IMPROVED RETRIEVAL OF GLOBAL LAND EMISSIVITY FROM AMSR-E OBSERVATIONS

by

Hamidreza Norouzi

A dissertation submitted to the Graduate Faculty in Civil Engineering in partial fulfillment of the Requirements of the degree of Doctor of Philosophy.

The City University of New York

2011

This manuscript has been read and accepted for the Graduate Faculty in Engineering in satisfaction of the dissertation requirement for the degree of the Doctor of Philosophy.

Date — Dr. Reza Khanbilvardi
Professor of Civil Engineering and
Chair of Examining Committee

Date — Dean. Mumtaz K. Kassir
Executive Officer

Supervisory Committee:

Dr. Sid-Ahmed Boukabara

Dr. Reza Khanbilvardi

Dr. Shayesteh Mahani

Dr. Fabrice Papa

Dr. Catherine Prigent

Dr. William Rossow

Dr. Marouane Temimi

THE CITY UNIVERSITY OF NEW YORK

ABSTRACT

IMPROVED RETRIEVAL OF GLOBAL LAND EMISSIVITY FROM AMSR-E OBSERVATIONS

by

Hamidreza Norouzi

Advisors: Drs. Reza Khanbilvardi, Marouane Temimi, and William Rossow

This research dissertation aims to improve our understandings of land surface emissivity using estimates from the Advanced Microwave Scanning Radiometer - Earth Observing System (AMSR-E) and to investigate the effect of penetration depth of the microwave signal and its effect on the retrieval of this variable. Microwave observations at low frequencies exhibit more sensitivity to surface and subsurface properties with little interference from the atmosphere. The AMSR-E sensor has two additional lower frequencies, at 6.9 and 10.65 GHz (C- and X-band, respectively) with respect to its preceding sensors. Observations at these low frequencies penetrate deeper into the soil layer. Ancillary data used in the analysis, such as surface skin temperature and cloud mask, are obtained from International Satellite Cloud Climatology Project (ISCCP). Atmospheric properties are obtained from the TIROS Operational Vertical Sounder (TOVS) observations to determine the small upwelling and downwelling atmospheric emissions as well as the atmospheric transmission.

The difference in depth of originations causes an inconsistency between diurnal variation of infrared and microwave brightness temperatures, which can lead to more than 10% difference

between day and night estimates of land emissivity. In this study, the diurnal cycle of microwave brightness temperature is constructed at different channels using a constellation of satellites which comprises AMSR-E and other SSM/I sensors. Differences in phase and amplitude were observed between the microwave and infrared diurnal cycles. These differences seem to be consistent with land cover and soil texture maps. A principal component analysis (PCA) is conducted to evaluate spatial variation of diurnal cycle of brightness temperature at global scale. A lookup table of effective physical temperature representative of the contributing layers of the microwave signal at each channel and month is adopted based on the diurnal cycle of brightness temperature. The implementation of the proposed effective temperature diurnal cycle lookup table showed that it can significantly mitigate the differences between day and night retrieved emissivities from AMSR-E observations. Therefore, a global product of instantaneous land emissivity that accounts for the difference in penetration depth between thermal and microwave temperatures is proposed.

ACKNOWLEDGEMENTS

It is a pleasure to convey my thanks to a number of people who have contributed in assorted ways to the research and making of the thesis. Over the course of my PhD at the City University of New York / City College, my advisors, Prof. Reza Khanbilvardi, Dr. Marouane Temimi and Prof. William Rossow have had a major impact on the dissertation with their supervision, advice, and guidance during my doctoral study and research. I would like to thank Prof. Reza Khanbilvardi who believed in my potentials, which encouraged me and inspired me. Without his supports, it was impossible to do this research.

Prof. Rossow provided me persistent encouragement and support in various ways. I gratefully thank him for his advice and contribution for four years, and using his precious time to read my manuscripts and this thesis and giving his critical comments about them. He also kindly provided his group facilities such as office space, data sets, and computers for this research.

I sincerely thank my dedicated adviser Dr. Temimi who was supportive from the first day, by helping me to remember basic principles and the big picture when feeling overwhelmed. He patiently reviewed my works and kept my hand through every step.

I feel sincerely thankful to my supervisor, Cindy Pearl, at my student job for her helps, advice, and suggestions. I convey my thanks to Dr. Catherine Prigent, Dr. Sid Boukabara, Dr. Fabrice Papa, Dr. Shayesteh Mahani, Dr. Filipe Aires, Dr. Yudong Tian, and Dr. Fuzhong Weng for their supports, discussions, and their suggestions for this dissertation. I thank NOAA-CREST administrative staff especially Dr. Shakila Merchant. Faculty and academic staff, Narges Shahroudi and other fellow graduate students in the department.

Finally, I would like to express my deepest appreciations to my lovely wife Marzi who is my love, my best friend, and my colleague. I want also to thank Ryan, my son, for bringing the joy of life to me. I thank my parents for their unconditional love and support.

Table of Content

LIST OF TABLES

LIST OF FIGURES:

CHAPTER 1: INTRODUCTION

Microwave remote sensing has a great potential in understanding the geophysical and atmospheric phenomena. Microwave radiation is emitted from atmosphere and the surface of the earth. Atmosphere contribution comes from column water vapor, clouds, and precipitating particles. To understand the atmospheric phenomena such as rain rate, cloud liquid water, and total precipitable water the contribution of the surface should be accounted and be removed from the microwave signal. On the other hand, to extract geophysical information such as snow, soil moisture, vegetation structure, and sea ice the effect of the atmosphere should be removed. Therefore disaggregating the effect of these two sources (i.e. atmosphere and the surface) is important, and directly using the brightness temperature in these applications without removing the effect of the other does not give accurate results. Over the ocean with approximately spatially homogeneous surface properties microwave radiation can be approximated more routinely. However, over land, the surface contribution depends on the vegetation type and water content, soil moisture, soil texture, and surface roughness. These properties are highly variable spatially over land, which makes the modeling of the passive microwave much more complicated than over ocean. This problem gets more complicated when the microwave information are used in atmospheric retrievals with strong emission by the land surface, and leaves smaller fraction for the atmosphere (Ruston, 2004). Therefore, accurate estimation of the surface effect in shape of land surface emissivity is very crucial.

This dissertation aims to bring new emissivity estimates from the Advanced Microwave Scanning Radiometer - Earth Observing System (AMSR-E) that with other available estimates from other sensors and algorithms increase our understanding about the microwave radiations

over land. It investigates the potential and sensitivity of microwave land surface emissivity at lower frequencies to surface properties. Also, the difficulties of using infrared thermal temperature as physical temperature of emitting layers in emissivity retrievals is discussed and a lookup table for the effective temperature diurnal cycle is proposed to decrease the discrepancies due to using infrared temperature.

1.1. Background

Assuming that the land surface is flat and specular and considering the atmosphere as a nonscattering plane-parallel medium and cloud free condition, the brightness temperature at top of atmosphere can be written as:

$$Tb_{(p,\upsilon)} = \varepsilon_{(p,\upsilon)}.e^{-\tau(0,H)/\mu}.T_{surf} + (1-\varepsilon_{(p,\upsilon)}).T_{atm}^{\downarrow}.e^{-\tau(0,H)/\mu} + T_{atm}^{\uparrow} \qquad (1\text{-}1)$$

where $\varepsilon_{(p,\upsilon)}$ and $Tb_{(p,\upsilon)}$ are the land surface emissivity and the measured brightness temperatures at polarization p and frequency υ, respectively. T_{surf} is the surface temperature and $T_{atm}^{\downarrow}$ and $T_{atm}^{\uparrow}$ are the downwelling and upwelling brightness temperatures from the atmosphere, respectively:

$$T_{atm}^{\downarrow} = \int_{H}^{0} T(z).[\alpha(z)/\mu].e^{-\tau(z,0)/\mu}dz \qquad (1\text{-}2)$$

$$T_{atm}^{\uparrow} = \int_{0}^{H} T(z).[\alpha(z)/\mu].e^{-\tau(z,H)/\mu}dz \qquad (1\text{-}3)$$

In these equations, *T(z)* is the atmospheric temperature profile, $\alpha(z)$ the atmospheric absorption at altitude z, μ the cosine of incidence angle and τ the atmospheric extinction between two altitudes which is written as:

$$\tau(z0,z1) = \int_{z0}^{z1} \alpha(z)dz \qquad (1\text{-}4)$$

The implementation of this algorithm requires an accurate characterization of the atmosphere, particularly temperature and humidity composition, to determine atmospheric transmissivity. Another key parameter is the surface physical temperature. This temperature should be representative of all emitting layers from where microwave signals originate. Due to lack of global information of physical temperature profile, it is common to use infrared thermal temperature as effective temperature. This is equivalent to an assumption that the microwave originates from the top surface rather than the deeper layer.

According the equation 1-1 and depending on the frequency, some amount of the signal that reaches to the sensor at satellite has contribution with surface (land or ocean). For example, figure 1-1 shows the weighting function or contribution of different altitudes in the atmosphere for different channels of Advanced Microwave Sounding Unit (AMSU). Channels such as 3, 6, and 15 show some part of the brightness temperature belongs to the surface. To retrieve temperature and humidity profiles from special sensor microwave/temperature (SSM/T) and advanced microwave sounding units (AMSU), it is important to quantify the contribution of the Earth surface emission (Prigent et al., 2000). These parameters are playing key role in hydro climate and weather prediction topics. Therefore, reliable estimation of the emissivity is crucial to disaggregate the effect of the atmosphere and surface in equation 1-1.

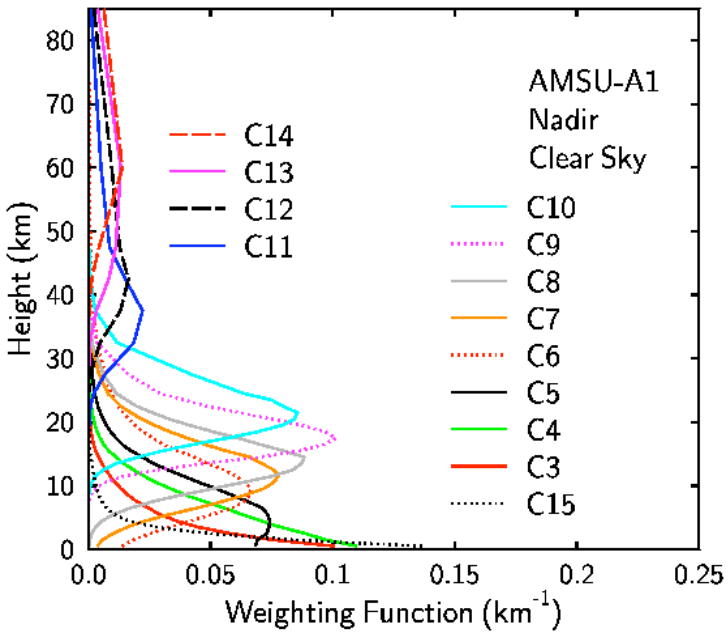

Figure 1- 1: Weighting function diagram of AMSU-A1 channels at different altitudes (Greenwald et al., 1999)

The contrast between ocean and atmosphere emission is great, as the atmosphere emission is largest over ocean in non-scattering condition than over land. Since, the ocean has homogeneous properties spatially; removing the effect of the surface is less challenging. However, over land by strong microwave emission from the surface, there is a smaller signal has left for the atmosphere. This makes the atmospheric retrieval much more complicated than over oceans. The land surface has a great variability in terms of vegetation type, water content, and soil moisture content that can affect the amount of emission by the surface, which makes the simulation of the microwave radiation much more complicated. Therefore, estimation and characterization of the microwave emissivity over land is more challenging. Land surface emissivity from passive microwave depends on several parameters such as soil wetness and roughness, vegetation cover, and also sensor configuration such as frequency, polarization, and incidence angle.

Land surface emissivity is being used as a boundary condition for Numerical Weather Predictions (NWP) models. These models use microwave data at different channels (relatively high frequencies ranging from 50 to 190 GHz). Land emissivity values at higher frequencies near the window regions can be extrapolated to microwave sounding frequencies to provide this boundary condition in NWP models (Prigent et al., 2005b; Aires et al., 2011). Neural network approach has been developed that uses a first guess of emissivity (Aires et al., 2001). The neural method retrieves the surface skin temperature, the integrated water vapor content, the cloud liquid water path and the microwave surface emissivities between 19 and 85 GHz over land from Special Sensor Microwave Imager (SSM/I) observations for all weather conditions including clear sky and cloudy scenes. Microwave land surface temperature retrieval presents a very attractive complement to the infrared estimates in cloudy areas (Aires et al., 2001). In similar study, the Microwave Integrated Retrieval Systems (MIRS) (Boukabara et al., 2007) running operationally since 2007 at NOAA-NESDIS makes use of microwave observations through a data assimilation process in order to infer a variety of land surface and atmospheric parameters, the microwave land emissivity being one of them at both clear and cloudy conditions. MIRS exploits observations from several sensors such as SSM/I, AMSU, and AMSR-E.

Recently, there is a Land Surface Working Group (LSWG), which specifically works to find an accurate estimation of microwave land surface emissivity for the Global Precipitation Measurement (GPM) mission. The first satellite is scheduled to fly in 2013. Microwave emissivity is needed to improve the development of physically based precipitation retrievals over land under all weather conditions such as clear, cloudy and precipitating sky from 10 – 190 GHz.

Moreover, passive microwave emissions especially at lower frequencies are more sensitive to the surface than the atmosphere. Removing the effect of atmosphere can help to have

a strong signal from the surface. Due to great variability of the land surface such as vegetation type, soil moisture content, roughness, and soil texture type, different contribution of the surface can be recognized from satellite observations. This variability can help to extract useful information from the surface properties. Because of this surface variability and the effect of the atmosphere, direct application of brightness temperature is not very useful, and an accurate estimation of emissivity is important, as it is “surface temperature free” and “atmosphere free”. As soil moisture increases, the surface emissivity decreases. Also, microwave measurements especially at low frequencies represent the temperature in sub layer part of the soil in smaller moisture situation. This may leads to more information about the soil moisture. Therefore, microwave emissions and in particular emissivity could be a good surrogate for changes in soil moisture and vegetation cover.

In figure 1-2, the relation between different frequencies and the penetration depth has been depicted. Water as moisture in the soil has higher thermal capacity compared to dry soil. It shows that with increasing the moisture, the penetration depth of the microwave radiation decreases. Consequently, we expect to have much lower amplitude of temperature diurnal cycle in moist soils with higher thermal capacity and evaporation. In figure 1-2, as frequency decreases the penetration depth increases.

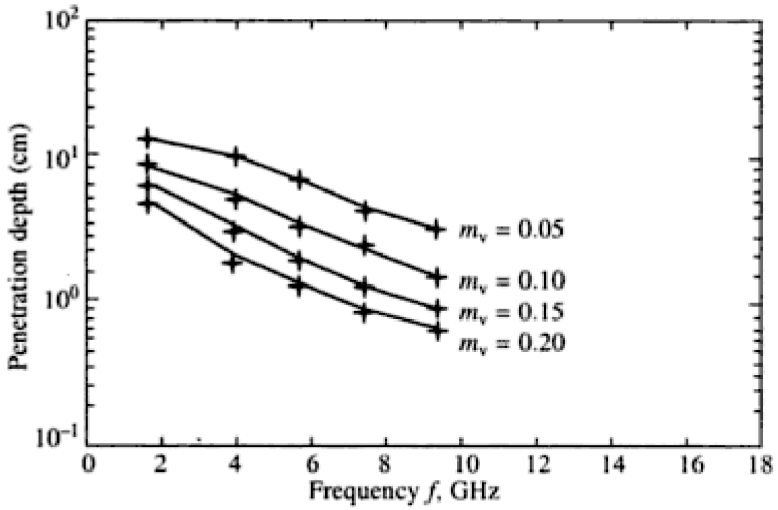

Figure 1- 2: Depth of penetration in a sandy-loam soil at different moisture contents and for different observation frequencies (Troch et al., 1997)

Based on these descriptions, several surface property studies have used microwave observations and emissivity in their applications such as soil moisture estimation, snow cover detection, freeze/thaw state, land surface temperature, surface inundation, and vegetation structure (e.g. Fily et al., 2003; Njoku et al., 2003; Aires et al., 2005; Prigent et al., 2005a; Cordisco et al., 2006; Papa et al., 2006; Tedesco and Kim, 2006; Entekhabi et al., 2010; Min et al., 2010).

The level of required accuracy for the brightness temperature and emissivity varies depending on application and the frequency that is being used. In other word, the emissivity should be more accurate than the signal that can be detected for a specific application. For instance in figure 1-3, 5 percent change in volumetric soil moisture content can change 8 percent of emissivity in bare soil regions and 5 percent change in a plot planted regions (Jackson et al., 1997). This means that 10 percent error in emissivity will miss most of the sensitivity to soil moisture content (it is worth noting that the range of soil moisture in global scale is between 0 to

30 percent).

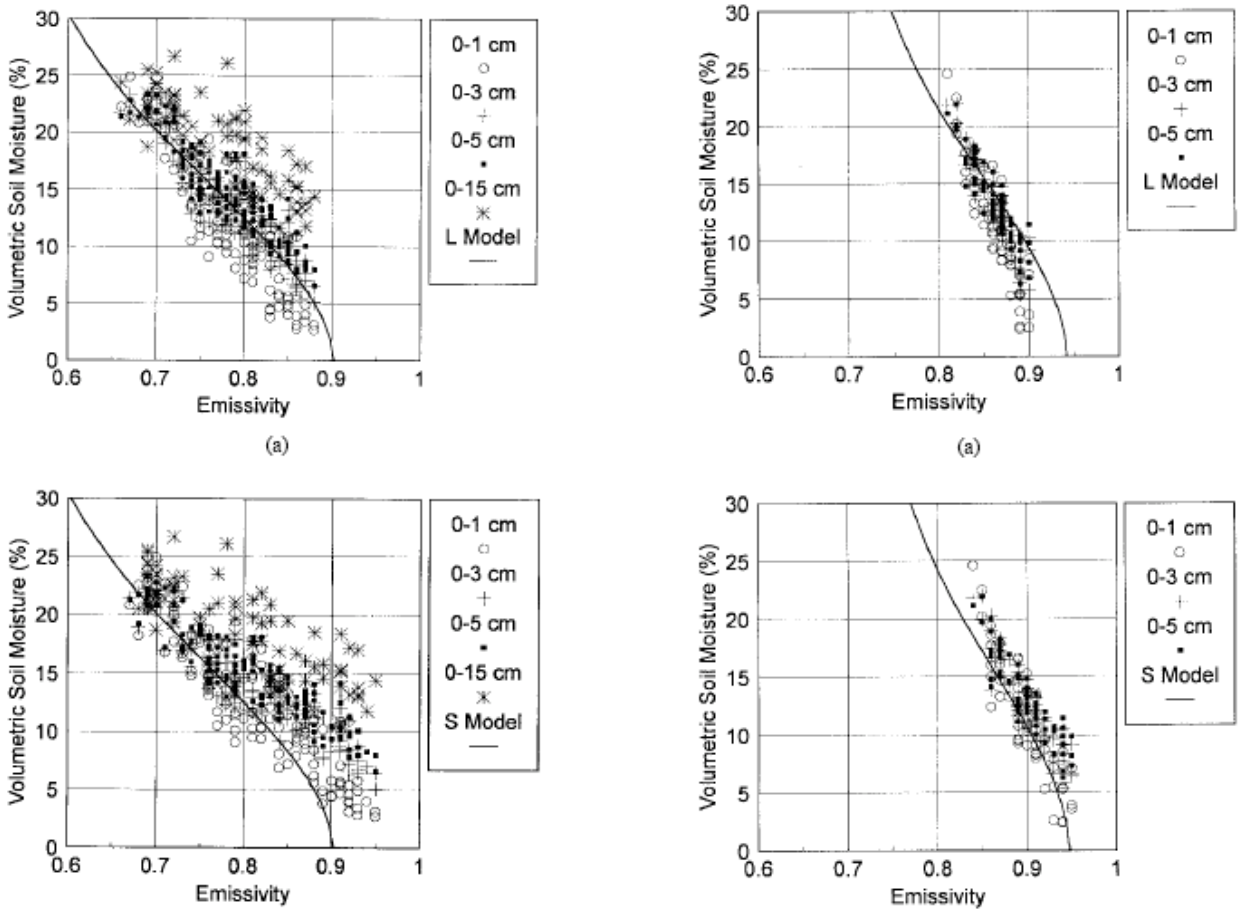

Figure 1- 3: Comparisons of emissivity and soil moisture at four depths for bare soil (left) and for a plot planted (right): (tops) L band and (bottoms) S band (Jackson et al., 1997).

In another study (Calvet et al., 2011), the signal of brightness temperature at different frequencies to detect soil moisture and vegetation water content was examined (figure 1-4). It shows that especially in lower frequencies the brightness temperature is more sensitive to these physical parameters. Therefore, either the estimation of brightness temperature or emissivity is essential in these applications.

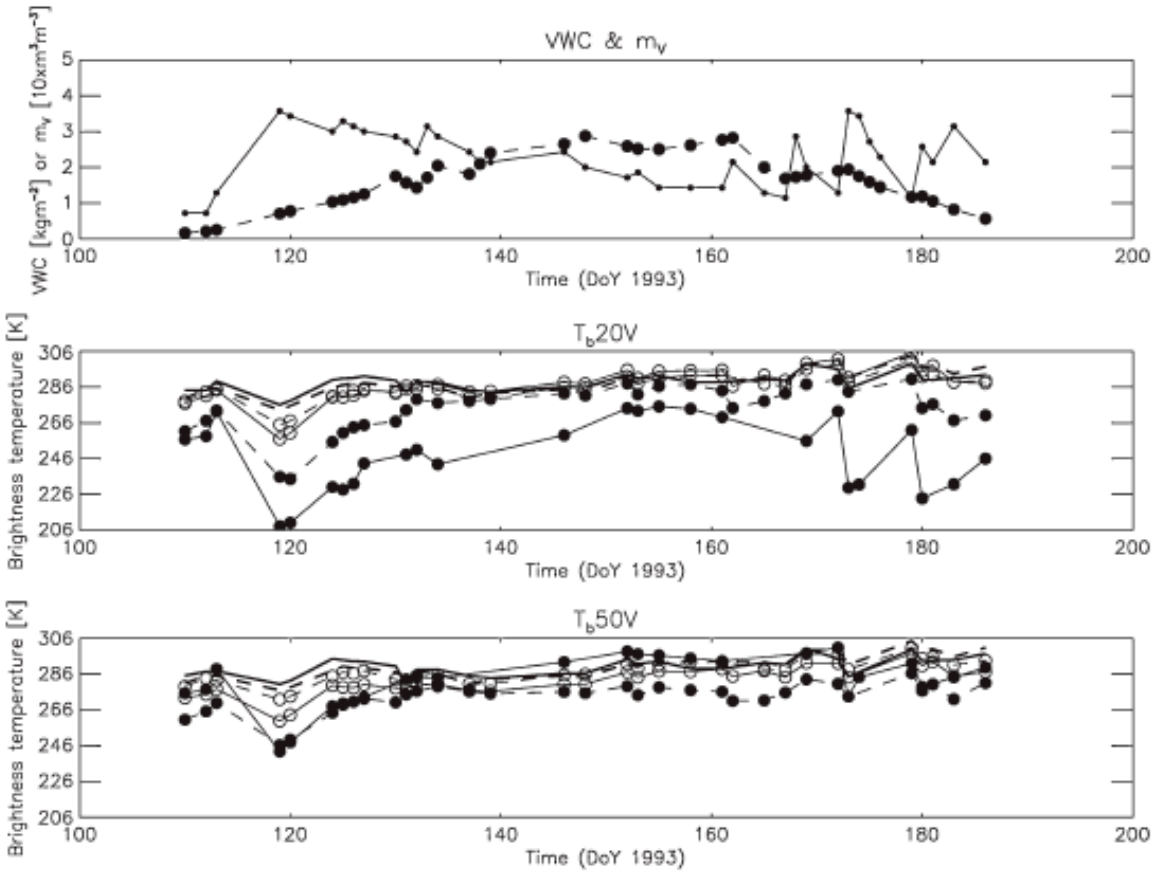

Figure 1- 4: Example of variables observed over a wheat field during PORTOS-93 experiment. From top to bottom: VWC and surface soil moisture measured at 2.5 cm and V-polarized brightness temperatures (Tb) at two incidence angles of 20^o and 50^o for six frequencies (1.41 GHz, closed circles and solid line; 5.05 GHz, closed circles and dashed line; 10.65 GHz, open circles and solid line; 23.8 GHz, open circles and dashed line; 36.5 GHz, solid line; 90 GHz, dashed line) (Calvet et al., 2011).

The relationship between emissivity and rain rate was investigated in another study (Calvet et al., 2011). Figure 1-5 shows daily mean AMSU-A and AMSU-B emissivities at 89 GHz, for an eight-month period, over a relatively flat area in northern France (0.5◦ W−4◦ E and 46◦ N−49◦ N) covered to a large extent by annual crops. The mean daily emissivity estimates at 89 GHz are shown together with the average daily accumulated precipitation measured in situ at about 810 stations. On average, 152 emissivity observations are available each day within the

considered area, including observations from AMSU-A NOAA-15, NOAA-16, NOAA-18, METOP, and AQUA and observations from AMSU-B, NOAA-16, NOAA-17, and NOAA-18. The emissivity deviates its average value of 0.95 ranges from −0.04 to +0.02. Figure 1-5 shows that, when rain occurs, the emissivity may drop by 0.02–0.04. For instance, an increase in precipitation in early September corresponds to a decrease of the emissivity of more that 0.02. Similarly, soil freezing may affect the emissivity (Calvet et al., 2011). This confirms that missing more than 4 percent of emissivity will diminish the sensitivity of emissivity to surface properties after precipitations.

However, according previous studies there are several difficulties in emissivity retrieval and achieving an estimate that can detect these surface physical characteristics. One of these challenges is the lack of global information of physical or effective temperature profile in emissivity retrieval that can cause more than 10 percent differences in emissivity estimates for day and night (Prigent et al., 1999; Galantowicz et al., 2011). Therefore, this research study aims to focus on this issue in emissivity retrieval.

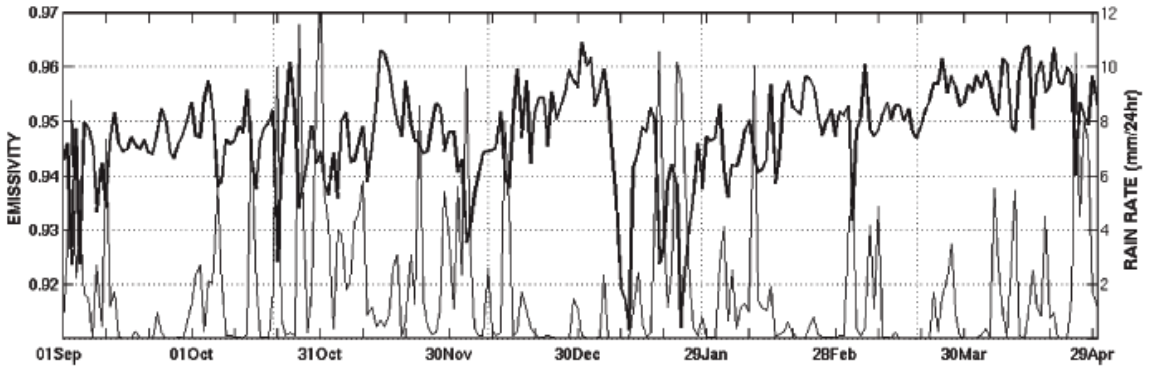

Figure 1- 5: (Dashed line) Daily mean AMSU-A emissivities at 89 GHz in northern France and (solid line) daily precipitation measured in situ (Calvet et al., 2011).

Several observations and estimates from different sensors have been utilized in these studies. In the next section, some of available land surface emissivity estimates that are useful for the mentioned applications are discussed.

1.3 Literature review

Satellite based land surface emissivity products have been retrieved globally since the 1990's. Choudhury (1993) investigated the inter-annual variation of land surface microwave reflectivity (reflectivity = 1-emissivity). Since then few groups have worked on this issue. In the following, some of the leading works in emissivity retrievals are discussed:

1.3.1. SSM/I-based emissivity products

Microwave emissivities of land surfaces have been estimated from special sensor microwave / imager (SSM/I) observations by removing the contributions from the atmosphere, clouds, and rain using ancillary satellite data (International Satellite Cloud Climatology Project (ISCCP) and TIROS Operational Vertical Sounder (TOVS) products) (Prigent et al., 1997). These estimations were first limited to MeteoSat observation area, and then were extended to whole globe using other geostationary and polar orbit products of ISCCP (Prigent et al., 1998). In the first step of their model, cloud-free SSM/I observations were isolated with the help of collocated visible / infrared satellite observations (ISCCP data). The cloud- free atmospheric contribution was then calculated from an estimate of the local atmospheric temperature-humidity profile (TOVS retrieval). Finally, with the surface skin temperature derived from IR observations (ISCCP estimate), the surface emissivity was calculated for all the SSM/I channels. In the global product, instead of TOVS data, National Centers for Environmental Prediction (NCEP) analyses (Kalnay et al., 1996) was used (Prigent et al., 1998). Using a neural network technique,

emissivities were estimated for cloudy pixels based on cloud-free estimates as first guess (Aires et al., 2001). These emissivity estimates are nowadays available for more than 16 years. Using this product, correspondences between the microwave emissivity and the vegetation distribution was found which suggests the possibility of using microwave emissivities to monitor vegetation phenology at regional and continental scale. The SSM/I land emissivities have also shown a strong sensitivity to flooding and to snow cover, sea ice characteristics and snow characterization and could be further used to monitor these parameters (Prigent et al., 2001; Cordisco et al., 2006; Papa et al., 2006).

In vegetated regions the emissivity difference reacts primarily to the vegetation increase, not to soil moisture variations; in semiarid regions, at the beginning of the rainy season when the vegetation density is very small, the emissivity difference is sensitive to the soil moisture at first, but as soon as the vegetation density increases, the emissivity reacts primarily to the vegetation variability. However, a rather strong correlation has been found between the passive microwave polarization difference and the soil moisture in some regions, making it possible to retrieve soil moisture from passive microwave observations around 19 GHz (Prigent et al., 2006).

The role of the vegetation in this correlation has been questioned: is passive microwave signal strictly related to the soil moisture or is it related to it through a correlation between the vegetation and the soil moisture? This relationship has been examined in detail with SSM/I microwave emissivities in coincidence with in situ soil moisture from a large number of stations (Prigent et al., 2005a) as well as with soil moisture as derived from land surface models (Aires et al., 2005). The passive microwave polarization differences are expected to react in a similar way to an increase of soil moisture or to a decrease in vegetation. As a consequence, in regions where soil moisture and vegetation are anti-correlated (i.e., in mid-latitude regions where vegetation

density tends to increase in spring and summer when soil moisture decreases) it is difficult to tell to which parameter the passive microwaves are reacting. Therefore, there is a complex sensitivity of the microwave emissivities to both vegetation and soil moisture. As a consequence, direct and simple retrieval of soil moisture solely from the passive microwave frequency range is unlikely for global application (Prigent et al., 2005a).

Another try for emissivity retrieval for SSM/I has been done by Jones et al (1997) over United States for 70 days using a data assimilation techniques (Jones and VonderHaar, 1997). Later they expanded their work to AMSU measurements (Jones et al., 2004).

1.3.2. AMSU-based emissivity products

Prigent et al (2000) tried to see the potential of using their SSM/I products to estimate the Advanced Microwave Sounding Unit (AMSU) emissivities by interpolating in frequency and angle. The SSM/T and AMSU temperature and humidity sounders are cross-track scanners, and they both have channels that are sensitive to the surface (figure 1-1). To analyze the feasibility of deriving SSM/T and AMSU land surface emissivities from SSM/I emissivities, the spectral and angular variations of land surface emissivities were studied with the help of ground-based emissivity measurements, emissivity models, and satellite emissivity estimates. They found up to 100 GHz for snow and ice-free areas, the SSM/T and AMSU emissivities can be derived with useful accuracy from the SSM/I emissivities. For a given zenith angle, the emissivities can be linearly interpolated in frequency. The scanning and polarization patterns of SSM/T and AMSU are such that the angular dependence of the emissivity seen by these instruments is rather small. Based on ground-based emissivity measurements of various surface types, a simple model was proposed to estimate SSM/T and AMSU emissivities for all zenith angles knowing only the emissivities for the vertical and horizontal polarizations at 53 zenith angle (Prigent et al., 2000).

A similar method to the one used for SSM/I emissivity retrieval, was used to retrieve the emissivity for AMSU channels at different zenith angles (Karbou and Prigent, 2005). The calculation uses an up-to-date radiative transfer model (RTM) and was performed for cloud-free AMSU observations. Ancillary data included the ISCCP cloud flags and surface skin temperature, along with the temperature and water vapor profiles from the ECMWF re-analysis. The day-to-day variability of the emissivities within a month was lower than 0.02 for all window channels, for small incidence angles. The angular and spectral dependence of the AMSU emissivity were examined for various surfaces. An instrumental AMSU-A problem was evidenced related to an asymmetry in the scan angle behavior. For low incidence angles, the land surface emissivities in the sounding channels (50-60 GHz and 150-183 GHz) could successfully be extrapolated from the calculation in the closest window channels (Karbou et al., 2005a).

Jones et al (2004) retrieved emissivity for AMSU channels at different angles over United States. They used a 1D-var method, the retrieval scheme requires a first guess of the water vapor, and temperature profiles as well as surface emissivities at the relevant microwave frequencies. This first guess for moisture can come from climatology, or from global model output such as from NCEP GDAS (Global Data Assimilation System). An a priori distribution of the retrieval parameters is used to constrain a non-linear iterative optimal-estimation scheme, which uses a method to minimize the cost function to find the optimal solution.

A NWP-independent 1D-VAR system was developed to carry out the simultaneous restitutions of atmospheric constituents and surface parameters in all weather conditions (Boukabara et al., 2007). This model estimates the emissivity as one of the outputs. Their consistent treatment of all components that have an impact on the measurements allowed an optimal information-content extraction. Their study focused on the data from the NOAA-18

satellite (AMSUA and MHS sounders). The retrieval of the precipitating and non-precipitating cloud parameters was done in a profile form, taking advantage of the natural correlations that does exist between the different parameters and across the vertical layers. The use of empirically orthogonal-function decomposition leaded to a dramatic stabilization of the problem. The goal of this inversion system was to be able to retrieve independently, with a high-enough accuracy and under all conditions, the temperature and water-vapor profiles, which are still the two main prognostic variables in numerical weather forecast models (Boukabara et al., 2007). The model has also been tested for AMSR-E observations as well.

A simulated land surface emissivity was developed by Weng et al (2001). Their study developed a model to quantify the land emissivity over various surface conditions. For surfaces such as snow, deserts, and vegetation, volumetric scattering was calculated using a two-stream radiative transfer approximation. The reflection and transmission at the surface-air interface and lower boundary were derived by modifying the Fresnel equations to account for cross-polarization and surface roughness effects. Several techniques were utilized to compute the optical parameters for the medium, which was used in the radiative transfer solution. In the case of vegetation, geometrical optics was used because the leaf size is typically larger than the wavelength. For snow and deserts, a dense medium theory was adopted to take into account the coherent scattering of closely spaced particles. The emissivity spectra at frequencies between 4.9 and 94 GHz were simulated and compared with the ground-based radiometer measurements for bare soil, grassland, and snow conditions. It was shown that the features including the spectra, variability, and polarization agree well with the measurements. The simulated global distribution of land surface emissivity was also compared with the satellite retrievals from the Advanced Microwave Sounding Unit (AMSU). It is found that the largest discrepancies primarily occur

over high latitudes where the snow properties are complex and least understood (Weng et al., 2001; Weng, 2007).

1.3.3. AMSR-E emissivity

Up to now there are no published long records of AMSR-E land emissivity. The only work that has been done is by Atmospheric and Environmental Research, Inc (AER) and estimates through previously mentioned MIRS estimations. AER has global gridded monthly emissivity products at the AMSR-E 10.7 GHz, 18.7 GHz, 23.8 GHz, 36.5 GHz, and 89.0 GHz Vertical Pol. and Horizontal Pol. channels (6.9 GHz is not included). The microwave land surface emissivity is derived from a combination of AMSR-E brightness temperature and MODIS LST and NCEP GFS data. The database is composed of two datasets: a multi-product database containing multiple AMSR-E channel emissivity products retrieved by so-called "1a", "1b" and "classification" algorithms, and a merged database derived from the multi-product database to provide the "best" available estimates of the average effective emissivities.

The 1a dataset is retrieved directly from AMSR-E brightness temperatures, using MODIS LST to represent the emitting temperature of the surface and ancillary data to define the atmospheric contribution.

The 1b algorithm estimates the microwave emission depth and effective emissivity by fitting the solution of a thermal diffusion equation to a one-month time series of clear-sky measurements, assuming sinusoidal diurnal surface forcing. It is produced as an alternative to the 1a product over arid or semi-arid regions where the microwave penetration depth effect is substantial. In their revised estimates, Prigent et al (1999) physical model has been used to extract the effective temperature over the regions with large day and night differences. This physical model can estimate the monthly mean surface emissivity, as it uses a non-linear least

square model (Moncet et al., 2011). Therefore, still the problem of the penetration depth effect for instantaneous retrievals remains and should be addressed.

1.4. Problem statement

Land emissivity estimates lack ground-truth measurements to be validated. Therefore, retrieval of emissivity using different sensors at different frequencies with different algorithms can help to have more information to build a better picture for this crucial parameter. In the previous section, several techniques and sensors were discussed. AMSR-E sensor is a "newer" sensor compared to mentioned sensors with two unique characteristics. It has two lower frequencies and unique overpass times close to daily minima and maxima of temperature. So, having another estimation based on what we have learned from SSM/I and AMSU would be useful. But there would be some difficulties with emissivity retrieval from AMSR-E observations as it has shown in earlier studies (Prigent et al., 1999; Grody and Weng, 2008; Moncet et al., 2011).

For solving the described equation 1-1, we need brightness temperature from remote sensing. Also, since there is no global ground measurement of skin temperature, infrared-based skin temperature is being used. The issue with using this information is that infrared-based temperature is sensitive to the skin of the surface, while brightness temperature of passive microwave can come from deeper level of the soil. This causes an inconsistency between these two measurements. The previous studies have shown this inconsistency has two problems. Firstly, the diurnal cycle of temperature has lower amplitude in deeper levels than the top surface especially in some land types such as sand dunes in desert area. Secondly, there is a phase lag between the peak of the diurnal cycle at top of the surface and deeper level in the soil, as it takes

some time to transfer the heat from top surface to deeper levels. This issue is more pronounced in lower frequencies due to their deeper penetration, and also the microwave measurements that are close to daily minima and maxima. Prigent et al (1999) studied the emissivity retrieval in desert and arid environments. They found that there is some specific microwave signatures exist in these regions. These phenomena can be explained by emissions of microwave radiations from different layers in the subsoil, depending on the soil type and on the microwave radiation frequency. They analyzed their results in detail for the Sahara desert and the Arabian Peninsula. They developed a one-dimensional heat transfer model to simulate the skin temperature for different layers by assuming a constant thermal diffusivity for the soil. The penetration depth of microwave was estimated to be larger than five wavelengths in some locations, indicating extremely dry conditions. They found that there is a phase lag between infrared or top skin temperatures and microwave radiation (figure 1-3) (Prigent et al., 1999).

Based on these studies, primarily using the infrared thermal temperature as physical temperature is unavoidable, since there is no global temperature profile available. Therefore, estimating the emissivity from AMSR-E observations would have the same issue especially at two lower frequencies with larger penetration depth.

Most of the available passive microwave sensors have the over passing time of 6:00 to 9:00 pm/am at equator (for example SSM/I, WindSat, AMSU…). This means that they may miss the minima and maxima of the temperature in the diurnal cycle. However, the Advanced Microwave Scanning Radiometer - Earth Observing System (AMSR-E) sensor of NASA which is on board on Aqua satellite has the over passing time of 1:30 am/pm local time at equator, which can help for more exploitation of the capabilities of operational microwave satellite sensors and diurnal variation coverage.

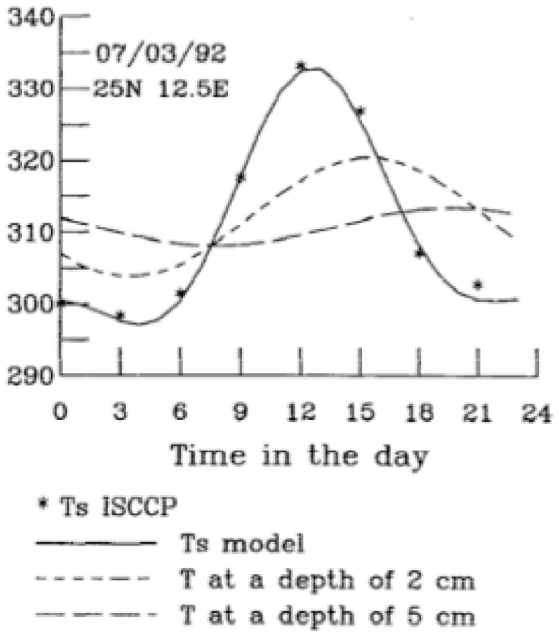

Figure 1- 6: Diurnal cycle of the surface skin temperature, along with the fit obtained from a two term expansion of the Fourier equation at the surface, at 2 cm below the surface, and at 5 cm below the soil surface (Prigent et al, 1999)

AMSR-E is more sensitive to atmosphere in higher frequencies, which is similar with other sensors in this case. Its two lower frequencies (10.65 and 6.925 GHz) are more sensitive to the soil compared to higher frequencies. Therefore, somehow it can give a better picture of frequency dependency of the soil moisture and land cover characterizations. This sensor gives us this opportunity to extent our knowledge with soil moisture with having more frequencies and penetration depth information.

Other issue with AMSR-E that is worth to be investigated is the contamination of the C and X bands with Radio Frequency Interference (RFI) especially over the US, the Middle East, and Europe. This RFI contamination problem can reduce the value of C- and X-band measurements. A spectral difference technique has been developed for AMSR-E and WindSat to

quantify the RFI magnitude and extent over the U.S. and at global scale (Njoku et al., 2005; Li et al., 2006). In this research, the RFI issue is not discussed and is left for future studies.

1.5 Scopes and Sequence

The main objective of this study is to have a better understanding of land surface emissivities using AMSR-E observations. The difficulties in retrieval and sensitivity to surface properties are discussed. The results of this research study compliments the existing emissivity estimates from other sensors or other algorithms by providing more information. In this dissertation, first emissivity is retrieved analytically based on a multi satellite approach. Different satellites provide information about brightness temperatures, skin temperature, cloud flag, and atmospheric information. The results are assessed at different levels and difficulties of using infrared-base temperature in emissivity retrieval are discussed. The sensitivity of AMSR-E frequencies especially at the two lower frequencies to surface properties is investigated. Using multi platform/multi sensor data for brightness temperatures, diurnal cycle of the brightness temperature is constructed. Spatial variability of microwave diurnal variation is studied. Based on the constructed diurnal variation of brightness temperature a lookup table of effective temperature diurnal cycle is generated that leads to resolve the discrepancies in instantaneous emissivities at day and night. The new generated effective temperature diurnal variation is general and can be used in any other sensor emissivity retrieval. This model is an improvement in emissivity retrievals and different with previous studies, as the difference between day and night emissivities is resolved instantaneously. The lookup table is limited to similar frequencies between AMSR-E and SSM/I (i.e. the C and X bands diurnal variation of effective temperature is not available yet). However, the methodology is general and can be extended to these lower frequencies by utilizing the other sensors.

The core parts of this dissertation are presented in chapter 3, 4, and 5 where the methodologies, problems and results are discussed. In chapter 2 the data sets used in this dissertation are introduced. Chapter 6 presents the conclusions of this research and future works. In following part, chapter 3 to 5 that forms the base of this research dissertation are introduced and summarized.

1.5.1. AMSR-E emissivity retrieval and the sensitivity of land emissivity estimates at C and X bands to surface properties (chapter 3)

The first objective of this study is to develop a global land emissivity estimates using passive microwave observations from the Advanced Microwave Scanning Radiometer - Earth Observing System (AMSR-E) and to investigate its sensitivity to land surface properties. A methodology based on previous studies is introduced after some adjustments due to different AMSR-E configuration. A sensitivity test is conducted to investigate the effect of the atmosphere parameters, skin temperature, and brightness temperature accuracy on emissivity estimates. Retrieved emissivities at C- and X-bands and their polarization differences are compared with changes in land cover type, soil moisture, and vegetation density. Moreover, differences between emissivity estimates from ascending and descending overpasses are examined as a test for the quality of emissivity estimates.

1.5.2. The analysis of the diurnal cycle of microwave brightness temperatures using a multi satellite approach (chapter 4)

Better understanding of the diurnal cycle of brightness temperature is needed for a better characterization of surface conditions. Diurnal cycles of microwave brightness temperature are constructed using observations from AMSR-E and SSM/I sensors, which are onboard four

operational satellites. Measurements from similar channels on both sensors are studied using a Principal Component Analysis (PCA). The effect of the surface properties in terms of vegetations land cover on diurnal cycle of brightness temperature is examined. Diurnal amplitudes and phase differences between infrared thermal and microwave brightness temperature diurnal cycle are then compared.

1.5.3. Using microwave brightness temperature diurnal cycle to improve emissivity retrievals over land (chapter 5)

In emissivity retrievals, it is common to use infrared thermal temperature as the physical temperature since there is no global physical temperature profile. The difference in depth of originations causes an inconsistency between diurnal variation of infrared and microwave brightness temperature, which can cause differences in retrieval of emissivities at day and night larger than 0.1. A lookup table of effective physical temperature representative of the contributing layers of the microwave signal at each channel and each month is adopted based on the diurnal cycle of brightness temperature. The implementation of the proposed effective temperature diurnal cycle lookup table mitigates the differences between day and night retrieved emissivities significantly from Advanced Microwave Scanning Radiometer – Earth Observing System (AMSR-E) observations. An error analysis for the proposed method is conducted to account the uncertainty of the assumptions made.

CHAPTER 2: DATA SETS

In this chapter, all the data sets used in this dissertation are discussed. Different data sets are utilized in emissivity retrieval and evaluation of the estimates.

2.1. AMSR-E microwave brightness temperatures

The Advanced Microwave Scanning Radiometer for EOS (AMSR-E) is a twelve-channel, six-frequency, total power passive-microwave radiometer system. It measures brightness temperatures at 6.925, 10.65, 18.7, 23.8, 36.5, and 89.0 GHz (Njoku and Li, 1999). Vertically and horizontally polarized measurements are made at all channels (table 1). The Earth-emitted microwave radiation is collected by an offset parabolic reflector 1.6 m in diameter that scans across the Earth along an imaginary conical surface, maintaining a constant Earth incidence angle of 55°. The spatial resolution of the individual measurements varies from 5.4 km at 89.0 GHz to 56 km at 6.9 GHz. The AMSR-E/Aqua L2A Global Swath Spatially-Resampled Brightness Temperatures (both ascending and descending) from National Snow and Ice Data Center (NSIDC) is used in this study. This data set contains resampled and non-resampled data. Higher frequency observations are upscaled and resampled to the lower frequencies spatial resolution. For each frequency we selected the resampled data having the closest spatial resolution to the original satellite footprint at that channel.

Sensor	Satellite	Temporal Coverage	Equator Crossing Time	Channels (GHz)	Polarization	Spatial Resolution (km)	Incident Angle
AMSR-E	Aqua	Jun. 2002 - present	1:30 A.M./P.M.	6.925	V, H	75 x 43	55^0
				10.65	V, H	51 x 29	
				18.7	V, H	27 x 16	
				23.8	V, H	32 x 18	
				36.5	V, H	14 x 8	
				89.0	V, H	6 x 4	

Table 2 - 1: AMSR-E sensor information.

2.2. ISCCP-DX data

In this study satellite infrared-based products from the International Satellite Cloud Climatology Project (ISCCP) are used for surface skin temperatures and cloud cover. The ISCCP-DX version provides information on skin temperature and cloud coverage every 3 hours since 1983 (Rossow and Schiffer, 1991; Rossow and Schiffer, 1999) at a ~ 30 km spatial resolution, based on merged observations from geostationary and polar-orbiting satellites. ISCCP products were resampled to match the 0.25° equal area grid adopted for the passive microwave observations. In production of skin temperatures in ISCCP-DX data infrared emissivity has been assumed to be unity, which it may not necessarily true for every surface type. Therefore, they are actually infrared brightness temperature, not actual skin temperature. This infrared brightness temperature despite of microwave emissivity which has proportional relation with actual temperature is proportional with following relationship:

$$TB^4_{\inf rared} = \varepsilon_{\inf rared}.TS^4 \qquad (1\text{-}5)$$

Although the effect of this emissivity is not as significant of microwave emissivity because of the power of 4 in the formula, it may have some effects in some regions especially arid area. In most of other places, this emissivity is close to unity. In this study, we will revise this temperature using equation (1-5) with appropriate infrared emissivity from ISCCP data (Zhang et al., 2007).

2.3. TOVS data

The TIROS Operational Vertical Sounder (TOVS) dataset available with ISCCP has a resolution of 280 km (Rossow and Schiffer, 1991) and provides global information on air temperature and water vapor profiles at 9 vertical layers ranging from 900 to 15 mb pressure. These profiles are available on a daily basis. We assume that the impact of their diurnal variation on the observed brightness temperature is minimal. Data are originally available in the 280 km equal area map resolution. They are processed and regridded to coincide with AMSR-E grid. These atmospheric parameters are used to calculate the upwelling, down-welling brightness temperatures, as well as the atmospheric transmission. The reason for choosing this data set is its consistency with ISCCP products, as ISCCP uses TOVS observations. As mentioned in section 4.2, there are some flaws with TOVS data that can affect ISCCP products including DX. These flaws obviously will affect the atmospheric corrections that we are trying to do in this research.

2.4. Emissivity products

For evaluation of this study, the microwave land surface emissivity data set provided by Prigent et al (2006) is used. These products are now available for 1993-2008, using the Special Sensor Microwave/Imager (SSM/I) observations, along with ISCCP-DX data (skin temperature and cloud cover), and NCEP Reanalysis data (Kalnay et al., 1996) (for atmospheric

corrections) have been used. Emissivities at all channels are available in monthly composite maps. More information about this product is available in section 1.3.1.

A microwave emissivity database has been developed (Moncet et al., 2011) with data from the Advanced Microwave Scanning Radiometer-EOS (AMSR-E) and with ancillary land surface temperature (LST) data from the Moderate Resolution Imaging Spectroradiometer (MODIS) on the same Aqua spacecraft. The accuracy of the emissivities in deserts and semiarid regions is enhanced by applying, in those regions, a version of the emissivity retrieval algorithm that accounts for the penetration of microwave radiation through dry soil with diurnally varying vertical temperature gradients. Emissivity coverage in areas where persistent cloudiness interferes with the availability of MODIS LST data is achieved using a classification-based method to spread emissivity data from less-cloudy areas that have similar microwave surface properties. Evaluations and analyses of the emissivity products over homogeneous snow-free areas are presented, including application to retrieval of soil temperature profiles (Moncet et al., 2011). More information about this product is available in section 1.3.3.

2.5. SSM/I brightness temperatures

The Defense Meteorological Satellite Program (DMSP) Special Sensor Microwave/Imager (SSM/I) is a seven channel passive microwave radiometer operating at four frequencies (19.35, 22.235, 37.0, and 85.5 GHz) and dual-polarization (except at 22.235 GHz which is V-polarization only) (Table 2). SSM/I data became operational in July 1987 on DMSP's F-8 satellite (Colton and Poe, 1999). Subsequent SSM/Is were flown on the DMSP's F-10 (November 1990), F-11 (December 1991), F-12 (August 1994), F-13 (March 1995), F-14 (April 1997) and most recently, F-15 (January 2000) satellites. At present, NESDIS receives data from

the F-15 satellite only; however, its channels have been deemed unusable for climate products as of January 2010. In this research, the measurements of this sensor from F13, F14, and F15 will be used to construct the diurnal cycle of microwave along with AMSR-E measurements. This data sets are in swath format, which are being re-projected to a 0.25 gridded equal area map at equator.

Sensor	Satellite	Temporal Coverage	Equator Crossing Time (2005)	Channels (GHz)	Polarization	Spatial Resolution (km)	Incident Angle
SSM/I	F13	May 1995 - present	6:30 A.M./P.M.	19.35	V, H	43 x 25	53^0
	F14	May 1997 - Aug 2008	7:00 A.M./P.M.	22.235	V Only	40 x 25	
				37.0	V, H	28 x 25	
	F15	Jan. 2000 - present	9:00 A.M./P.M.	85.5	V, H	13x12.5	

Table 2 - 2: SSM/I sensor information.

2.6. Land cover vegetation classes

Vegetation and land use global data set compiled from a large number of published sources at 1° equal area grid resolution by Matthews (1983) and regrouped by (Prigent et al., 2001) is used as land cover vegetation classification. The classes include rain forest, evergreen forest, deciduous forest, evergreen woodland, deciduous woodland, cultivation, grassland, tundra, shrubland, and desert. This data set is utilized for studying the effect of land cover on the diurnal cycle of microwave brightness temperature and also sensitivity analysis of the estimated emissivities.

2.7. AMSR-E soil moisture product

This gridded Level-3 land surface product (AE_Land3 provided by NASA) includes daily measurements of surface soil moisture and vegetation/roughness water content interpretive

information, as well as brightness temperatures and quality control variables. Ancillary data include time, geolocation, and quality assessment. Input brightness temperature data, corresponding to a 56 km mean spatial resolution, are resampled to a global cylindrical 25 km Equal-Area Scalable Earth Grid (EASE-Grid) cell spacing. Data are available from 19 June 2002 to the present. Spatial coverage is global except for snow-covered and densely vegetated areas (Njoku et al., 2003).

2.8. ASCAT soil moisture product

Another soil moisture product that is used in this dissertation is from the Advanced Scatterometer (ASCAT) provided by the European Organization for the Exploitation of Meteorological Satellites (EUMETSAT). This product was chosen, because it prodvides independent estimates of soil moisture that are not based on passive microwave observations. However, it has spatial coverage limitation as it uses active microwave observations. The ASCAT soil moisture product has originally 25 km spatial resolution and daily temporal resolution. ASCAT is a real aperture radar operating at 5.255 GHz (C-band) and using vertically polarized antennas. It transmits a long pulse with Linear Frequency Modulation ('chirp'). Ground echoes are received by the instrument and, after de-chirping, the backscattered signal is spectrally analysed and detected. In the power spectrum, frequency can be mapped into slant range provided the chirp rate and the Doppler frequency are known. The above processing is in effect a pulse compression, which provides range resolution (Bartalis et al., 2008).

2.9. Normalized Difference Vegetation Index (NDVI)

Global MODIS vegetation indices provide consistent spatial and temporal comparisons of vegetation conditions. Blue, red, and near-infrared reflectances, centered at 470-nanometers,

648-nanometers, and 848-nanometers, respectively, are used to determine the MODIS daily vegetation indices. Global MOD13C2 data are cloud-free spatial composites of the gridded 16-day 1-kilometer MOD13A2, and are provided monthly as a level-3 product projected on a 0.05 degree (5600-meter) geographic Climate Modeling Grid (CMG). Cloud-free global coverage is achieved by replacing clouds with the historical MODIS time series climatology record. These data are distributed by the Land Processes Distributed Active Archive Center (LP DAAC), located at the U.S. Geological Survey (USGS) Earth Resources Observation and Science (EROS) Center (lpdaac.usgs.gov).

CHAPTER 3: AMSR-E EMISSIVITY RETRIEVAL AND THE SENSITIVITY OF LAND EMISSIVITY ESTIMATES AT C- AND X-BANDS TO SURFACE PROPERTIES

Microwave observations at low frequencies exhibit more sensitivity to surface and subsurface properties with little interference from the atmosphere. The objective of this chapter is to develop a global land emissivity product using passive microwave observations from the Advanced Microwave Scanning Radiometer - Earth Observing System (AMSR-E) and to investigate its sensitivity to land surface properties. The developed product complements existing land emissivity products from SSM/I and AMSU by adding land emissivity estimates at two lower frequencies, 6.9 and 10.65 GHz (C- and X-band, respectively). Observations at these low frequencies penetrate deeper into the soil layer. Ancillary data used in the analysis, such as surface skin temperature and cloud mask, are obtained from International Satellite Cloud Climatology Project (ISCCP). Atmospheric properties are obtained from the TIROS Operational Vertical Sounder (TOVS) observations to determine the small upwelling and downwelling atmospheric emissions as well as the atmospheric transmission. A sensitivity test is conducted to investigate the effect of the atmosphere parameters, skin temperature, and microwave brightness temperature accuracy on emissivity estimates. Retrieved emissivities at C- and X-bands and their polarization differences are compared with changes in land cover type, soil moisture, and vegetation density. Finally, differences between emissivity estimates from ascending and descending overpasses are testes as a quality control of the retrievals.

3.1. Introduction

At lower frequencies, passive microwave observations are less affected by the atmosphere and are more sensitive to the surface and subsurface properties like soil moisture and soil texture (Choudhury, 1989; Choudhury, 1993). Because of this greater sensitivity and a greater penetration depth, land emissivity estimates at these lower frequencies are appropriate for applications like soil moisture estimation, snow cover detection, freeze/thaw state, land surface temperature, and vegetation structure (e.g. Njoku et al., 2003; Tedesco and Kim, 2006; Jones et al., 2007; Min et al., 2010; Zhang et al., 2010). In addition, land emissivity values at higher frequencies near the window regions can be extrapolated to microwave sounding frequencies to provide the critical boundary condition in numerical weather prediction (NWP) models (Weng et al., 2001; Karbou et al., 2005a). Interpretation of microwave emissivity over land is not very straightforward as it is affected by several factors such as soil wetness and roughness, vegetation cover, macroscopic mixtures of vegetation, soil and rock, and terrain slopes, as well as sensor properties (i.e. frequency, polarization, and incidence angle).

Land emissivity estimates at higher frequencies (19 GHz>) are sensitive only to the topsoil layer, of the order of few millimeters, depending on the soil wetness, texture and frequency, and vegetation cover. Measurements at these frequencies are therefore not as useful as lower frequencies to infer subsurface parameters (Njoku et al., 2003).

The Advanced Microwave Scanning Radiometer - Earth Observing System (AMSR-E) sensor has two channels at 6.925 and 10.65 GHz (the C and X bands) beside those available onboard SSM/I and AMSU. These channels penetrate deeper and are more sensitive to the surface and subsurface. Also, this sensor is on a polar orbiting satellite with different overpass times in early afternoon and morning (1:30 am/pm), as compared with most SSM/I overpass

times between 6:00 to 9:00 (am/pm local time). Since the AMSR-E overpass time is closer to maxima and minima temperature of the day, the contrast between early morning and early afternoon measurements might be used to infer surface and subsurface properties: the early morning (1:30 am) observation occurs when the soil temperature profile tends to be more nearly uniform within the sensed soil layer and the afternoon observation occurs when the temperature difference between the skin and deeper layers is large (Njoku et al., 2003). When combined with other microwave sensors, such as SSM/I and WindSat, the AMSR-E measurements could also provide a better characterization of the diurnal temperature cycle.

3.2. Determination of AMSR-E land surface emissivities

The algorithm adopted to determine land emissivities in this study is similar to the approach proposed by (Prigent et al., 1997; Prigent et al., 1998). Although the approach was initially tested using SSM/I observations the algorithm is extendable to lower frequencies as well. A few adjustments are needed to account for minor differences in incidence angles, spatial resolution, and channel frequencies.

AMSR-E overpass times are near 1:30 am (ascending) and 1:30 pm (descending) local time at the equator. Since skin temperatures from ISCCP-DX data are available every 3 hours, microwave and thermal observations are not necessarily coincident. Therefore, a Spline interpolation between the eight available skin temperature measurements every day is used to infer the complete skin temperature diurnal cycle. The Spline method better estimates the daily maxima and minima that can occur between two 3-hourly samples (Aires et al., 2004). Actual acquisition times for each microwave pixel are used in the Spline interpolation to estimate more accurately the physical temperature. This may be critical in arid regions where the temperature

diurnal cycle has much larger amplitude. Also, if either of two consecutive (before and after AMSR-E acquisition times) cloud flags indicates cloudy conditions, the microwave pixel is flagged as cloudy.

The upwelling and downwelling atmospheric emissions are estimated using the Liebe's MPM model to determine the atmospheric absorption (Liebe, 1989; Liebe et al., 1993). This model is a broadband model for complex refractivity to predict propagation effects of loss and delay for the neutral atmosphere at frequencies up to 1000 GHz. Contributions from dry air, water vapor, suspended water droplets (haze, fog, cloud), and rain are addressed (Liebe, 1989). Upwelling and downwelling brightness temperatures, as well as atmospheric transmission, are calculated using Eq. (1-2), (1-3), and (1-4) for the AMSR-E incidence angle of 55°. Atmospheric corrections are applied to the ascending and descending overpasses. Because of the TOVS daily resolution, the same atmospheric profiles are used to correct atmospheric effects for both the ascending and descending overpasses.

Monthly composite emissivity maps are created for each frequency and polarization from the instantaneous cloud-free land surface emissivity maps. In the case of persistent cloud (longer than 30 days, which is possible in some tropical locations), land emissivity is not retrieved. Figure 3-1 presents the flow diagram of the instantaneous and monthly emissivity retrieval.

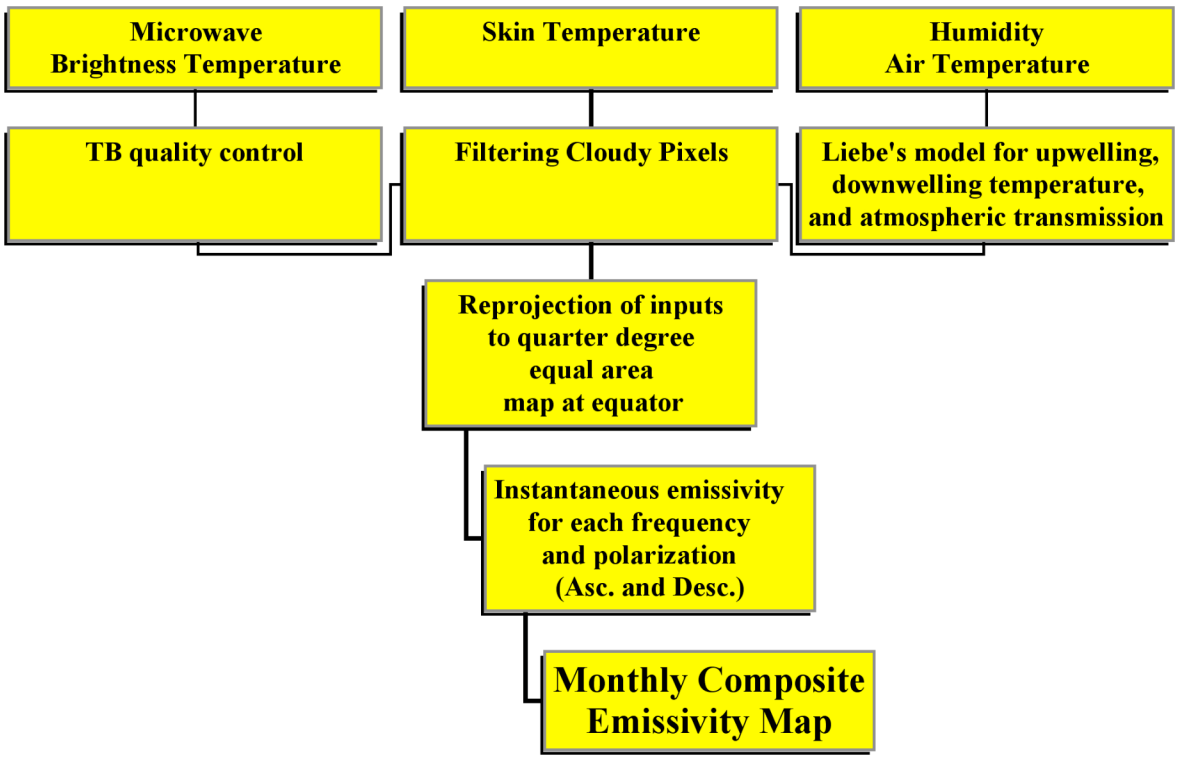

Figure 3- 1: Flow diagram for retrieval of land microwave surface emissivity

3.3. Land emissivity sensitivity analysis and evaluation

3.3.1. Sensitivity analysis

The inputs to the retrieval (skin temperature, column water vapor and brightness temperature) were tested to determine the sensitivity of the emissivity retrieval to errors in these parameters. The uncertainty in the atmospheric water vapor profile can be as much as 10 percent (Lin and Rossow, 1994; English, 1995). The sensitivity of the retrieved emissivity to the atmospheric water vapor was assessed by introducing biases into the atmospheric profile and determining their impact on the emissivity. A constant increase of 5, 10, and 25 percent was applied globally to the water vapor profiles. The sensitivity was assessed for all AMSR-E frequencies. The results (Table 3-1) show that the sensitivity of land emissivity to water vapor

errors decreases as frequency decreases. Sensitivity at C- and X- bands is the smallest. A 25 percent change in water vapor leads to a global mean 0.0016 change of emissivity at 6.9 GHz and 0.03 at 89.0 GHz. The amount of the water vapor is much larger near the equator compared with higher latitudes. Therefore, the effect of the water vapor errors on emissivity retrievals is greater in the tropics and arid regions close to the equator. Moreover, given the seasonal variation of water vapor, larger errors are expected in summer than in winter. These results are similar to the test results for SSM/I (Prigent et al., 1997).

The physical skin temperature plays an important role at lower frequencies, since the microwave radiation is more sensitive to the surface rather than the atmosphere. Recent studies show that available global skin temperatures have significant differences, generally only a few degrees but up to 20 K in deserts (Jimenez et al., 2011). The relationship between emissivity and physical skin temperature from thermal infrared is reciprocal according to Eq. (1-1). The sensitivity analysis showed that the difference in global mean emissivity retrieval could be as much as 0.06 for skin temperature differences of 20K. Therefore, at lower frequencies, skin temperature is the most important source of inaccuracy. Although possible biases in skin temperatures from ISCCP can affect the absolute emissivity value, its effect on emissivity variability should not be significant during the AMSR-E period because the ISCCP results are homogeneous in quality over this time period (Zhang et al., 2006).

Changes implemented	Variability in global mean emissivity				
	6.9 GHz	10.7 GHz	18.7 GHz	36.5 GHz	89 GHz
+5%	0.00034	0.0006	0.0013	0.0029	0.0063
+10%	0.00065	0.0012	0.0025	0.0057	0.0127
+25%	0.0016	0.003	0.0063	0.0145	0.0323

Table 3 - 1: Sensitivity of the emissivity retrieval in terms of global average change of emissivity (horizontal polarization) to 5, 10, and 25 percent increase in water vapor profile

The uncertainty of microwave calibration and its effect on the emissivity retrieval are similar to results from previous studies (Prigent et al., 1997; Karbou et al., 2005b). For instance, a 3K decrease in observed brightness temperature leads to 0.01 decrease of emissivity at 36.5 GHz (H. polarization). The absolute accuracy of AMSR-E brightness temperatures has been reported as 1.0 K (Kawanishi et al., 2003), therefore TB biases will not significantly affect the accuracy of emissivity retrieval.

Infrared emissivity was used to correct the skin temperature from ISCCP-DX product. The uncertainty of the infrared emissivity is less than 0.02 (Li et al., 2010; Li et al., 2011). This level of uncertainty can only cause small differences (less than 1.5 k) in skin temperature based on the quadratic relationship of infrared brightness temperature and surface physical temperature. Therefore, its effect on microwave emissivity retrieval should not be significant (less than 0.005) according error analysis of the effect of uncertainty of skin temperature explained above.

One of the assumptions in this emissivity retrieval is specularity of the land surface. The specular approximation is not strictly valid for all surface types and observation conditions.

However, the error related to the specular approximation is limited, well within 1% even for close-to-nadir observations in the case of natural snow-free surfaces as measured from satellites (Karbou and Prigent, 2005). Large differences between the two approximations have been calculated or observed for very specific cases as reported in (Matzler, 2005), but they are not representative of natural snow-free surfaces over land. Introducing a specularity parameter could eventually reduce the already limited noise associated to the specular approximation but anyhow; no method exists yet to derive such a parameter on a global basis (Karbou and Prigent, 2005).

3.3.2. Comparison to the other products

We evaluate our AMSR-E emissivity product by comparing it with the SSM/I-based emissivity product (Prigent et al., 2006) at three frequencies (19.35, 37.0, and 85.5 GHz). The common channels between AMSR-E and SSM/I have small differences in their spectral responses and incidence angles: AMSR-E frequencies are centered at 18.7, 36.5, and 89.0 GHz with an incidence of angle of 55^0 compared to 53^0 for SSM/I. Moreover, the overpass times of both sensors do not match. It is necessary to accurately determine the systematic discrepancies introduced by these differences.

Liebe's radiative transfer model (RTM) was used to assess the effect of the differences in the viewing geometry and frequency. Simulated brightness temperatures at 37 and 36.5 GHz (also between 18.7, 19.35 GHz, and 89, 85.5 GHz) with the 2 degree difference in incidence angle were compared by using the same skin temperature, atmospheric air temperature, and water vapor profiles. Skin temperatures matched with the descending orbits of AMSR-E for July 2005 were used in order to minimize the effect of the diurnal cycle. The model was forced by the monthly mean emissivity at descending overpass for SSM/I frequencies and incidence angle. SSM/I emissivities were retrieved with the exact model and information used in this study for the

AMSR-E descending overpass. The global mean difference between two simulated brightness temperatures at 37 GHz is 0.3K with a standard deviation of 6.5K. This simulated brightness temperatures difference can be translated to emissivity difference between AMSR-E and SSM/I sensors due to geometry and frequency difference.

SSM/I derived emissivities (Prigent et al., 2006) are compared with our AMSR-E product after removing the differences caused by geometry and frequency (figure 3-2). Figure 3-3 shows histograms of the differences at 18.7, 36.5, and 89.0 GHz (horizontal polarization). The mean and standard deviation of the differences between the two products are respectively 0.006 and 0.0225 (at 36.5 GHz), which indicates good agreement. The mean and standard deviations of the differences between two emissivity products (at 36.5 GHz, horizontal polarization) are respectively 0.0061 and 0.031 without accounting for differences in geometry and frequencies. The largest differences appear in arid and mountainous locations (figure 3-2) and may be caused by the difference in overpass times and the difference of the diurnal temperature cycle amplitude at the surface and at deeper layer below surface (Prigent et al., 1999). This difference is exaggerated at the AMSR-E overpass times as compared to the SSM/I overpass times near dawn and dusk. In coastal areas, the different resolutions of the two sensors can produce large differences as well because of differing amounts of open water included in the pixel. The bias at 89.0 GHz can be attributed to differences between the two different atmospheric correction data sets (Zhang et al., 2006), as the effect of atmosphere is larger at higher frequencies; the SSM/I-based emissivity product used the NCEP reanalysis (Kalnay et al., 1996) for atmospheric information, while this study used the TOVS product.

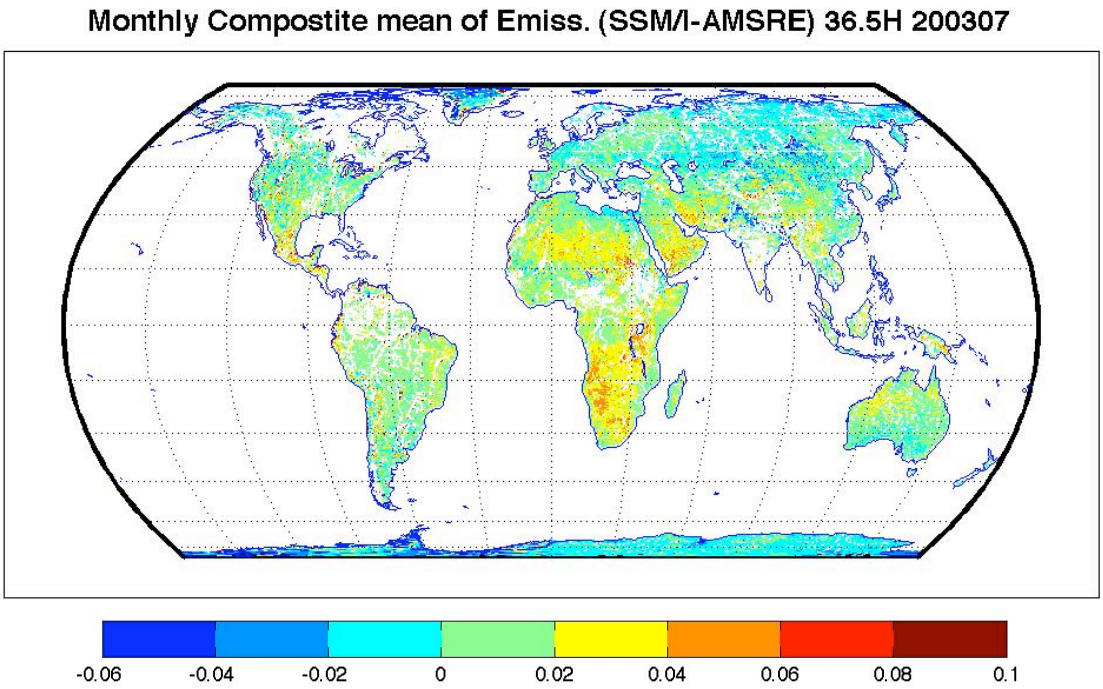

Figure 3- 2: Global map of land surface emissivity difference between SSM/I (Prigent 2006) and AMSR-E at 36.5 GHz horizontal polarization

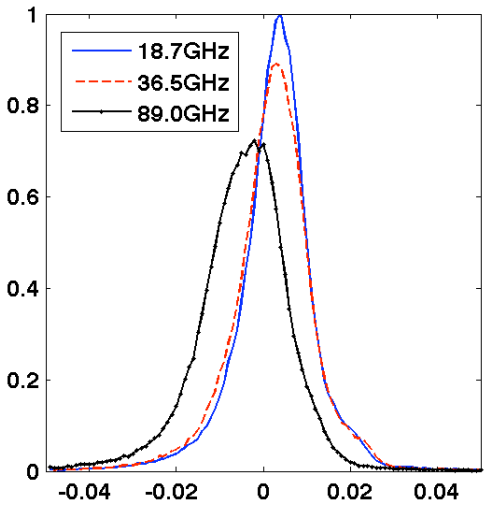

Figure 3- 3: Normalized histogram of the difference between SSM/I and AMSR-E products at close to 18.7, 36.5, and 89.0 GHz (horizontal polarization) for July 2003.

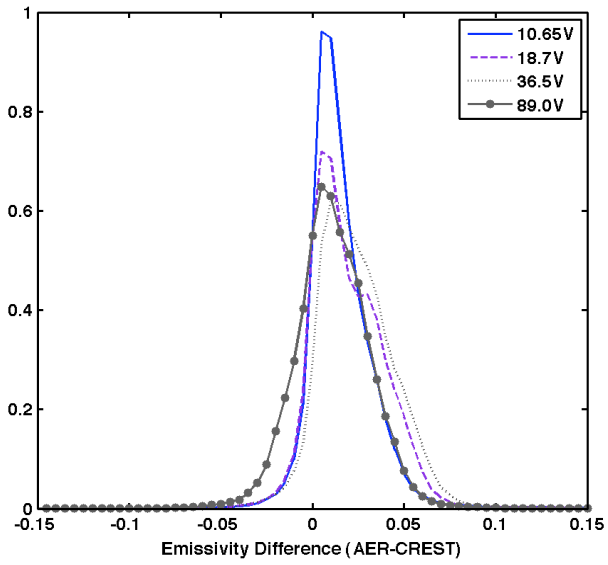

Figure 3- 4: Normalized histogram of AMSR-E emissivity differences between this study and Moncet et al (2011) at 10.65, 18.7, 36.5, and 89.0 GHz (vertical polarization) for July 2003.

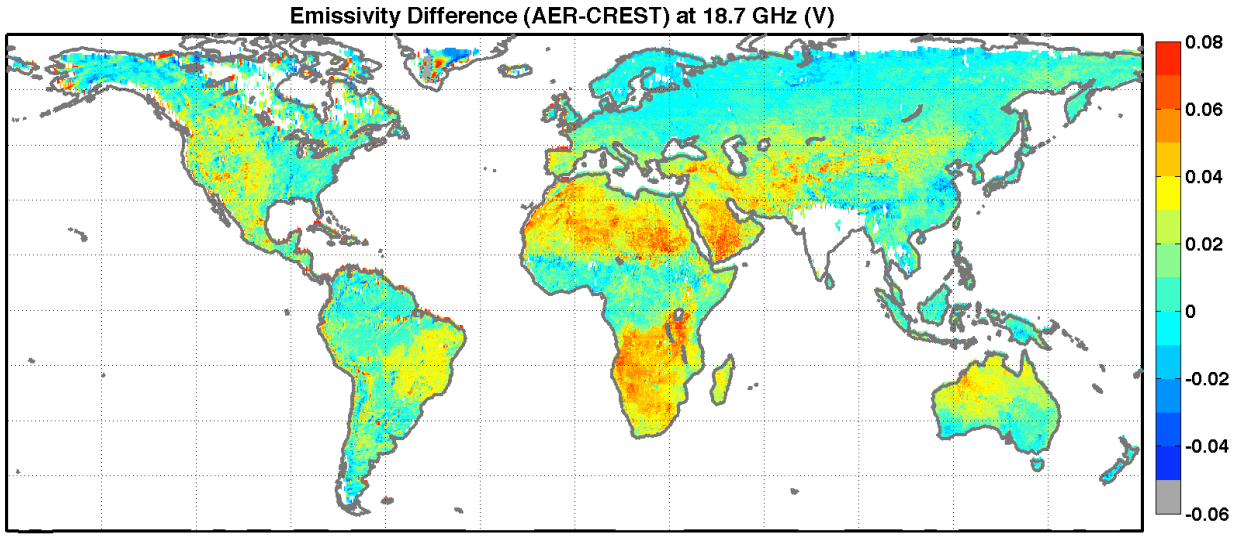

Figure 3- 5: Map of AMSR-E emissivity estimates differences between this study and Moncet et al (2011) at 18.7V GHz for July 2003.

The result of this study also was compared to AMSR-E emissivity product (Moncet et al., 2011) that has been recently released. This product as mentioned in data section uses MODIS skin temperature in emissivity retrieval. The results for one month are compared at different frequencies (figure 3-4). Generally, they are in good agreement according the histograms. Lower frequencies have better agreement which could be attributed to less atmospheric interferences. The map of differences between two products is shown in figure 3-5 at 18.7 GHz vertical polarization for July 2003. Most of the vegetated areas have the differences less than 1 percent. However, arid regions show the differences more than 3 percent. Different skin temperature products in the retrievals can be cause of this difference. In this research, ISCCP- DX has been utilized while the other product uses MODIS skin temperature. Some analysis has revealed that these two products have big differences in arid regions (figure 3-6). The differences can be up to 20 k in arid regions such as North Africa that can be translated to 5 percent difference between two emissivity estimates. This highlights the importance of finding the right skin temperature in emissivity retrievals.

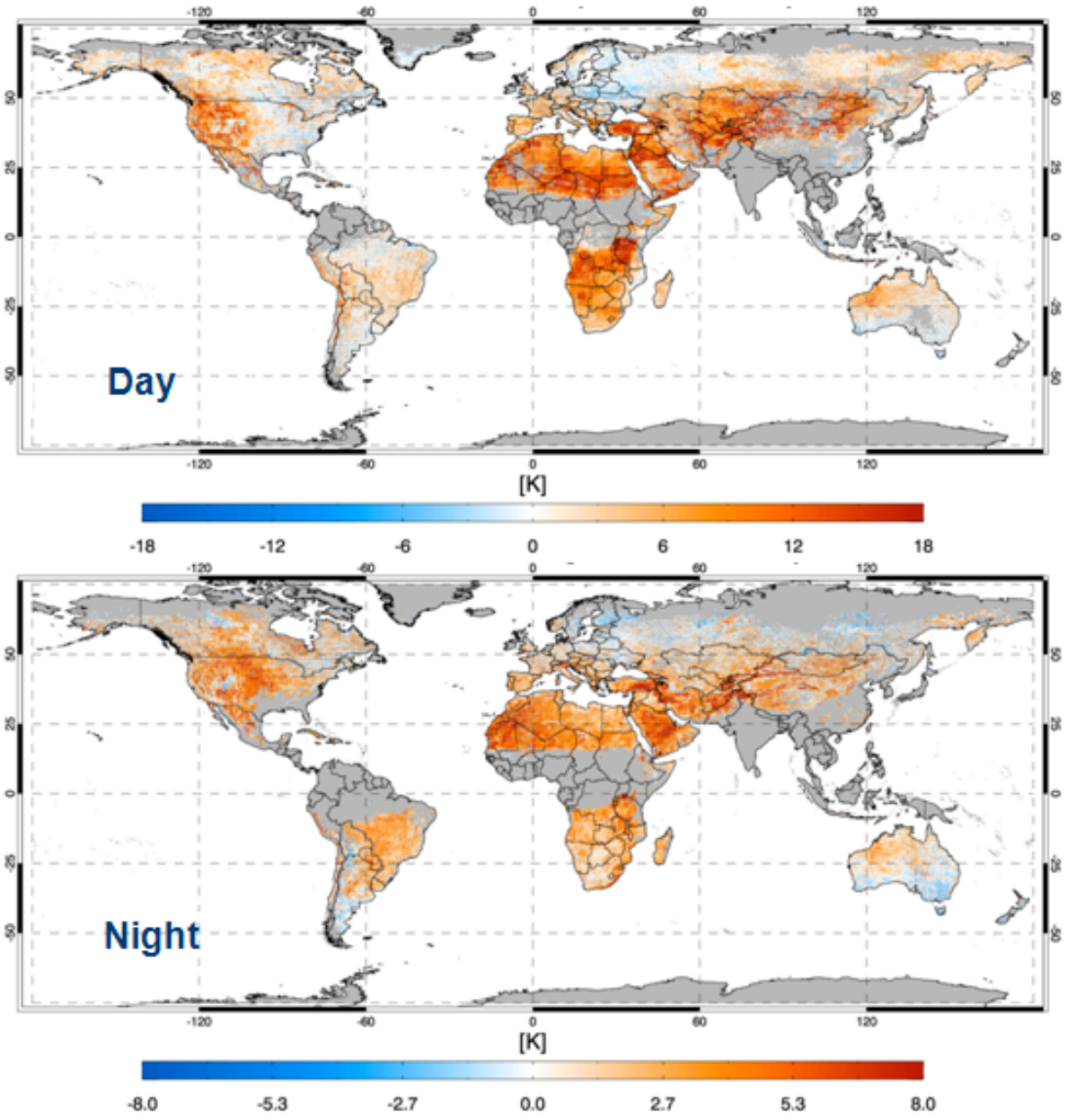

Figure 3- 6: Map of differences between ISCCP-DX and MODIS skin temperature during day and night for July 2003 (Moncet et al, 2011)

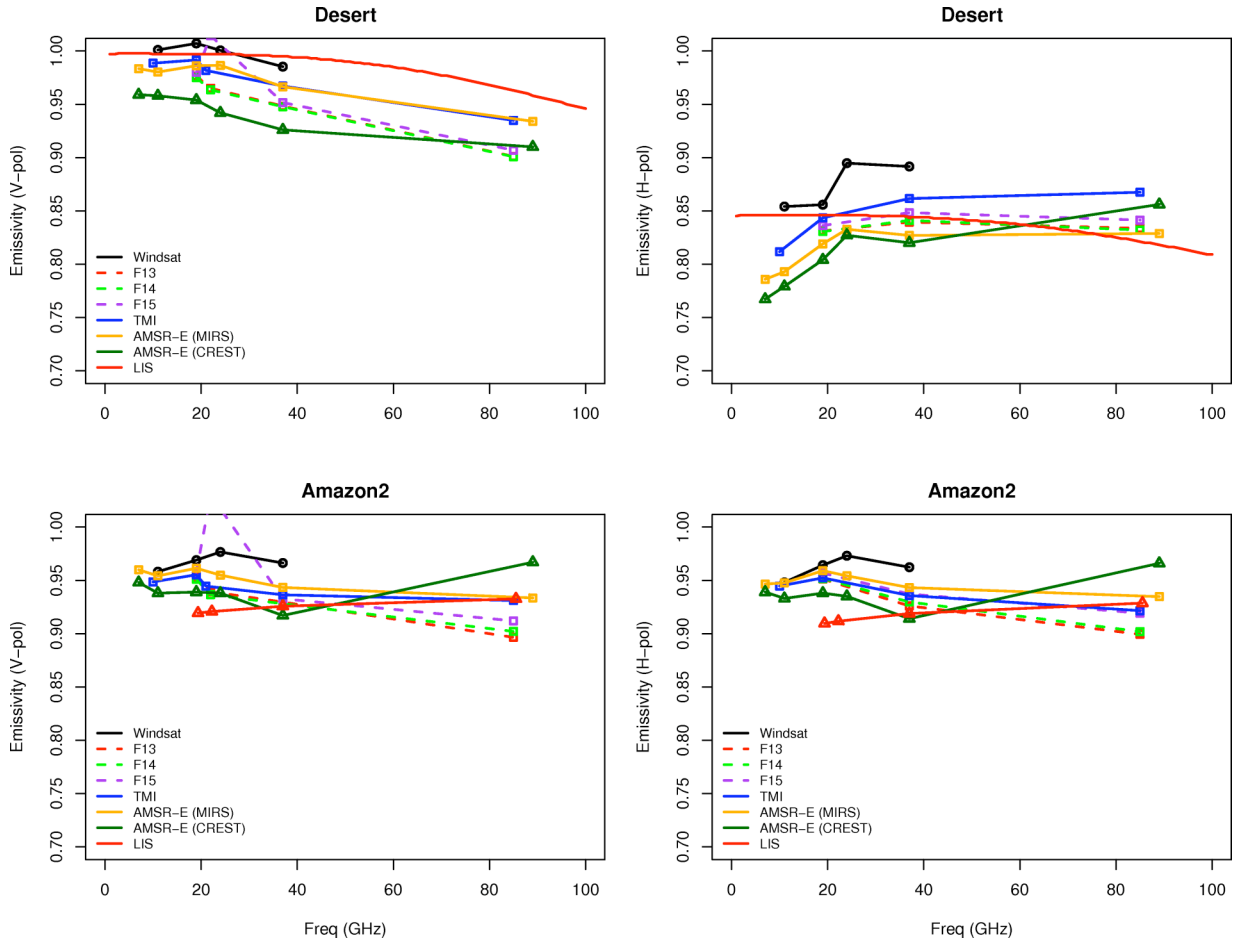

Figure 3- 7: Spectral analysis of emissivity using different products and this study over desert and Amazon (Tian 2011, personal communication).

The spectral analysis of the emissivity estimates and comparison to other emissivity products are shown in figure 3-7. This figure exhibits large discrepancies between different emissivity estimates, which are very difficult to validate the products in lack of direct measurement emissivity parameter. The results of this study that has been shown as AMSR-E (CREST) emissivity show higher emissivity estimates at higher frequencies that could be because of some atmospheric residuals in our retrieval. To check this issue, the differences between emissivity estimates at lower frequencies with less atmospheric interference and higher frequency (89 GHz) estimates are plotted against water vapor amount (figure 3-8). It shows that

in higher water vapor amount, the differences between two emissivity estimates increase, which could be an atmospheric residual in emissivity retrieval (figure 3-8). Moreover, the spectral relationship between emissivities at different land cover types is not fully understood, which limits this analysis for possible atmospheric contamination in retrieved emissivities. More analysis about this issue is included in our future works.

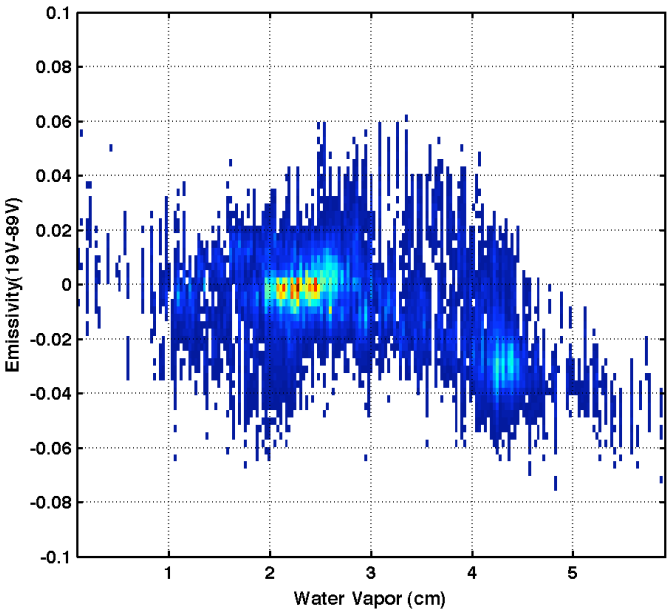

Figure 3- 8: Comparison of global emissivity difference (19V-89V) and water vapor for July 2003.

3.4. Results

Cloud-free AMSR-E brightness temperatures from June 2002 through June 2008 are used to retrieve land surface emissivities. The ISCCP cloud mask indicates that, on average, more than 50 percent (monthly average) of the land, is cloud covered (Rossow and Schiffer, 1999), which significantly limits the instantaneous spatial coverage. In addition, gaps between consecutive orbit swaths induce further loss of data and reduce the coverage. The instantaneous coverage of the product varies between 25 and 35 percent seasonally.

3.4.1. Land emissivity and surface physical properties

Examples of monthly mean composites of estimated land emissivities for January and July 2003 for horizontal polarization at 10.7 and 36.5 GHz are presented in figure 3-9. For relatively smooth bare soils, land surface emissivity is smaller in horizontal polarization compared to vegetated areas. For instance, in North Africa and Saudi Arabia, which are mostly dominated by bare soil and desert, a noticeably smaller emissivity can be seen compared to highly vegetated regions such as Amazon or Congo, which exhibit relatively larger emissivities. Generally, the 10.7 GHz shows smaller emissivity values in arid and semi-arid regions (North Africa and Australian desert) compared with the same locations at 36.5 GHz. This is also observed in Australia, where smaller emissivities are obtained in deserts, whereas the vegetated western coast shows larger horizontal emissivity values. Figure 3-9 shows horizontal polarizations; but results at vertical polarization are the opposite, with the largest emissivity values found in desert areas. This behavior is due to the different response of horizontal and vertical polarization emissivities to the dielectric constant (Njoku and Li, 1999; Owe et al., 2001). Also, seasonal variation of emissivity can be seen at some places such as in Russia where the 10.7 and 36.5 GHz show large differences in January and July with land and snow cover changes. The seasonal variations of land surface emissivities with land cover change are discussed later.

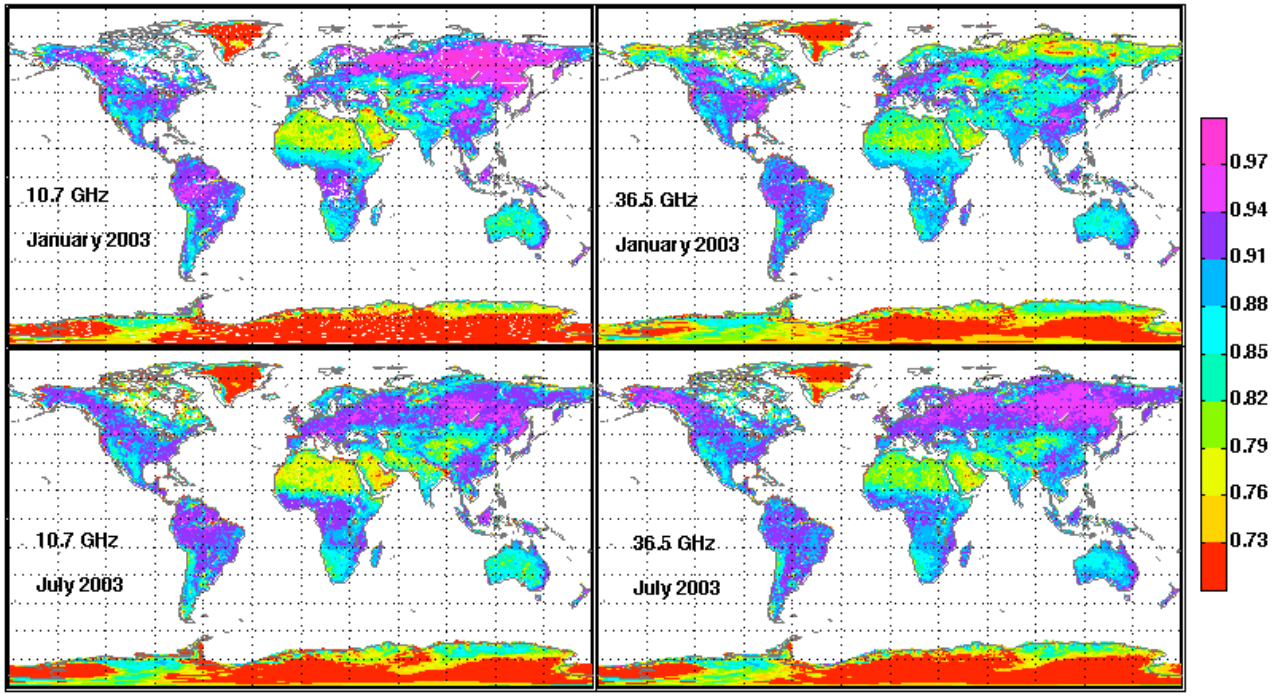

Figure 3- 9: Composite monthly mean land surface emissivity at 10.7, and 36.5 GHz (horizontal polarization) for January and July 2003.

The radiative properties of vegetated surfaces are controlled by the dielectric properties of the vegetation components, their density, and the relative size of the vegetation components with respect to wavelength. As the surface roughness and wetness decreases, the polarization difference increases (Choudhury, 1989). As vegetation density increases the surface roughness also increases, which causes more scattering of microwave radiation. Figure 3-10 shows that most vegetated areas have polarization differences less than 2%. The largest polarization difference is observed in arid and semi-arid regions such as North Africa. The polarization difference at 6.9 GHz in these regions is systematically larger than at 89.0 GHz, which can be attributed to greater relative size of desert roughness to wavelength at 89.0 GHz. Bare soil is rougher for observations at higher frequencies, as the relative size of the surface to the

wavelength and the scattering are greater. This will cause larger polarization differences at lower frequencies in desert areas (Prigent et al., 2001).

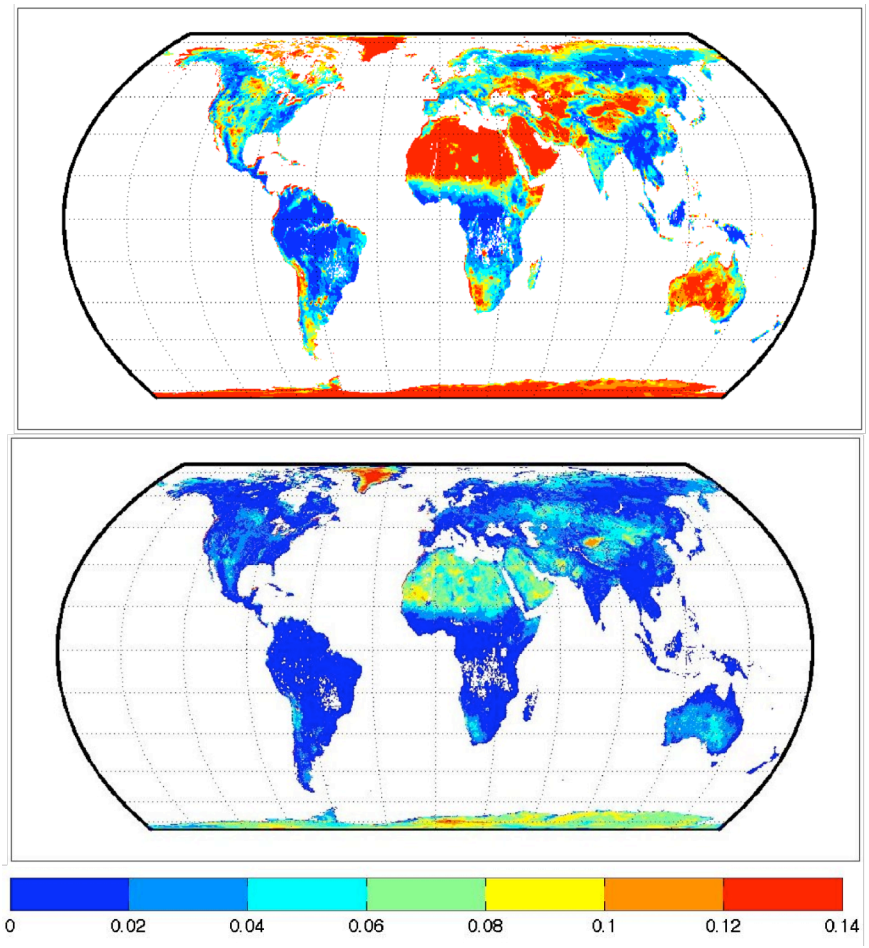

Figure 3- 10: Difference between vertical and horizontal polarizations land surface emissivity at 6.9 GHz (top), and 89.0 GHz (bottom) for January 2003.

Figure 3-11 shows the temporal variations of global monthly mean polarization differences at different frequencies for the whole globe as well as for desert and cold deciduous forest with evergreen areas, based on the Matthews (1983) vegetation classification. The plots are shown for Northern and Southern hemisphere separately to avoid the different seasonal variations. As expected, the difference between horizontal and vertical polarization emissivity

decreases with increasing frequency. The polarization gradient is larger at 6.9 GHz than at 89.0 GHz in all land classes (most not shown). Deserts have larger polarization differences but smaller interannual variability, since in

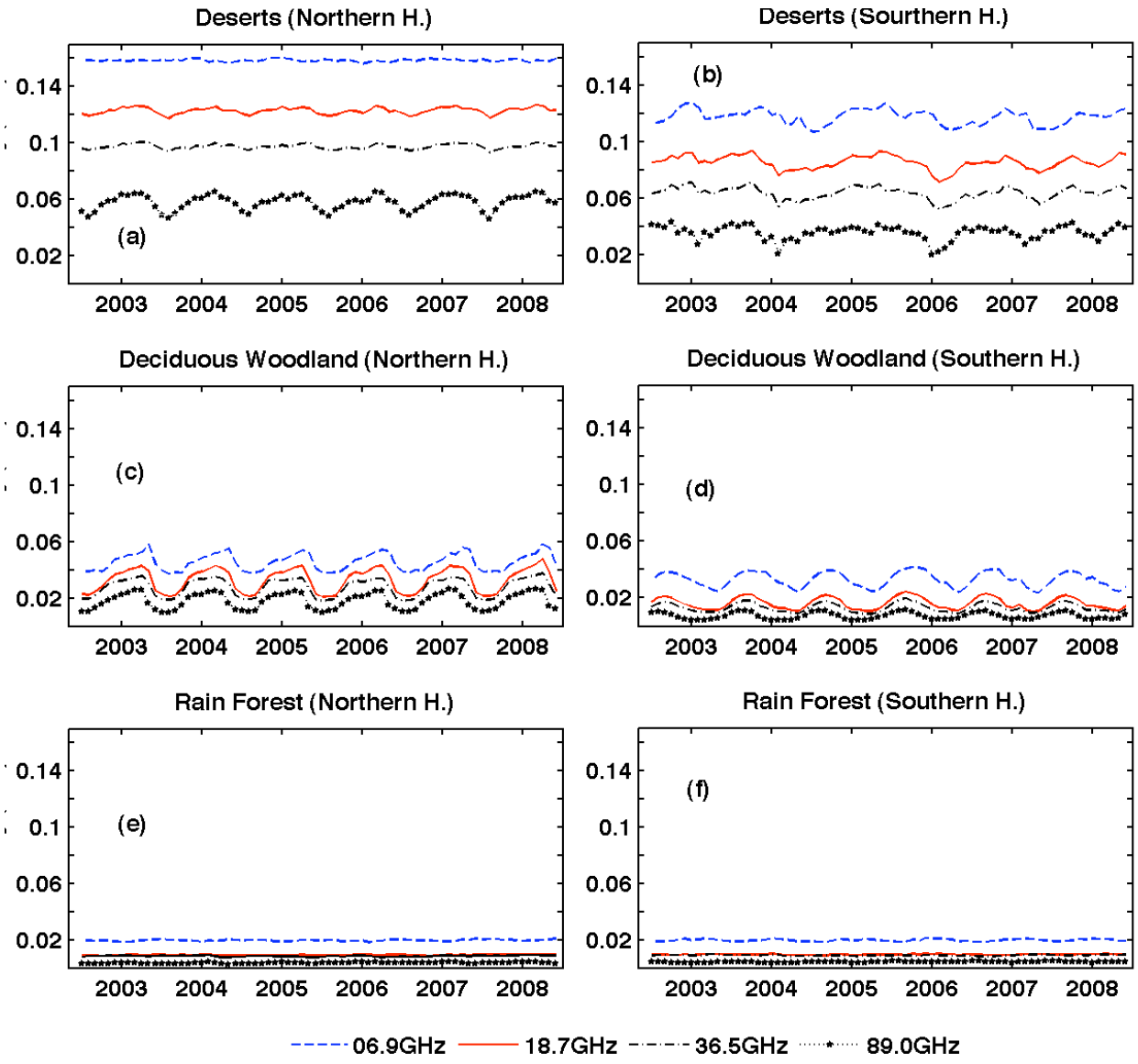

Figure 3- 11: Seasonal variation of the vertical and horizontal polarization differences at 6.9, 18.7, 36.5, and 89.0 GHz in (top) desert regions (middle) cold deciduous forest with evergreen (vegetation classification (Matthews, 1983)) (bottom) whole glob for Northern and Southern hemisphere.

arid regions the seasonal variation of soil moisture and vegetation cover is not significant (figure 3-11 top). Most of the frequencies confirm this small seasonal variation in desert areas, except 89.0 GHz, which may be caused by some residual atmospheric perturbations in the emissivity retrieval. However, vegetated areas (for example cold deciduous forests) show smaller polarization differences with larger seasonal variations that correspond to variations in vegetation density (figure 3-11 middle). In places with constant high-density vegetation, such as evergreen areas, the polarization differences exhibit smaller seasonal variation (not shown), as the change of the land cover is not significant.

The relationship between the retrieved land surface emissivity and physical properties, such as Normalized Difference Vegetation Index (NDVI) and soil moisture content, is investigated to assess the sensitivity of lower frequency emissivities to these parameters. The comparison between monthly average (July 2005) global emissivity polarization difference (V-H) at 6.9 and 10.7 GHz and NDVI values from MODIS observations distributed by the Land Processes Distributed Active Archive Center (LP DAAC) is displayed in figure 3-12a,b. Note that y-axis in this scatter plot is logarithmic to make the relationship clearer. The peak frequency of pixels occurs at small NDVI and large (logarithm of) emissivity differences. In general, the emissivity polarization difference decreases as NDVI increases. However, at larger NDVI values in high density vegetated regions, the correlations between emissivity polarization difference and NDVI are much lower. We check the places that have different pattern and relationship between emissivity and NDVI at NDVIs greater than 0.6 and found that the regions that don't follow the linear relationship in these plots are associates with regions at coasts and flooded regions and have seasonal variations. Figure 3-12c,d illustrates the emissivity polarization differences at 6.9 and 10.7 GHz versus the soil moisture product from ASCAT (Bartalis et al., 2008). The

correlation between emissivity polarization differences at 10.7 GHz and soil moisture content is less than 70 % and is 71 % at 6.9 GHz. Smaller correlations (between 65% to 70%) were found at higher frequencies (>19GHz) (not displayed). As soil moisture increases the logarithm of emissivity difference decreases. One should note that soil moisture and NDVI are correlated with each other and that this can be the reason for the similar relationship between emissivity and these parameters (Prigent et al., 2005a).

Time series correlations between monthly variations of NDVI and (H-V) emissivity at 10.7 GHz for each pixel at global scale were calculated for the period from January 2003 through December 2007. The results shown in figure 3-13 confirm that correlation of emissivity monthly variation with vegetation density variation is very small in desert areas (North Africa; Saudi Arabia) and in densely vegetated area such as Amazon and Congo basins. It should be noted that NDVI values are not representative of the vegetation density in such arid regions since there is almost no vegetation in these regions. In predominantly vegetated areas emissivity may be sensitive to other physical parameters such as surface roughness and moisture content.

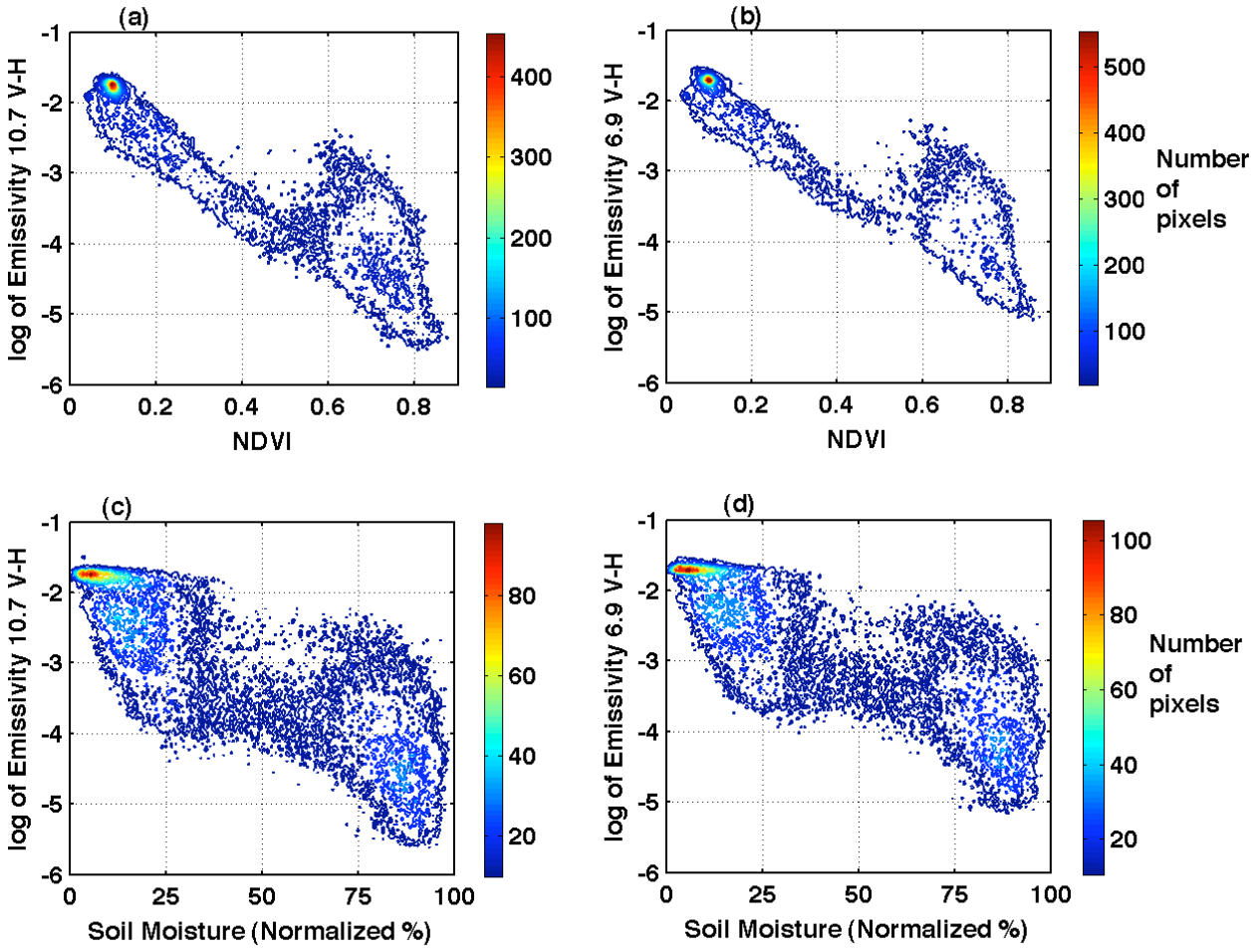

Figure 3- 12: (a-b) Scatter plot of logarithm of emissivity polarization difference at 10.7 GHz and 6.9 GHz (V-H) versus NDVI. (c-d) Scatter plot of logarithm of emissivity polarization difference at 10.7 GHz and 6.9 GHz (V-H) versus soil moisture from ASCAT

However, it is difficult to clearly characterize the effect of these physical parameters on land emissivity and its polarization difference, as separation of the exact relation between these parameters and emissivity is not fully clear (Prigent et al., 2001). When these two parameters are mixed and large amounts of soil moisture and vegetation density occur, it is difficult to determine exactly which parameter is the emissivity more sensitive to.

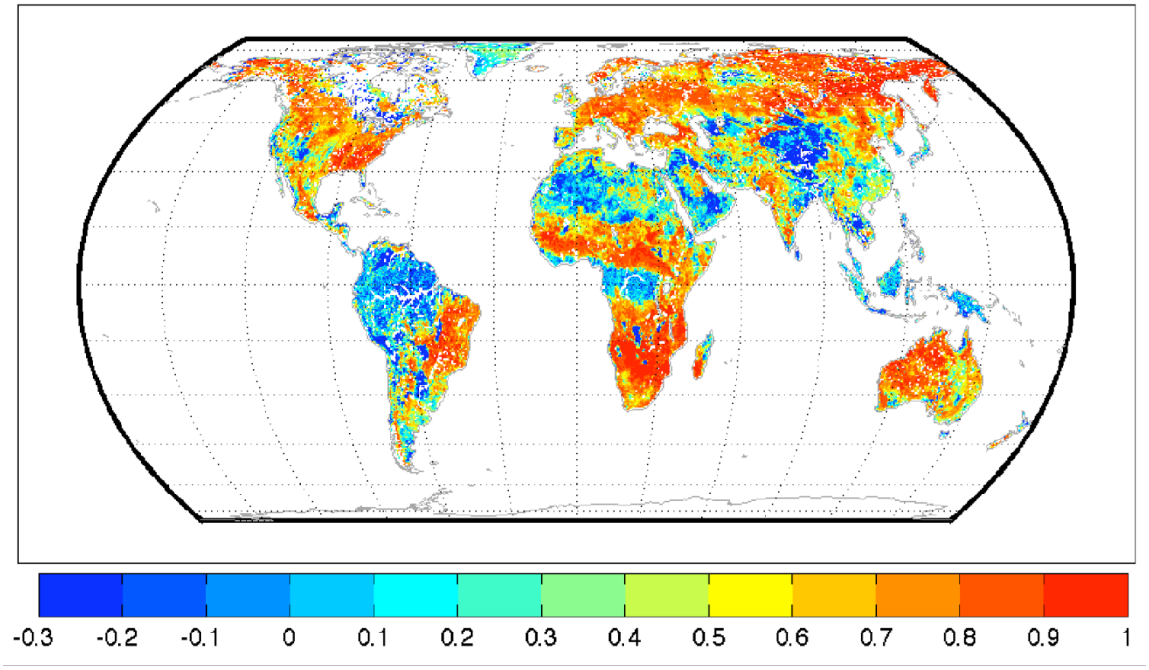

Figure 3- 13: Map of correlation between monthly variation (time series) of emissivity polarization difference at 10.7 GHz (H-V) and NDVI monthly mean variation for time period of January 2003 to December 2007.

The monthly variation of emissivity polarization differences at 10.7 GHz H-V (not V-H) and those of NDVI and soil moisture (AMSR-E product) at different locations is also examined. A selection of results is shown in figure 3-14 for different regions with moderate vegetation and large seasonal variation (densely vegetated and desert areas show low correlations with monthly variation of emissivity polarization difference). In general, they show a good relation in monthly variation with correlation coefficients of more than 0.9. At some places, such as Lat=15S and Lon=30E (figure 3-14a), the polarization difference shows more relation with NDVI variations. This region is at the edge of the North African desert and the effect of soil moisture changes is amplified by the seasonal variation of vegetation, so there is a stronger relationship with the emissivity difference. This might indicate that the soil moisture signal does not persist as the

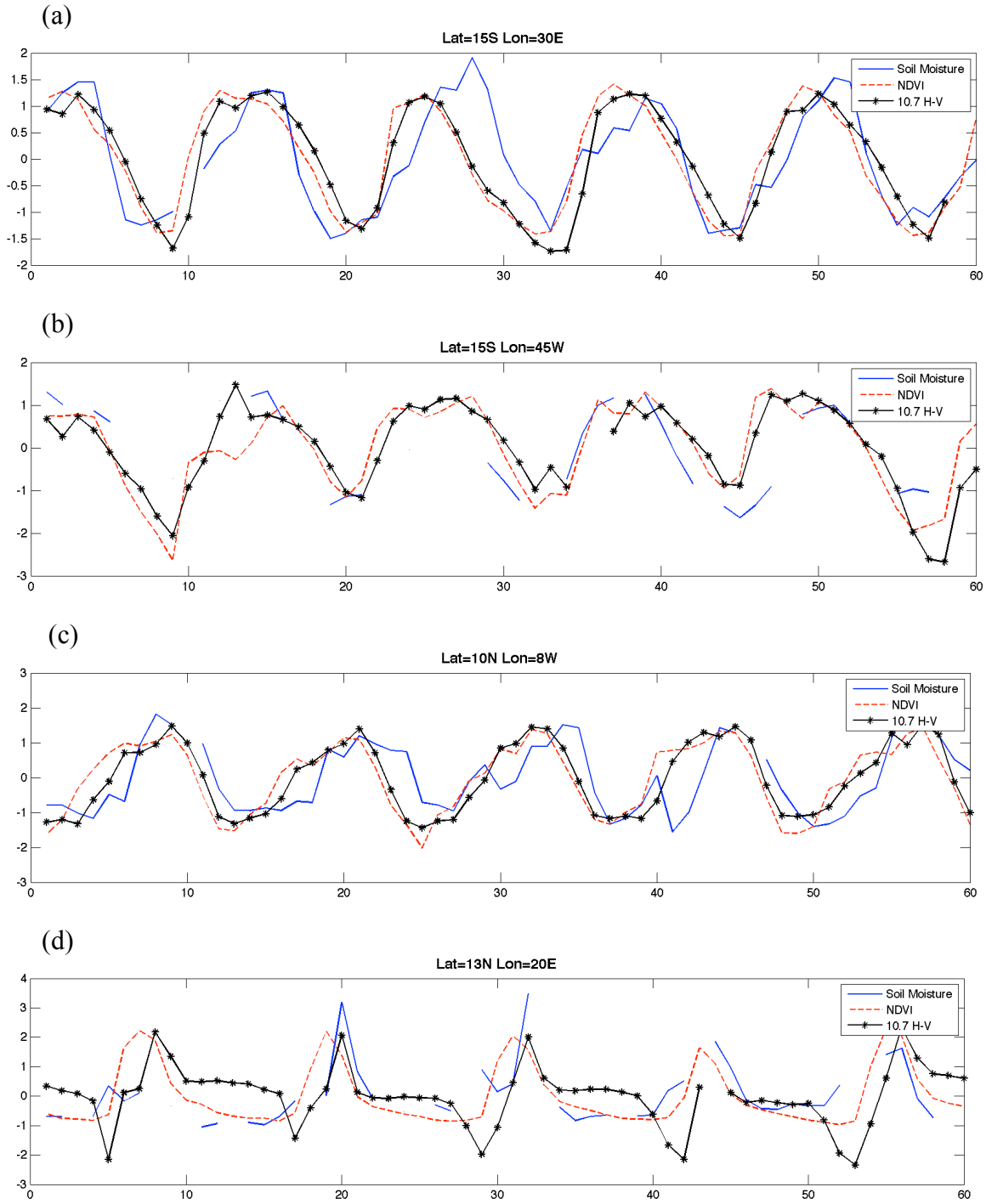

Figure 3- 14: (a-d) Normalized monthly mean variation of emissivity polarization difference at 10.7 GHz (H-V), NDVI, and soil moisture content at different locations from January 2003 to December 2007. The vegatation types of these locations are (a) deciduous woodland (b) shrubland (c) cultivation (d) grassland.

vegetation signal does because the moisture either evaporates or infiltrates more rapidly and does not remain in top surface layers. However, in other regions farther to the south, such as Lat=13S and Lon=20E, soil moisture is more persistent, which produces better consistency with the variability of emissivity difference (H-V) (figure 3-14c). Overall, these features of the results indicate that the retrieval of low frequency emissivity is consistent with known properties of the surface, such as soil moisture and vegetation structure.

3.4.2 Emissivity variability / ascending and descending differences

The day-to-day variability of emissivity at different frequencies is represented by the daily mean values (ascending and descending) to test the stability of the retrieval. The standard deviation of daily averaged emissivities (vertical polarization) for July 2003 is shown in Table 3-2 for different land cover types based on (Matthews, 1983). The RMS variability is less than 0.021, which demonstrates the consistency of the instantaneous emissivity product on monthly time scales. We assume that the geophysical properties of the land surface (such as vegetation cover) do not change dramatically on this time scale. Table 2 also shows that as vegetation density decreases, the day-to-day variability increases. The largest standard deviations of about 0.02 are seen in the desert areas and the smallest values around 0.01 occur in rain forest or densely vegetated regions. The frequency dependence of this variability is negligible in desert areas but in densely vegetated areas the standard deviation increases as the frequency increases. This might be due to larger atmospheric effects at higher frequencies.

	Day to day variability				
Land Class Type	**6.9 GHz**	**10.7 GHz**	**18.7 GHz**	**36.5 GHz**	**89 GHz**
Rain forest	0.0092	0.0093	0.0096	0.0103	0.0112
Evergreen forest	0.0107	0.0105	0.0109	0.0113	0.0136
Deciduous forest	0.0110	0.0106	0.0106	0.0111	0.0141
Evergreen woodland	0.0162	0.0148	0.0148	0.0148	0.0179
Deciduous woodland	0.0191	0.0179	0.0175	0.0173	0.0189
Cultivation	0.0148	0.0140	0.0133	0.0132	0.0154
Grassland	0.0190	0.0176	0.0167	0.0163	0.0187
Tundra	0.0175	0.0168	0.0158	0.0173	0.0233
Shrub land	0.0198	0.0180	0.0170	0.0164	0.0191
Desert	0.0249	0.0232	0.0212	0.0197	0.0218

Table 3 - 2: Day to day variability of global mean emissivity at vertical polarization for July 2003 at different land vegetation covers.

Figure 3-15 shows the standard deviation of emissivity at 18.7 GHz (horizontal polarization) for July 2003. Most of the places show standard deviations of the emissivity less than 2 percent, except in arid regions (e.g. North and South Africa). These regions have relatively higher standard deviations due to larger emissivity differences between ascending and descending overpasses.

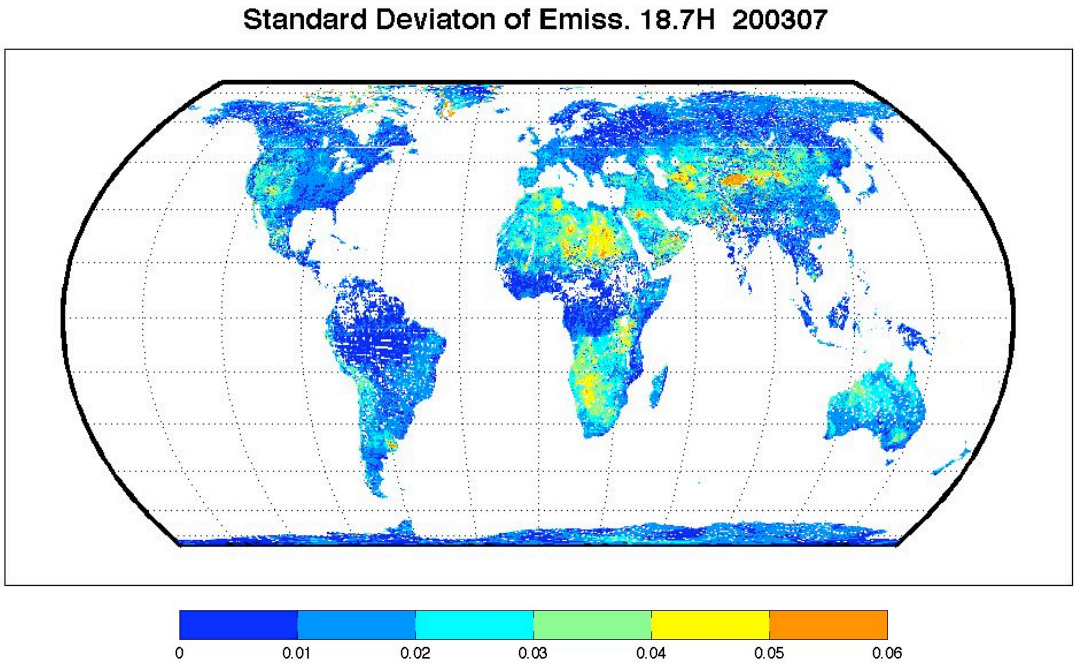

Figure 3- 15: Standard deviation of land surface emissivity at 18.7 GHz (horizontal polarization) for July 2003.

The difference between the retrieved emissivities from the ascending and descending parts of the orbits (day and night) is shown in figure 3-16 for 6.9, 10.7, 18.7, and 89.0 GHz horizontal polarization. Large differences occur in desert and mountainous locations even though we expect less difference because of small moisture changes from day to night. This larger systematic difference than seen in SSM/I results can be explained by the timing of the overpass: since the daytime overpass is closer to the daily maximum temperature but the nighttime pass is not near to the daily minimum temperature. The difference of diurnal temperature cycle phase will be larger during daytime than nighttime (Prigent et al., 1999; Grody and Weng, 2008). For some surface types, such as sand dunes, the microwave signal comes from a deeper layer than the surface with a different diurnal temperature amplitude and phase than the surface (Prigent et

al., 1999). Using the IR skin temperature in the emissivity retrieval causes this inconsistency. The fact that this inconsistency is even larger for the lower AMSR-E frequencies corroborates

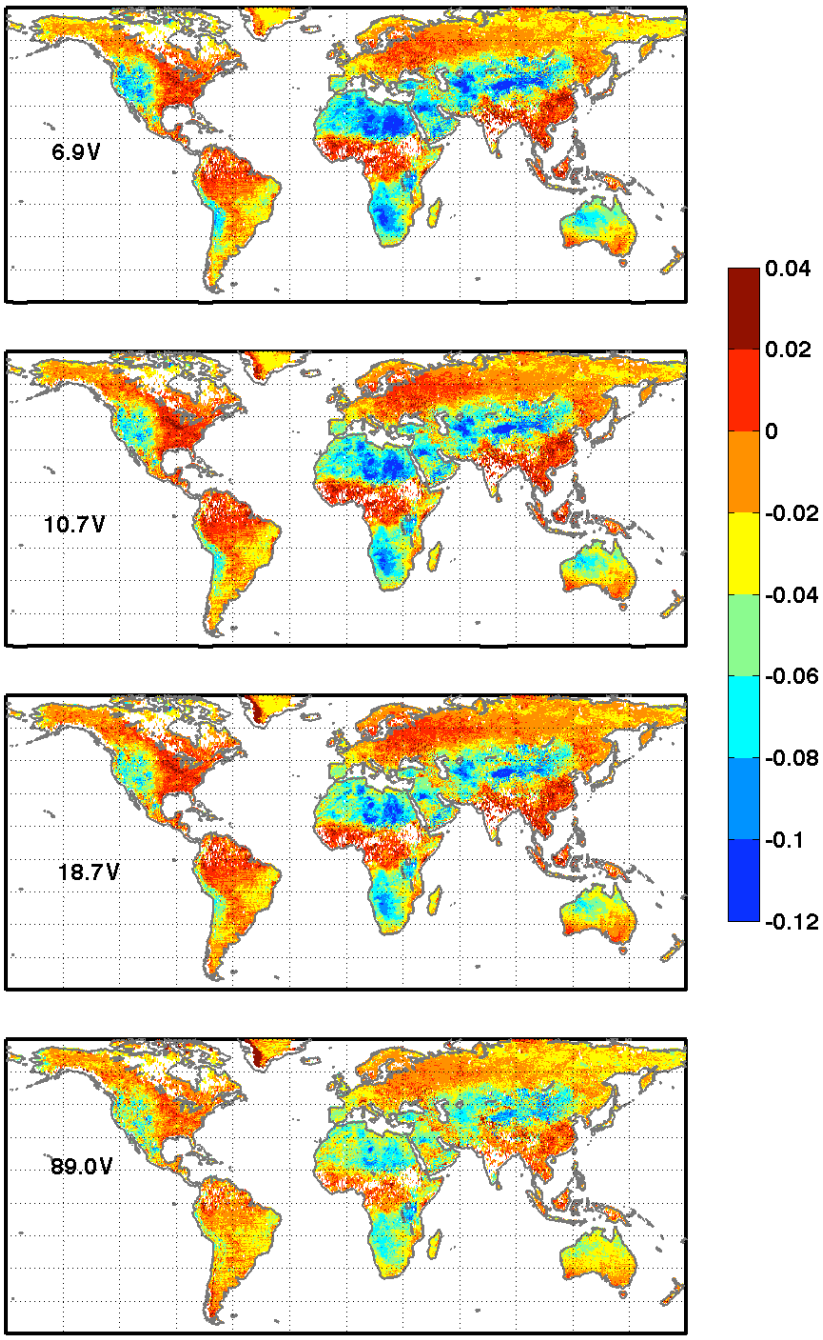

Figure 3- 16: Difference between ascending and descending monthly mean of AMSR-E emissivity at 6.9V, 10.7V, 18.7V and 89.0V GHz for July 2003.

previous findings that microwave emission at lower frequencies is generated from deeper soil layers. The lack of global soil temperature profiles makes removing this inconsistency challenging especially in arid regions. This effect is more pronounced in AMSR-E than SSM/I observations because they occur closer to the extremes of the diurnal temperature cycle. 10.7 and 89.0 GHz both have the same pattern of differences; but the emissivity difference between day and night at 89.0 GHz is noticeably smaller than 10.7 GHz at the same locations such as North and South Africa, due to small penetration depth of 89.0 GHz.

3.5. Discussion

Retrieval of land surface emissivity from different sensors and at different frequencies helps to understand the properties of land surface. Previous studies have shown that land surface emissivity can be used to classify the land cover using the difference between horizontal and vertical polarization emissivity (Prigent et al., 2001). Using two even lower frequency emissivities (C- and X-bands) can describe land cover variations in more detail because of their greater sensitivity to the subsurface. Polarization differences, especially at lower frequencies, can be interpreted as a roughness effect. As the vegetation increases, the roughness increases and decreases the difference between emissivities at horizontal and vertical polarization. These patterns may be used to quantify the polarization difference for land cover classification / vegetation detection (Prigent et al., 2001).

However, there are some difficulties in emissivity retrieval at lower frequencies. Significant differences in the emissivity maps between the ascending and descending overpasses were noticed particularly in deserts. The effect of the temperature diurnal cycle amplitude and phase lag between the microwave and infrared temperatures needs further investigation and

should be accounted for in future retrieval procedures. More similarity in term of penetration depth between the higher passive microwave frequencies and thermal wavelengths should produce more nearly synchronous brightness temperature and thermal skin temperature diurnal cycles, but at lower frequencies the microwave signal is sensitive to deeper soil layers (on the order of few ten centimeters at the L band) (Grody and Weng, 2008). This leads to a lag between the diurnal variations of the skin temperature and brightness temperature and inaccurate emissivity values. Revising the skin temperature in order to infer an effective temperature that is representative of the deeper layer in the soil could resolve this inconsistency.

3.6. Conclusion

A procedure using multi-satellite observations for retrieving instantaneous land surface emissivities from AMSR-E observations under clear sky conditions at all frequencies and both polarizations is tested. Instantaneous as well as monthly mean composite maps are produced at all frequencies and polarizations for more than six years. The results compared with previous studies show reasonable consistency. The remaining differences, after accounting for the differences due to the geometry and frequency, can be explained mostly by the difference in overpass times between two different sensors (AMSR-E and SSM/I). The methodology is general and can be expanded to other sensors, such as WindSat, to achieve better temporal and spatial coverage. In this study, the focus was on the potential and difficulties of retrieval at the two lower frequency emissivities that can be obtained from AMSR-E. Differences between the vertical and horizontal polarizations at C- and X-band were in good qualitative agreement with known variations of vegetation density and surface roughness and can be used as additional indicators of land cover or vegetation type variation at global scales. Large correlations were found in moderately vegetated areas with the large seasonal variations of the lower frequencies

polarization differences and physical properties such as soil moisture and vegetation density (represented by NDVI). The seasonal variations of the polarization difference may be used for quantifying changes in the amount of vegetation.

The difference between day and night emissivities was also examined. Larger differences are found in arid regions at lower frequencies than at higher frequencies, which can be explained by the difference between the skin temperature diurnal variations (amplitude and phase) and the temperature variations at the differing penetration depths for different frequencies. This effect is especially larger for AMSR-E because its overpass times are closer to the daily extremes of the skin temperature. A method is needed to account for this inconsistency between infrared thermal temperature and microwave brightness temperatures to remove the differences between emissivities at ascending and descending overpasses. Chapter 4 and 5 focused on this issue by analyzing the diurnal variation of brightness temperature using multiple satellite observations and generating the effective temperature diurnal cycle.

The approach proposed in this study may be extended to L band (about 1.4 GHz), which has been found to be more suitable for soil moisture retrieval. Such measurements are available since 2010 from the Soil Moisture and Ocean Salinity (SMOS) mission (Jorda et al., 2011). In 2014, Soil Moisture Active and Passive (SMAP) mission will be launched (Entekhabi et al., 2010). AMSR-E low frequency may be extrapolated to find the emissivities from L-Band observations.

CHAPTER 4: ANALYSIS OF MICROWAVE BRIGHTNESS TEMPERATURES DIURNAL CYCLE USING A MULTI SATELLITE APPROACH

Retrieval of microwave emissivity over land is challenging due to the complexity of the interaction of the signal with surface parameters. This interaction affects the variability of observed brightness temperatures and its diurnal cycle. Therefore, a better understanding of the diurnal cycle of brightness temperature is needed for a better characterization of surface conditions. Constructing diurnal cycles from microwave temperatures is more straightforward with respect to infrared temperature because of their limited sensitivity to atmosphere. In this chapter, diurnal cycles of microwave brightness temperature are constructed using observations from the Advanced Microwave Scanning Radiometer - Earth Observing System (AMSR-E) and the Special Sensor Microwave/Imager (SSM/I) sensors, which are onboard of four operational satellites. Measurements from similar channels on both sensors are studied using a Principal Component Analysis (PCA). The first three components of the PCA are related to the diurnal amplitude, the length of the daytime and the phase of the peak time of the diurnal cycle. This study shows that the diurnal amplitude of microwave brightness temperature increases with frequency as higher frequencies have smaller penetration depth and behave therefore like physical infrared temperature. The effect of the surface properties in terms of vegetations land cover is examined. Smaller diurnal amplitudes are seen in densely vegetated areas. Desert areas exhibit on the other hand large diurnal amplitude of brightness temperature except over certain regions with specific soil texture like sand dunes or loose siliceous rocks. Moreover, a phase lag was observed

between infrared and microwave brightness temperatures over areas where soil texture allows for deeper penetration of the microwave signal. These results demonstrate the necessity of addressing the discrepancies between infrared and microwave temperature for a better retrieval of land surface emissivity.

4.1. Introduction

Microwave brightness temperature depends on the thermal and geophysical properties of the surface (i.e. emissivity and physical temperature). The temporal variation of the physical temperature highly depends upon the incident solar radiation, while emissivity is related to dielectric of the surface type, roughness, vegetation density, and the moisture content (Njoku and Entekhabi, 1996; Owe et al., 2001; Stephen et al., 2010). Microwave brightness temperature, *Tb,* is sensitive to key surface parameters in lower frequencies as the attenuation by atmosphere is negligible under clear conditions (Prigent et al., 1997). Instantaneous measures of this variable have been largely used in a variety of applications such as water vapor and rainfall estimation, wind speed, ocean salinity, soil moisture estimation, snow cover detection, freeze/thaw state, land surface temperature, and vegetation structure (e.g. Njoku et al., 2003; Wilheit et al., 2003; McCollum and Ferraro, 2005; Karbou et al., 2006; Tedesco and Kim, 2006; Entekhabi et al., 2010; Min et al., 2010). Diurnal variation of land surface temperature and atmospheric temperature and water vapor profiles due to solar radiation affects the observed brightness temperature. The more frequent the observation of this variable throughout the day, the better our understanding of the variability of the retrieved parameters. Capturing the diurnal variation of microwave brightness temperature is therefore critical.

Operational polar orbiting satellites that are equipped with microwave radiometers provide at least two observations per day in most regions of the globe. Therefore, to ensure a frequent temporal coverage and capture the entire diurnal cycle of *Tb* a constellation of several polar orbiting satellites can be used. In deed, the existence of several operational satellites observing the surface of the earth at different local times, more information on the diurnal variation of Tb can be extracted. For instance passive microwave observations have been available, since 1978, with the advent of the Scanning Multi-channel Microwave Radiometer (SMMR), a 5-frequency microwave radiometer, which was flown onboard the Seasat and Nimbus 7 satellites (Njoku et al., 1980). Its successor, the Special Sensor Microwave/Imager (SSM/I), provides global passive microwave products from late 1978 to present at four-frequency and seven channels. It is flown onboard the United States Air Force Defense Meteorological Satellite Program (DMSP) satellites (F-8 to F-15) with different local overpass times ranging from 6:00 to 9:00 A.M. / P.M. (Colton and Poe, 1999). In 2002, the Advanced Microwave Scanning Radiometer - Earth Observing System (AMSR-E) sensor on NASA's Aqua satellite was launched which acquires microwave observations twice a day at 1:30 A.M./P.M. local solar time at twelve channels (Njoku et al., 2003). This sensor is essential in the understanding of diurnal variability as it provides measurements in the time range of daily temperature maxima and minima. More recently, WindSat onboard Coriolis, a polarimetric microwave radiometer developed by the Naval Research Laboratory Remote Sensing Division, started to provide passive microwave measurements daily at 6:00 A.M./P.M. (Bettenhausen et al., 2006).

There are not so many studies in characteristics of diurnal variation of microwave brightness temperature. Stephen et al (2010) modeled the temporal variation of the physical and brightness temperatures as a function of incident solar radiation for the Tropical Rainfall

Measuring Mission (TRMM) Microwave Imager (TMI). Moreover, TMI has shown that have some diurnal biases when it compared to other conical sensors such as AMSR-E and SSM/I due to solar heating of the its main reflector (Geer et al., 2010). In the ocean, intense diurnal warming of the surface occurs in low wind and clear sky conditions, and the diurnal variation is mostly consistent spatially (Pimentel et al., 2008). However, over land because of surface properties variability and their different thermal behavior, it is difficult to characterize the diurnal variation of the microwave brightness temperature. Brightness temperature measurements depend upon the surface emissivity and physical temperature (Njoku and Entekhabi, 1996). Up to now, the diurnal variation of physical temperature and its relation to land cover type has been examined (Aires et al., 2004). Principal Component Analysis (PCA) approach has been utilized to analyze the diurnal variation of the skin temperature provided globally by the International Satellite Cloud Climatology Project (ISCCP) every 3-hour interval. The first three components represent the diurnal amplitude, the phase, and the daytime duration. Moreover, in highly vegetated area skin temperature has lower diurnal variation than desert area with the highest diurnal amplitude (Aires et al., 2004).

Passive microwave brightness temperature is affected by the depth of the originating soil layer which varies with frequency, surface type, and mineral types of the region (Njoku et al., 1980). Prigent et al (1999) found that in some surfaces such as sand dunes in desert area microwave temperature has much lower diurnal amplitude comparing with the top surface physical temperature variation. In another study, Grody and Weng (2008) showed that at some desert regions the difference between microwave brightness temperature at 19 and 37 GHz have positive sign at 6:00 A.M., but changes sign at 9:00 A.M., as they are originating from different layers. A physical model was proposed by Prigent et al (1999) to simulate the effective

temperature variation at different depths based on a semi-infinite heat transfer equation and the first two terms of Fourier solution. The model showed that as the depth of the soil layer increases, the diurnal amplitude decreases and causes a phase lag with respect to the top surface temperature variation. In line with Prigent's et al. findings, in chapter 3, we noticed a difference between land emissivity determined from AMSR-E daytime and nighttime overpasses. These differences were attributed to the facts that skin temperature *Ts* and microwave *Tb* that were used in the retrieval of land emissivity were not sensitive to the same depth. Since the depths of the soil layers, which affect these two variables, *Ts* and *Tb*, were different and therefore their thermal inertia, the obtained diurnal cycles were not coincident. This led to a discrepancy between land emissivity estimates from ascending and descending overpasses.

This study elaborates on these previous findings and addresses on global scale diurnal variation of the passive microwave brightness temperature, *Tb*. In this chapter, first, we construct, analyze, and characterize the diurnal variation of microwave brightness temperatures observed at different local times using a constellation of multiple sensors. Principal Component Analysis (PCA) is then used to explore the spatial variation of microwave Tb diurnal cycle similar to Aires et al (2004) skin temperature diurnal cycle study. The effect of the frequency and land cover type on the shape of the microwave diurnal cycle is examined.

4.2. Constructing the diurnal cycle of microwave brightness temperature

Using three DMSP satellites (F13, F14, and F15) and Aqua with ascending and descending overpasses, 8 observations at each frequency are available in a daily basis. The time of observation at each location for all satellites is constant with respect to local solar time as their

orbits are sun-synchronous. The overpass time of SSM/I from 3 satellites are varying between 6:00 to 9:00 A.M./P.M. local time. Due to orbit degradation, overpass time of SSM/I satellites have to some extent changed since their launch date. Figure 4-1 (from http://www.remss.com) shows that variation of equatorial crossing time for different satellites throughout the years. As shown in figure 4-1, DMSP satellites have more variable crossing time comparing to AMSR-E and WindSat. AMSR-E with almost constant 1:30 A.M./P.M. overpass time seems to be more stable in this respect.

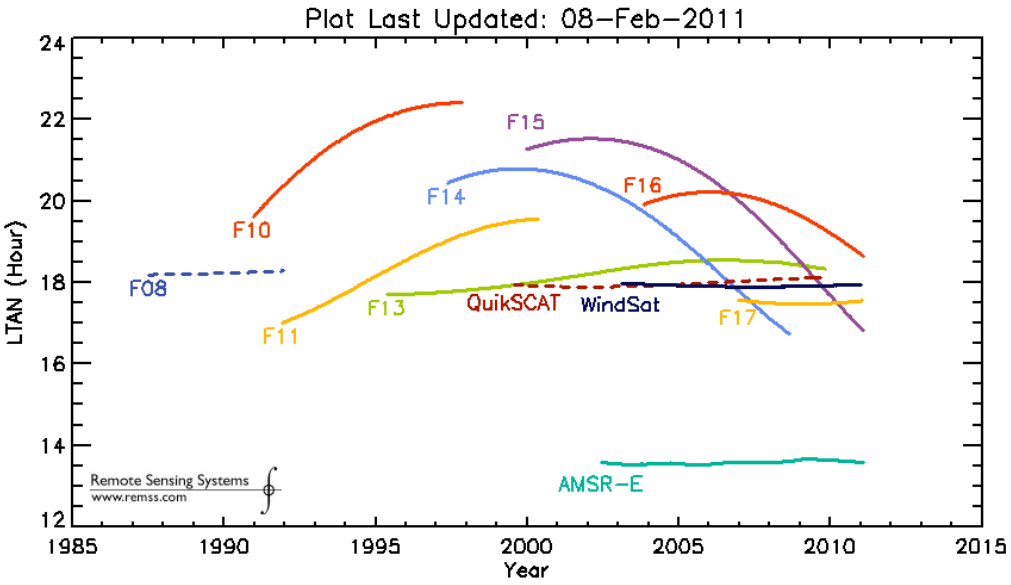

Figure 4- 1: Crossing local solar time of different satellites (from http://www.remss.com)

First, all data sets from both sensors are re-projected and gridded to a 0.25-degree (at equator) equal area map. Then, actual crossing time of each SSM/I observation (figure 4-1) are considered for the diurnal variation along with constant 1:30 A.M / P.M. local time for AMSR-E observations. The cloud mask information provided by the International Satellite Cloud Climatology Project (ISCCP) in DX product with 3 hourly temporal resolution are used to screen out the cloudy microwave brightness temperatures. Only cloud free observations are used to

construct the diurnal cycle, which significantly reduced the spatial coverage as well as temporal coverage in a day. Note also that if at least one of two consecutive (before and after microwave acquisition time) cloud flags indicate cloudy conditions over a given pixel, the pixel is automatically identified as cloudy pixel. In addition, orbit gaps between consecutive swaths introduce an inherent

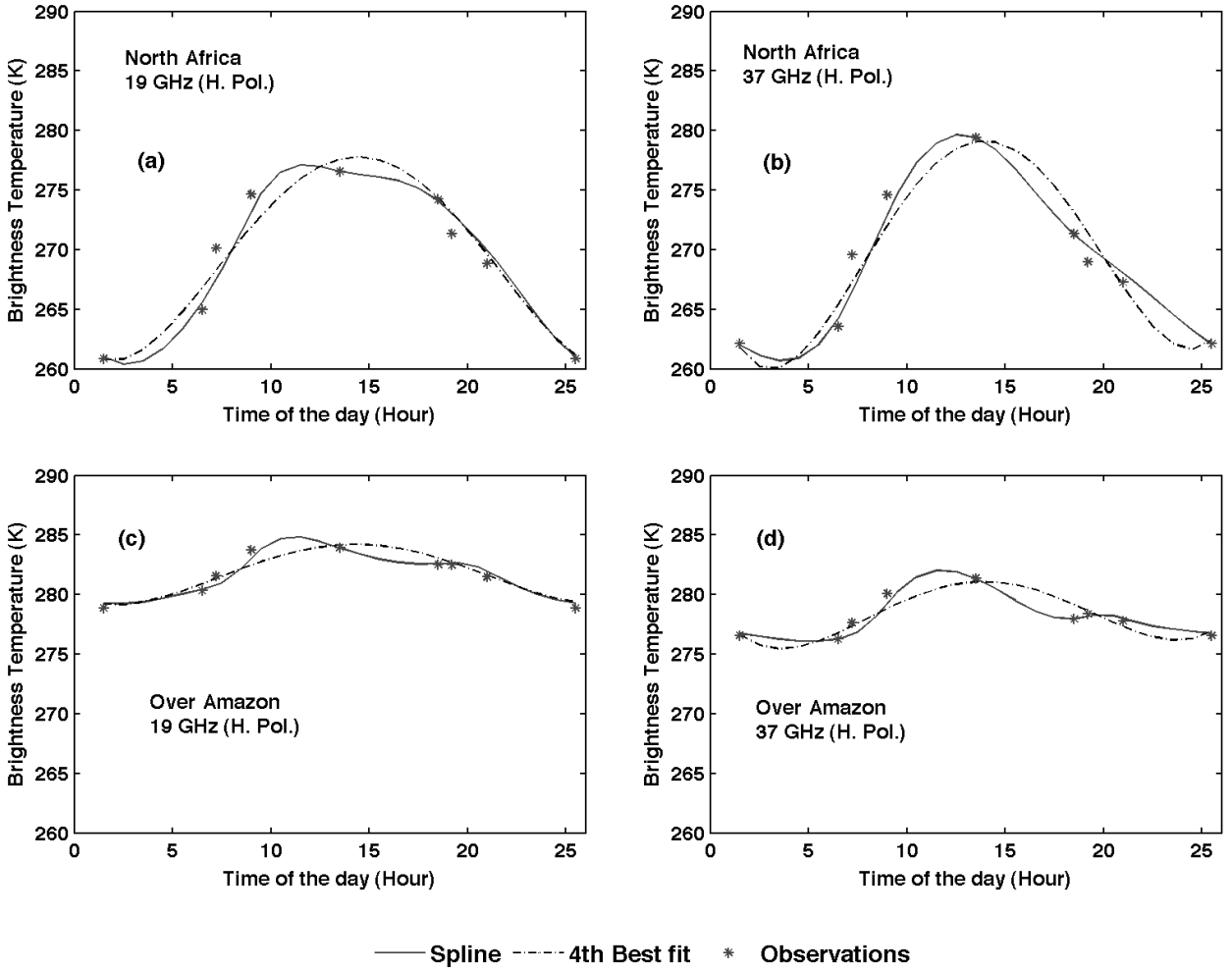

Figure 4- 2: (a, b) diurnal cycle of passive microwave brightness temperature at 19H and 37H using observations, Spline interpolation, and 4th degree best fit for July 2003 over North Africa (c, d) the same over Amazon.

loss of data and reduce the coverage further. Consequently, the chance for obtaining 8 clear sky microwave observations per day is very small. The average of the cloud free observations for each crossing time in a month is considered as the shape of diurnal cycle at pixel level. Figure 4-2 shows diurnal cycle of brightness temperature at 19 and 37 GHz using a Spline interpolation and a 4^{th} degree best-fit model over North Africa and Amazon with two extreme surface conditions. As it is noticeable, best-fit model shows more gradual and smooth diurnal variation, while Spline method is forced to pass through the observations. Calibration differences between the two sensors, errors due to the re-projection of original observations and small differences between sensors configuration (i.e. frequency and viewing angle) can cause discrepancies, which can prevent obtaining a smooth sinusoidal diurnal cycle. Therefore, hereafter, the best-fit model is being used as approximation of the diurnal cycle with an hour temporal resolution for each pixel, each month and each channel. The diurnal cycle amplitude is remarkably larger (more than 20K) at North Africa with arid surface compared to densely vegetated Amazon region (less than 5K) at both frequencies. Also, the higher 37 GHz frequency has noticeably larger amplitude than the 19 GHz at both places.

4.3. Principal component analysis

A principal component analysis (PCA) is used to investigate the constructed diurnal cycles of the microwave brightness temperature *Tb* and assess their spatial variability at different channels over the globe. The PCA technique is a mathematical procedure that uses an orthogonal transformation to convert a set of observations of possibly correlated variables into a set of values of uncorrelated variables called principal components. The number of principal components is less than or equal to the number of original variables. This transformation procedure is defined so that the first principal component accounts for as much of the variability

in the data as possible, and each succeeding component in turn has the highest variance possible under the constraint that it be uncorrelated with the preceding components (Jolliffe, 2002). A matrix T of $m \times n$ is the input for any principal component analysis, where m is the number of trials and n is the number of variables. First, a covariance matrix of $m \times m$ is calculated. Then, using a Singular Value Decomposition (SVD) the eigenvector V and the eigenvalue L of the covariance also are calculated. Finally, the original $m \times n$ matrix can be projected on to the new basis vectors (scores) in principal component space as following:

$$S=V^{t}.T \qquad (1)$$

S is the principal component score matrix, and t represents the transpose of the matrix.

PCA is applied to the built microwave brightness temperature diurnal cycles using the best-fit interpolation with 24 hourly values (based on best fit model) at different channels. Pixels that show persistent cloudy conditions over a given month are eliminated. Only pixels with complete diurnal cycle are considered. Brightness temperatures at different channels (i.e. 19V, 19H, 23V, 37V, 37H, 89V, and 89H) are analyzed separately. The diurnal mean of microwave temperature is subtracted at each pixel to center the data and PCA is performed on obtained anomalies. This step is necessary because it can avoid producing the first component as mean diurnal cycle temperature regionally.

The first three components (figure 4-3) show more than 98 percent variability and the first five components show all the variability in the brightness temperature diurnal cycle at different channels. PCA technique can smooth the variability between components. Part of this variability due to noises and inconsistency between sensors configuration (i.e. incidence angle and frequency) has been already eliminated through the application of the best-fit interpolation to construct *Tb* diurnal cycle. Figure 4-3 depicts the percent of the variability using the first five

components at different channels. As it is shown, the first component ranges between 70 to 80 percent of the variability at different channels. The second and the third components consecutively are between 15-25 and 3-6 percent of the variability (totally more than 98 percent). Additional tests were performed using the Spline interpolation instead of best fitting method. The total variability from the first three components was about 94 percents at different channels and lower than the variability obtained with the best fitting algorithm.

4.4. Results and discussion

The eigenvectors of the first three PCA components for 37 GHz (vertical polarization) are shown in figure 4-4. The other channels also have the same pattern of for their eigenvector with possible sign change (not shown). These components are similar to those obtained in previous studies (Aires et al., 2004) when PCA applied to diurnal skin temperatures from ISCCP. However, the order of the second and the third eigenvectors was different.

The effect of each component on the shape of the diurnal cycle by PCA was analyzed using different scores (Figure 4-5). The first two components affect the amplitude of the diurnal cycle. Also, the second component shows an existing relationship with the width of the diurnal cycle as well with applying higher scores (not shown). The third component represents mostly the change in phase or the timing of the maximum and minimum temperatures. Although the PCA analysis should theoretically de-correlate variables, the interaction between components may persist (Aires et al., 2002a; Aires et al., 2002b; Aires et al., 2004).

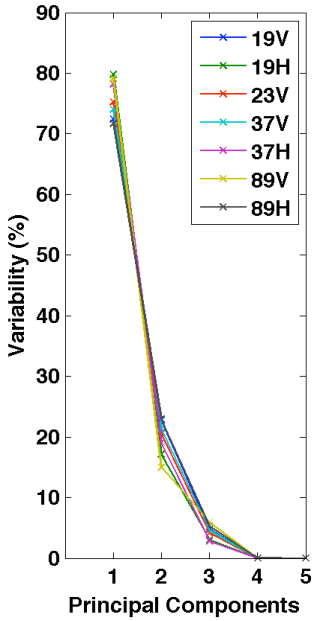

Figure 4- 3: Explained percentage variability of the PCA for the first five components at different channels (July 2005).

Individual maps displaying the spatial distribution of each component eigenvalue (score) are shown in figure 4-6. These maps represent the organization of each component geographically which may be related to land surface conditions. It is worth noting that these maps show PCA components with positive and negative sign. Different signs show different effects on the diurnal cycle. For instance, in the first component, high positive numbers tend to increase the diurnal amplitude and negative signs seem to diminish it. This sign can have opposite effect at other channels and components as their eigenvectors might have opposite sign.

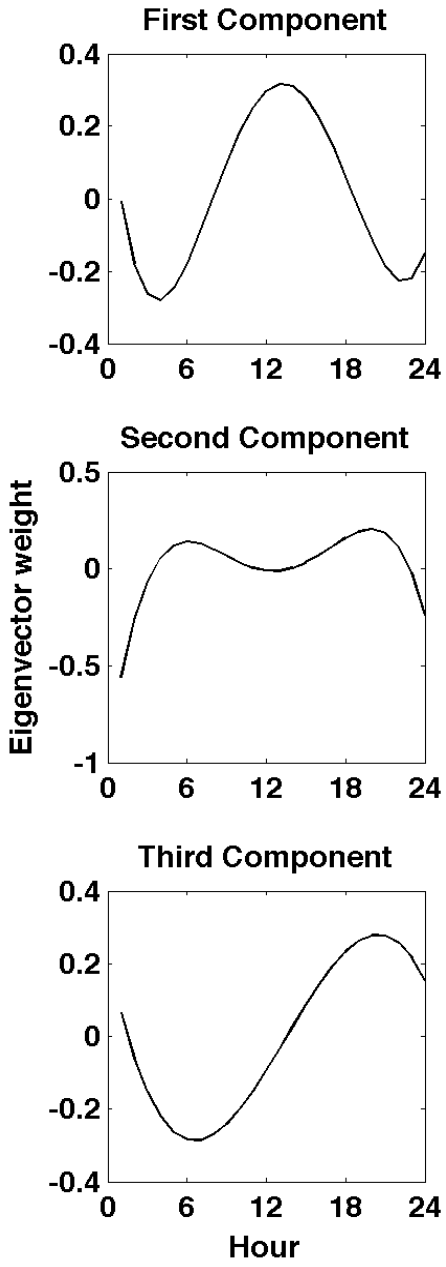

Figure 4- 4: The base function (eigenvector) variation of the first three PCA components of 37H for July 2005.

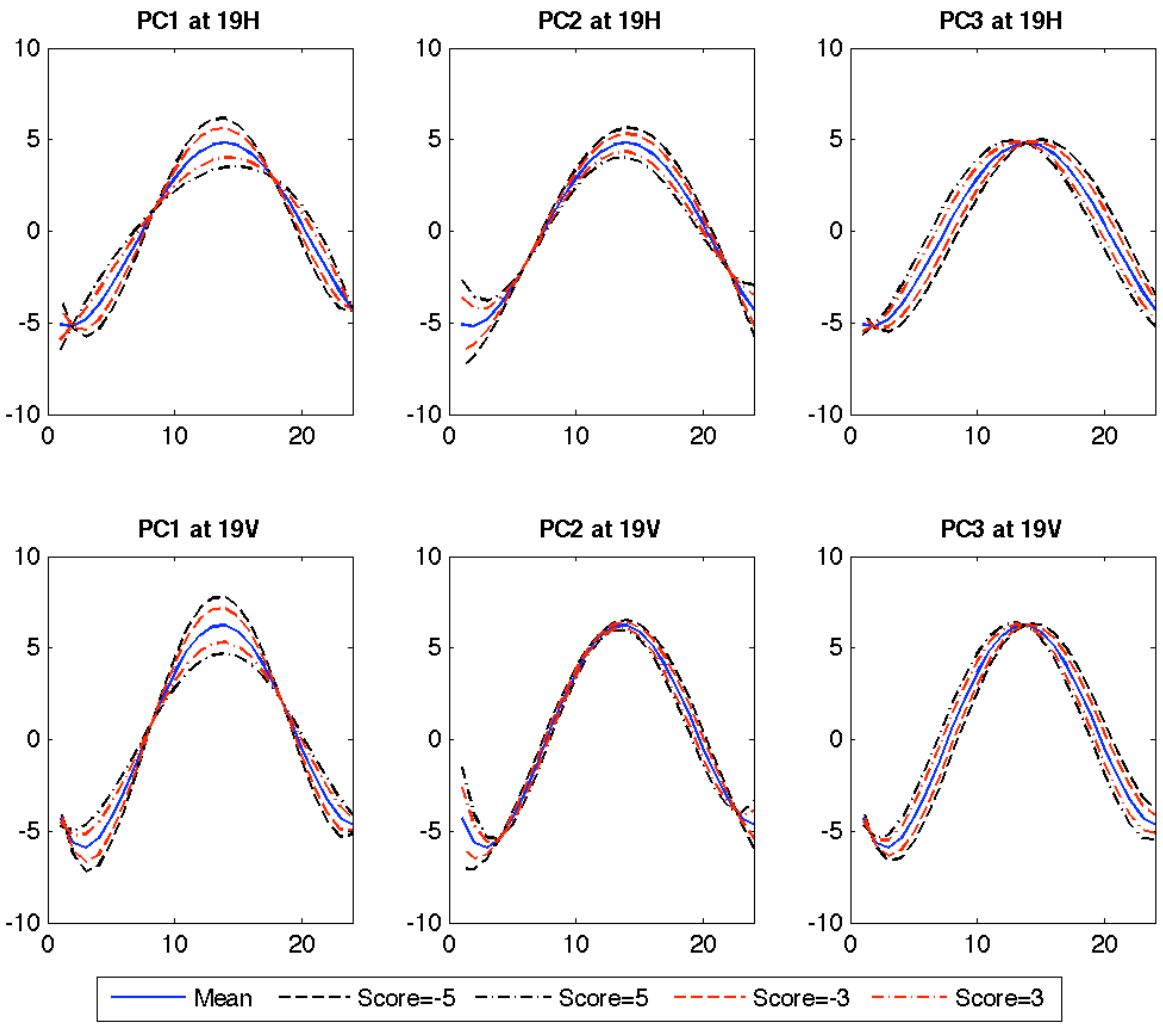

Figure 4- 5: The effect of score variation on the first three PCA components for 19 H and 19V for July 2005.

The first map (Figure 4-6, top) shows the first component with diurnal amplitude effect. The spatial variation of this component depicts some land cover effect on the diurnal cycle. Desert regions such as North Africa, Middle East, and Australian desert show large positive scores. On the other hand, more vegetated areas such as Amazon and Congo show small scores. This is reasonable, as water and wetlands should have lower diurnal amplitude because of the thermal inertia of the water (Lu et al., 2009). However, in desert area there are some regions that

show opposite values. These regions comprise sand dunes in Sahara desert that have low brightness temperature diurnal variation. This corroborates previous study that claimed lower fractional volume of sand dunes and lime stone will produce scattering in microwave signals (Prigent et al., 1999; Grody and Weng, 2008). This contradicts with the behavior of diurnal amplitude of skin temperature, which exhibits larger amplitude over the same dessert regions (Aires et al., 2004). This contrast can affect the emissivity retrievals when microwave brightness temperature and infrared thermal temperature are used together (Norouzi et al., 2011).

The second component also affects the diurnal amplitude. Moreover, the latitude dependency of the second component is noticeable, as this component reflects the variation of daytime duration (figure 4-6, middle). It has higher/lower values as it gets farther from/closer to the equator. The last map in figure (4-6, bottom) displays values of the third component that reflect the phase effect on the diurnal cycle. Highest phase lag of the temperature is observed in arid and semi-arid regions, as the soil wetness is much lower than in fairly vegetated area. Microwave observations originate from deeper soil layer in arid regions comparing with regions with higher soil moisture, as it takes time for heat from solar radiation to transfer from the surface to the deeper layer, which corresponds to the depth of microwave emanation (Prigent et al., 1999; Grody and Weng, 2008; Stephen et al., 2010).

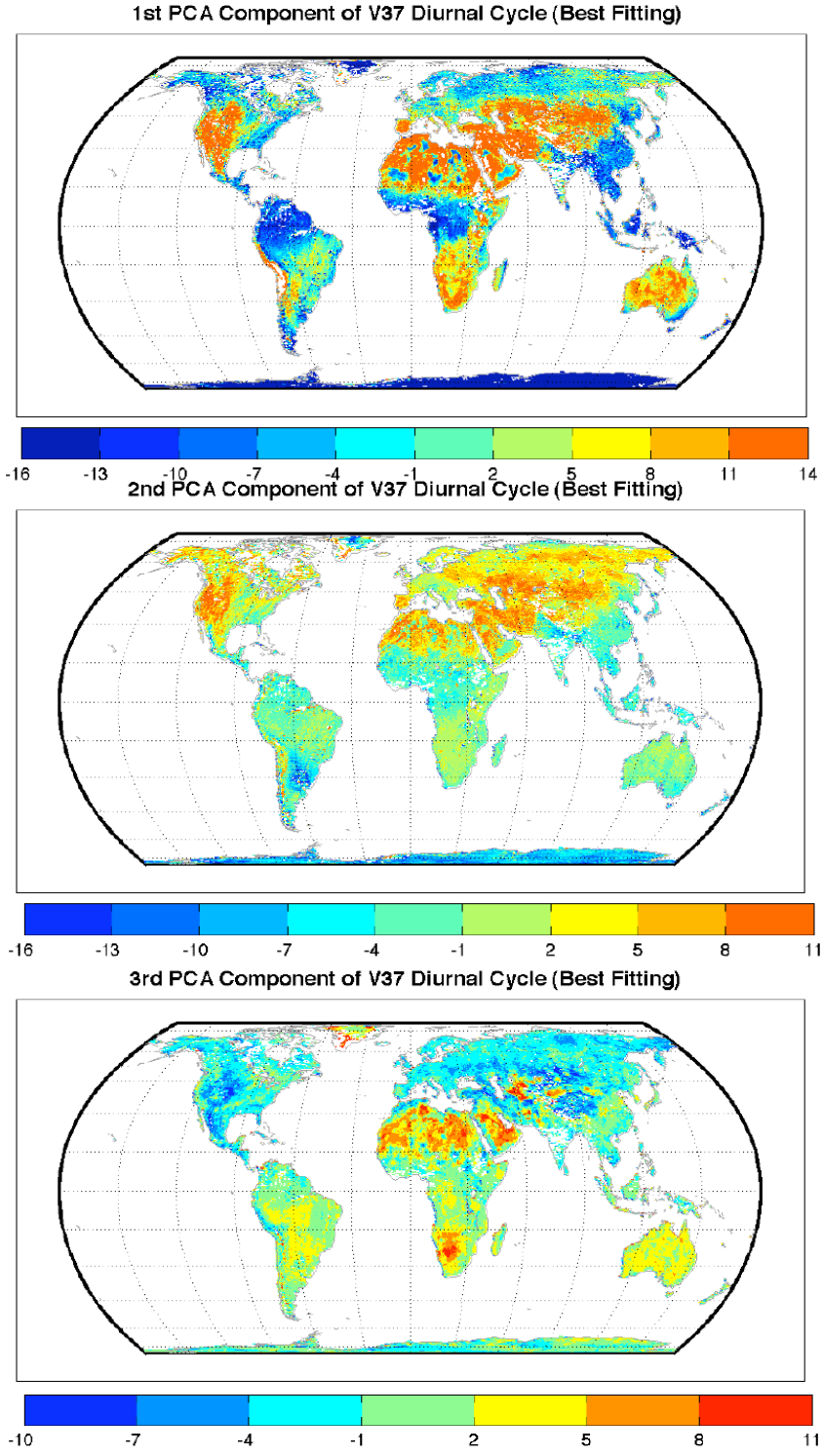

Figure 4- 6: The spatial variation of the first three PCA components score at 37V for July 2005.

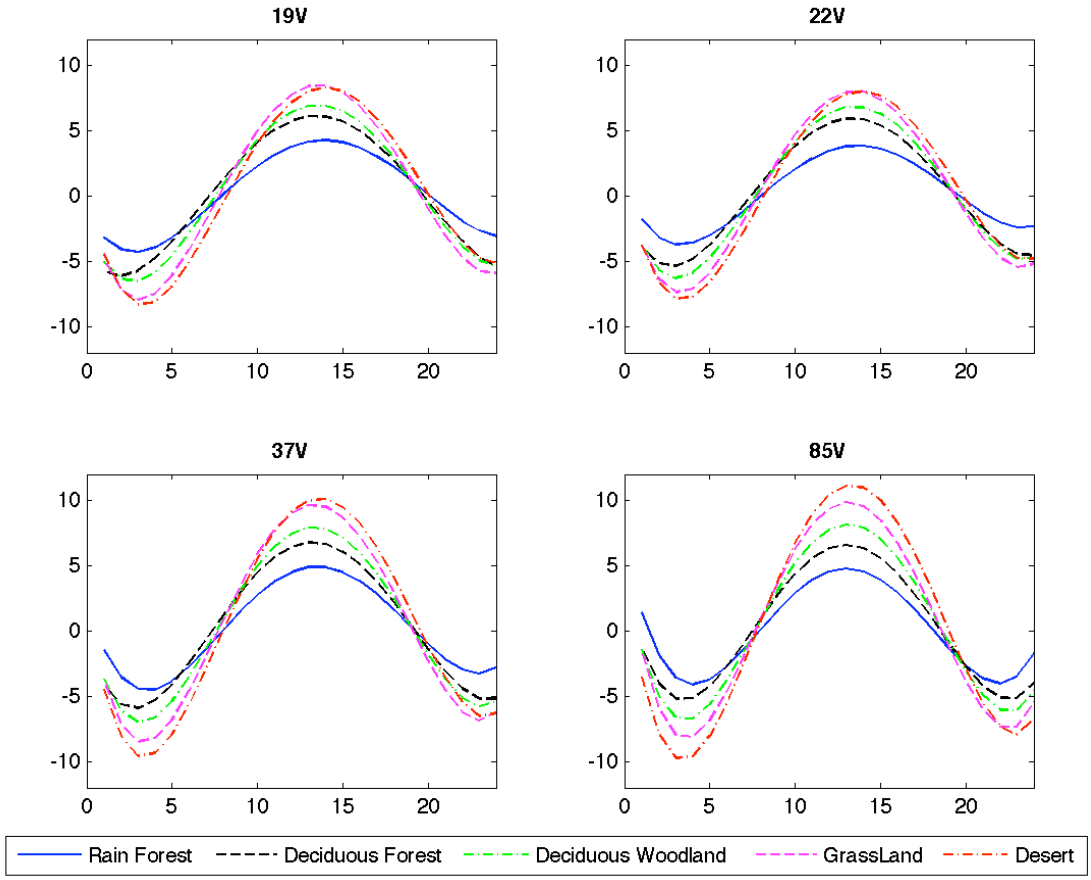

Figure 4- 7: Anomalies of diurnal cycle variation of microwave brightness temperature at different channels for different land vegetation classes (July 2005).

Effect of the land cover on the diurnal cycle of microwave brightness temperature *Tb* is also studied using global vegetation cover database provided by (Matthews, 1983). Figure 4-7 depicts the diurnal variation of the microwave brightness temperature at five different land cover types for 19, 23, 37, and 89 GHz (vertical polarization). The selected land cover classes ranges from densely vegetated areas to deserts with almost no vegetation. Figure 4-7 shows that the largest amplitude of diurnal cycle is associated with desert areas and the lowest related to highly vegetated area with rain forest land cover type. High amount of moisture and higher scattering in vegetated regions reduces the amplitude, as the physical temperature variation is not significant

with higher thermal capacity of the water (Lu et al., 2009). Moreover, the differences at 89 GHz in diurnal amplitude of different classes are more distinct than lower frequencies such as 19 GHz. This is because the 89 GHz microwave brightness temperature is more sensitive to the top surface while the 19 GHz microwave observation originates from deeper layer (Njoku and Li, 1999). Prigent et al (1999) showed that the deeper the layer or penetration, the lower the diurnal amplitude. However, as we showed in PCA maps (figure 4-6) some desert areas also have small diurnal cycle amplitude. Therefore behavior of the microwave diurnal cycle in this respect is not consistent with skin temperature diurnal cycle, as the brightness temperature not only depends on physical temperature, but also it is affected by emissivity (i.e. soil properties) as well. The dependency of the microwave brightness temperature diurnal cycle on the frequency is illustrated in figure 4-8 where the diurnal amplitude increases with frequency. The 89 GHz has the greatest diurnal amplitude in average over the globe whereas the 19 GHz shows the lowest one. Horizontal polarization at 89 and 37 GHz shows slightly lower amplitude than vertical. Also, at 23 GHz the brightness temperature is lower than 19 GHz, which is caused by the higher sensitivity of the 23 GHz brightness temperatures to water vapor profile (Prigent et al., 2005b).

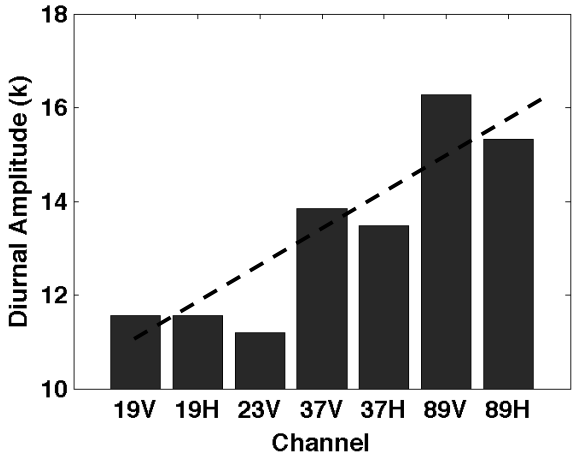

Figure 4- 8: Global diurnal amplitude of microwave brightness temperature at different channels for Jan. 2005.

As it was shown (Figure 4-6 bottom), the third PCA component of microwave diurnal variation reflects the phase effect (time of maximum temperature) on the diurnal cycle. This phase lag due to penetration depth can delay the peak time for the temperature (Prigent et al., 1999). Therefore, places with larger penetration depth display a longer phase in their diurnal cycle variation. To examine the spatial variation of the phase lag in microwave, the peak time in microwave diurnal cycle is compared to the timing of the peak of infrared-based skin temperature diurnal cycle from constructed diurnal cycle of ISCCP skin temperature. Skin temperature from infrared has theoretically almost zero penetration depth, while microwave especially in lower frequencies has higher penetration depth. Therefore, one can expect a considerable phase lag between the infrared and the microwave observations. This has been shown in figure 4-9top, when the difference between the peak time at infrared-based skin temperature (from ISCCP) and passive microwave brightness temperature at 19GHz (vertical polarization) diurnal cycle is mapped over North Africa and Arabian Peninsula. Large differences, up to three hours, between the peak times of both diurnal cycles are observed in desert. Areas where large time lag was observed between microwave and infrared temperatures coincide also show smaller diurnal amplitude (figure 4-6 top). By looking at the lithology map of the Sahara desert and Arabian Peninsula (figure 4-9 bottom) (Jimenez et al., 2010), one can observe that areas showing high phase lags are coincident with sand dunes or loose siliceous rocks. Grody and Weng (2008) also found that these regions with low fractional volume cause some scattering in microwave signals. This inconsistency between thermal and microwave brightness temperatures can lead to discrepancies in emissivity retrieval particularly when estimated emissivities from day/night overpasses are compared (Norouzi et al., 2011). In stable conditions in terms of moisture and vegetation, similar emissivity is expected during day and

night. However, the mismatch between thermal and microwave temperature can introduce an error up to 10% in emissivity retrievals (figure 3-16). These findings demonstrate the necessity of addressing this inconsistency in order to improve the retrieval of land emissivity.

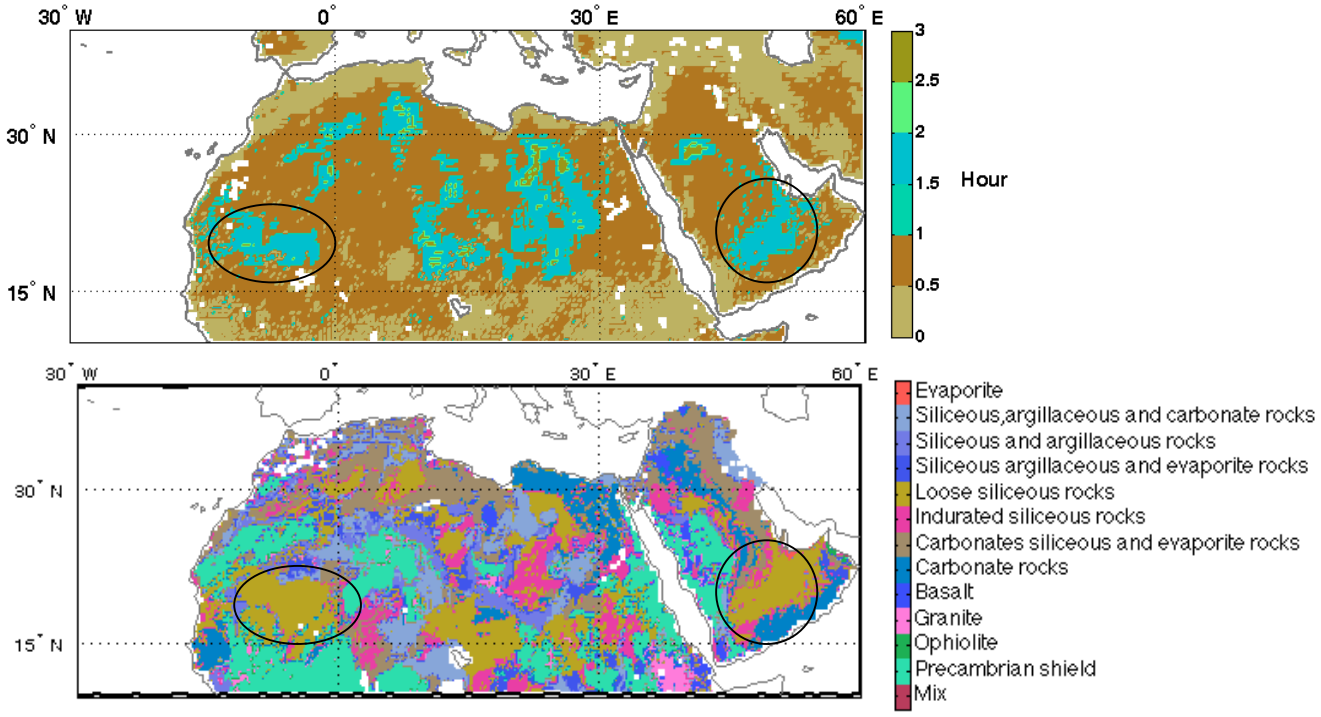

Figure 4- 9: (Top) The lag time between skin temperature and microwave brightness temperature diurnal cycle at 19V for July 2003 compared to Lithology map (Bottom) of Sahara desert and Arabian Peninsula (Jimenez et al., 2010)

4.5. Conclusion

In this chapter, diurnal cycles of microwave brightness temperature were constructed using AMSR-E and SSM/I observations at similar channels. A PCA approach was used to study the spatial variability of the microwave diurnal cycle. The first three components were found to be related to the diurnal amplitude, the duration of daytime, and phase time of the diurnal cycle of the brightness temperature. Strong frequency dependency was found in diurnal amplitude of microwave temperature as the high frequencies showed greater diurnal amplitude with smaller

penetration depth. The diurnal variation of the microwave was studied at different land cover types. It confirmed that in densely vegetated areas the diurnal amplitude is smaller and deserts have the greatest diurnal variation except places with sand dunes soil type. Overall, it was noticed that the brightness temperature diurnal variation does not quite match with the diurnal variation of the infrared temperature. Furthermore, the intercomparison of both temperatures may also be an indicator of several soil parameters like, soil texture, mineral type, and soil moisture and vegetation type. An analysis of the phase time between thermal and microwave brightness temperatures showed that large differences were found in places where soil texture is favorable for deeper penetration. The similar inconsistency is noticed in the diurnal amplitude of thermal and microwave temperatures, as diurnal amplitude of the microwave is significantly smaller in desert over loose siliceous rocks covered areas. This underscores the necessity of adjusting IR to improve the retrieval of land emissivity. This adjustment will be addressed in chapter 5 and its effect on the retrieval of land emissivity will be assessed.

CHAPTER 5: USING MICROWAVE BRIGHTNESS TEMPERATURE DIURNAL CYCLE TO IMPROVE EMISSIVITY RETRIEVALS OVER LAND

Passive Microwave emissions originate from deeper layers than the infrared. To retrieve microwave emissivities, infrared thermal temperatures are used as the physical temperature since there is no global information on physical temperature profiles. A difference in depth of origination can cause an inconsistency between diurnal variations of infrared and microwave brightness temperatures, which can lead to differences of emissivities from day and night retrievals of more than 0.1. A lookup table of effective physical temperature representative of the contributing layers to the microwave signal for each channel and month is constructed based on the diurnal cycle of brightness temperatures. The implementation of the proposed effective temperature diurnal cycle lookup table shows that it can mitigate the differences between day and night retrieved emissivities significantly from Advanced Microwave Scanning Radiometer – Earth Observing System (AMSR-E) observations.

5.1. Introduction

Microwave brightness temperature, *Tb*, is sensitive to key surface properties. Instantaneous measures of this variable have been used in a variety of applications to estimate column water vapor abundance, rainfall rate, wind speed, ocean salinity, soil moisture, snow cover, freeze/thaw state, land surface temperature, inundation fraction, and vegetation structure (e.g. Fily et al., 2003; Njoku et al., 2003; Wilheit et al., 2003; McCollum and Ferraro, 2005; Karbou et al., 2006; Papa et al., 2006; Tedesco and Kim, 2006; Boukabara et al., 2007; Entekhabi

et al., 2010; Min et al., 2010; Zhang et al., 2010). Diurnal variation of land surface temperature and atmospheric temperature and water vapor profiles affects the observed brightness temperature. The more frequent the observation of this variable throughout the day, the better our understanding of the variability of these retrieved parameters.

Microwave emissions can come from layers deeper than the surface skin depending on the frequency and the media, in particular its moisture. For instance, in vegetated areas, the 6.9 GHz (C band) passive microwave can pass through the vegetation and originate from the soil surface (Njoku et al., 2003). The diurnal variation of the passive microwave brightness temperature mainly depends on physical temperature variation at the depth of origination. In some desert regions at higher frequencies, where the penetration depth is smaller, the radiometric measurements display diurnal variations similar to those of the surface temperature, but conversely, at lower frequencies, where the penetration depth is larger, the radiation displays smaller diurnal variations than the surface temperature (Grody and Weng, 2008). Therefore, to retrieve microwave emissivities, estimates of the variation of physical temperatures with depth are necessary. A physical model has been used to simulate the physical temperature variation at different depths based on a semi-infinite heat transfer equation (Prigent et al., 1999; Grody and Weng, 2008). This type of model shows decreasing diurnal amplitude and increasing phase lag with respect to the skin temperature with depth.

A significant difference was found in chapter 3 between land emissivities determined from AMSR-E daytime and nighttime overpasses, using infrared thermal temperature as the physical temperature. Such large differences, up to 0.1, seem unlikely for stable surface conditions. These differences were attributed to the fact that the skin temperature, *Ts*, and microwave brightness temperature, *Tb*, did not correspond to the same depth, so the diurnal cycles were not the same.

This explanation is supported by the variation of the discrepancy magnitude with surface type – more densely vegetated locations that are also moister showed much smaller discrepancies than arid regions.

This study focuses to reduce globally the day-night discrepancy in land emissivity estimates instantaneously. First, the physical model proposed by Prigent et al (1999) is used globally to investigate the spatial variability of the penetration depth at different microwave frequencies. We determine the diurnal variation of microwave brightness temperatures observed at different local times using similar channels of AMSR-E and SSM/I on multiple satellites. A lookup table of effective temperature (i.e. a temperature that represents the vertical integration of microwave emissions over layer temperatures) diurnal variation for each frequency and month is constructed from the PCA results. This effective temperature is used to improve land surface emissivity retrieval by mitigating the differences between day and night estimates. Finally, the emissivities are estimated using the proposed look up table.

5.2. Statement of the problem

In our previous study (chapter 3), we estimated microwave land surface emissivities over the globe from AMSR-E observations at all frequencies and both polarizations. The effects of the atmosphere were removed using TOVS atmospheric temperature – humidity dataset available with ISCCP and an appropriate radiative transfer approximation. The ISCCP-DX product provided land skin temperature and cloud mask.

The brightness temperature at the surface after removing the effect of the atmosphere can be written as:

$$Tb_{(p,\upsilon)} = \varepsilon_{eff_{(p,\upsilon)}} . T_{eff} \qquad (5\text{-}1)$$

where $\varepsilon_{eff_{(p,\upsilon)}}$ and $Tb_{(p,\upsilon)}$ are the land surface emissivity and the brightness temperatures (at the surface) at polarization p and frequency υ, respectively. T_{eff} is the effective physical temperature. The emissivity is a physical parameter, which depends on the surface characteristics such as moisture, vegetation, fractional volume, dielectric, and sensor configuration (i.e. viewing angle and frequency). Therefore, the variation of the brightness temperature should be similar to the effective temperature variation with stable surface condition and emissivity during day and night.

The emissivity retrieval is based on the assumption that infrared skin temperature is the effective physical temperature, equivalent to assuming that the microwave brightness temperature originates from the skin. This assumption is not necessarily true, but necessary because of lack of general global information on penetration depth and temperature profile. A measure of the accuracy of this assumption is provided by the differences of the retrieved emissivities between ascending and descending (day/night) orbits (figure 3-16). The largest differences are found in more arid and less vegetated regions even though we expect less difference because of small moisture changes from day to night. The 10.7 and 89.0 GHz frequencies both have the same pattern of differences; but the emissivity difference between day and night at 89.0 GHz is noticeably smaller than 10.7 GHz at the same locations such as North and South Africa, due to smaller penetration depth of 89.0 GHz (figure 3-16).

A physical model has been proposed (Prigent et al., 1999) to account for the effect of penetration depth in emissivity retrievals by revising the physical temperature. This method is based on a one-dimensional heat transfer by conduction and has been tested over North Africa, Saudi Arabian desert, and Australia. We implement this model globally to analyze the spatial variation of the penetration depth at different frequencies and polarizations. The method provides

the temperature diurnal cycle for a given depth and time of the day using the first two terms of the Fourier solution as follows:

$$T(d,t) = T_0 + \sum_n A_n \exp(-d\sqrt{\frac{n\omega_0}{2\kappa}})\cos(n\omega_0 t + \phi_n - d\sqrt{\frac{n\omega_0}{2\kappa}}) \qquad (5\text{-}2)$$

$T(d,t)$ is the temperature at depth, d, and time t. T_0, A_n, and ϕ_n are the coefficients of the Fourier solution. κ is the thermal diffusivity and $\omega_0 = \frac{2\pi}{3600 \times 24} rad/\sec$ is angular frequency for a period of 24 hours. $d\sqrt{\frac{\omega_0}{2\kappa}}$ known as "Alpha" (α) can be representative of penetration depth as it has the d parameter embedded in.

The surface skin temperature variation as a boundary condition can be used to determine the T_0, A_n, and ϕ_n by setting $d=0$ in equation (5-2) and using a nonlinear least square solution:

$$T(0,t) = T_0 + \sum_n A_n \cos(n\omega_0 t + \phi_n) \qquad (5\text{-}3)$$

The emissivity and alpha over a month then can be estimated by minimizing the differences between measured and simulated brightness temperatures in a radiative transfer equation. AMSR-E microwave observations at different channels along with the upwelling and downwelling temperature and atmospheric transmission for each month are used. The root mean square (RMS) errors of the fit at different channels are 3.6 k to 4.5 k at global scale.

The global maps of alpha (α) obtained for July 2003 at 6.9, 18.7, 36.5, and 89.0 GHz (vertical polarization) are shown in figure (5-1). The value of alpha is larger in arid and semi-arid regions (more than 0.4). For instance, large alpha is found in the Sahara desert, Middle East, South Africa, and Western United States. These regions correspond to regions with larger differences between day and night (figure 3-16). This can be confirmed by figure 5-2, which

shows that as the alpha increases the differences between estimated emissivities at day and night increases as well. The pixels with high Alpha and small day and night differences belong to coastal regions. The regions with larger alpha contain smaller amounts of the moisture compared with densely vegetated areas such as Amazon, Congo, and Eastern United States (figure 5-1). Water (in moister areas) has higher thermal capacity and smaller microwave penetration depth (Njoku and Entekhabi, 1996). In North Africa and Saudi Arabia the pattern of the alpha map is consistent with Prigent et al (1999). As expected, the penetration depth decreases with frequency, for instance the alpha values decrease at North Africa with frequency (figure 5-1).

The relationships between alpha parameter at different frequencies can be seen using the scatter plots in figure 5-3. The figure shows the relation between alpha at 6.9 V versus alpha at 6.9H, 18.7 V, 36.5 V, and 89.0 V. The microwave brightness temperature originates from the same depth at the same frequency with different vertical and horizontal polarization, as the relationship in scatter plot of alphas between 6.9 vertical and horizontal is almost unity. However, as frequency increases the alpha parameter or the penetration depth decreases. This is in line with previous study (Prigent et al., 1999), but this time the alpha values are provided globally.

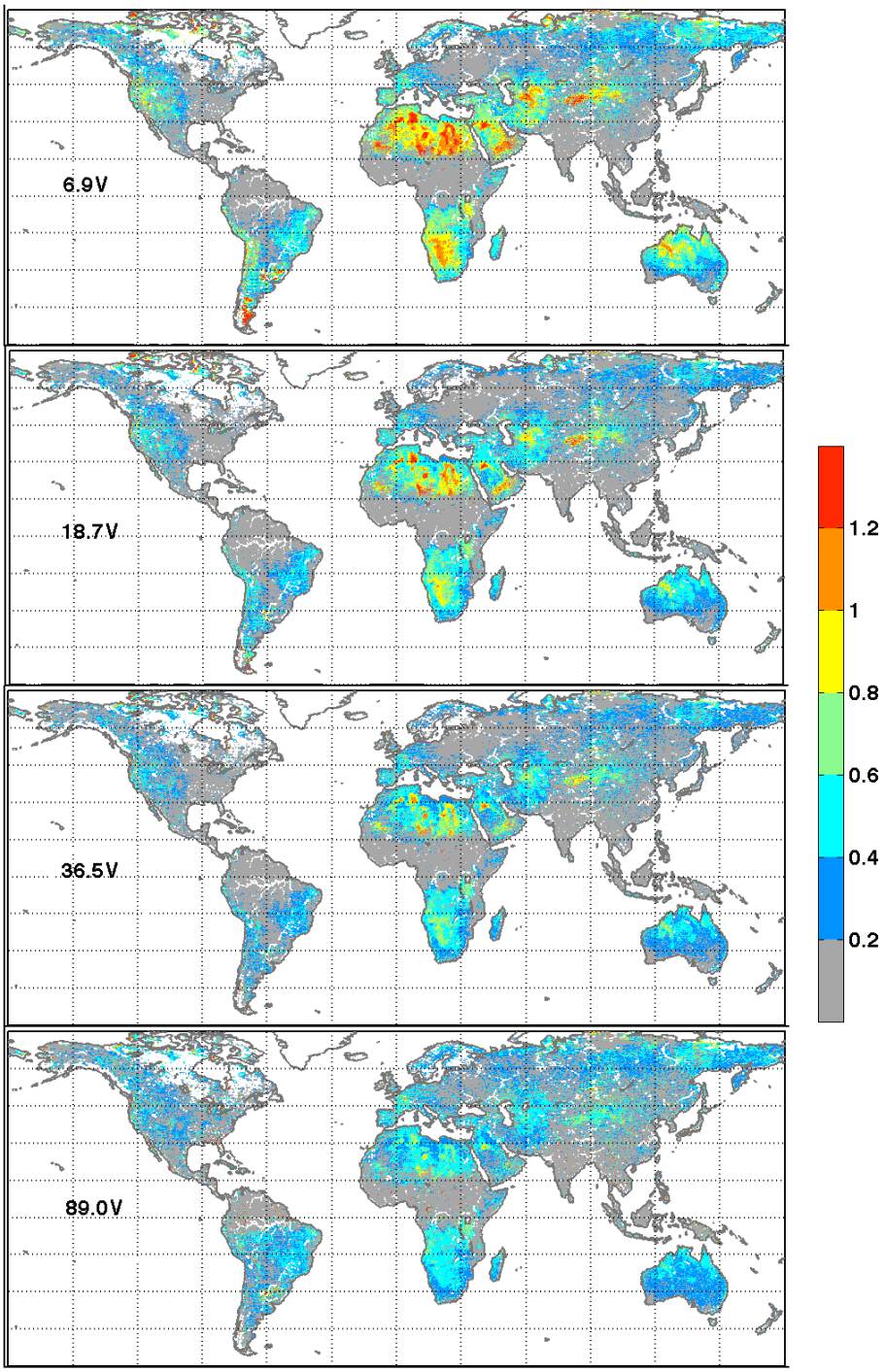

Figure 5- 1: Global map of alpha at 6.9, 18.7, 36.5, and 89.0 GHz (vertical polarization) from physical model for July 2003.

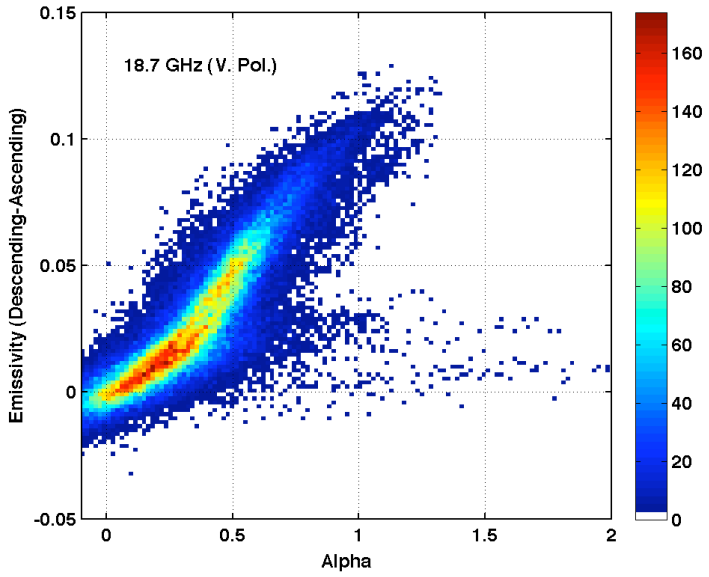

Figure 5- 2: Alpha versus descending and ascending emissivity differences at 18.7V for July 2003. Color bar represents number of pixels.

The described physical model are in monthly scale, however instantaneous emissivity retrieval with consideration of the effect of penetration depth is not possible using the physical model, as it uses a nonlinear least square model for all observation within a month to estimate the fitted emissivity and penetration depth. But, nowadays there are more sensors are available with different orbit times such as AMSR-E, which can provide observations at daily maximum and minimum temperature and therefore better daily variation coverage. In the following sections, we propose a method and show its ability to mitigate the discrepancies between ascending and descending emissivity estimates using a constructed microwave diurnal cycle.

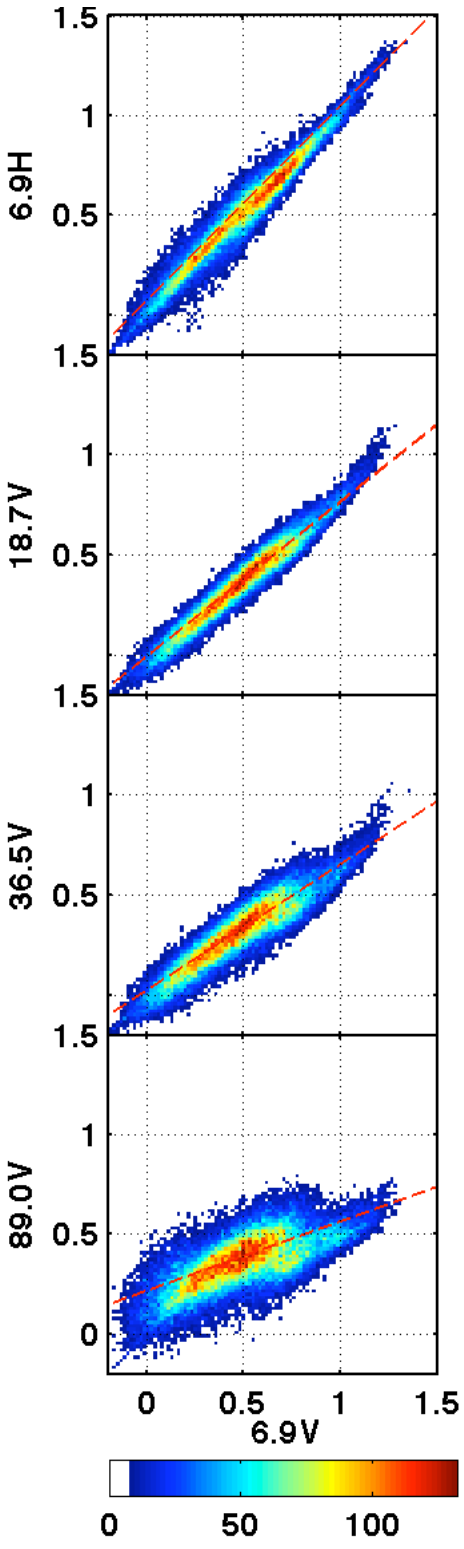

Figure 5- 3: Scatter plots of Alpha at 6.9V versus 6.9H, 18.7V, 36.5V, and 89.0V for July 2003. Color bar represents number of pixels.

5.3. Methodology

The diurnal variation of infrared temperature and microwave brightness temperatures are investigated at a variety of different locations, depending on whether differences between day and night emissivities are smaller or larger. A location with small day-night emissivity difference (figure 5-4a) is in densely vegetated area (lat= 60N, lon= 30E) and the one with large differences (figure 5-4d) is in the Sahara desert in North Africa (lat= 25N, lon= 12.5E) with sand dunes. Two other locations with intermediate emissivity differences are also depicted (figure 5-4b,c). The Spline-interpolated ISCCP-DX diurnal cycle of the skin temperature is shown at each location along with diurnal cycle of microwave brightness temperatures at 19, 37, and 89 GHz for vertical polarization from AMSR-E and SSM/I observations. The diurnal cycle of the skin temperature and microwave observations have similar amplitude in the region with small differences between day and night retrieved emissivities (figure 5-4a). However, noticeable differences in amplitude between skin temperature and microwave brightness temperature appear in the other regions with larger day-night emissivity differences (figure 5-4c,d). Moreover, the difference in amplitude and phase lag increases as frequency decreases as expected. Figure 5-5 depicts the diurnal variation of the retrieved emissivities at the same locations if the microwave diurnal cycle is used along with skin temperature diurnal cycle. Figure 5-5 shows that the emissivity has a small variation diurnally, when the differences between microwave and skin temperature amplitude is small and increases the apparent diurnal variation of emissivity to as much as more than 0.1, when the diurnal amplitude differences increase. We conclude that the apparent diurnal variation of emissivity is caused by the discrepancy between the infrared skin temperature used in the retrieval and the effective temperature at deeper levels sensed by microwave channels.

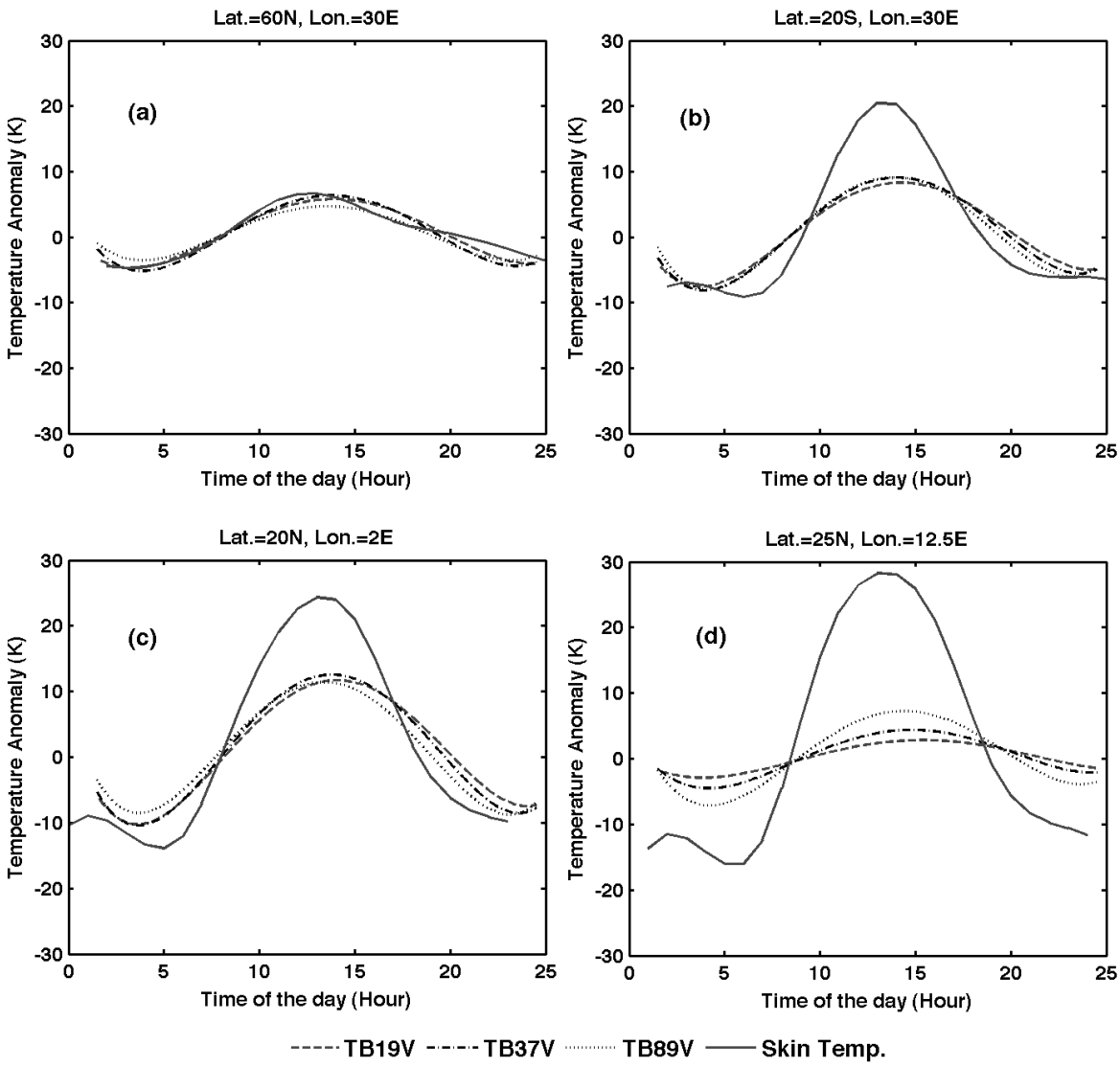

Figure 5- 4: Diurnal cycle of skin temperature from ISCCP and microwave brightness temperatures at 19V, 37V, and 89V for Jul. 2003.

The brightness temperature can be written in a simplified equation by ignoring the effect of the atmosphere as follow:

$$\overline{Tb_{(p,\upsilon)}} = \overline{\varepsilon_{(p,\upsilon)}.T_{eff}} \qquad (5\text{-}4)$$

This shows that the monthly mean brightness temperature, $\overline{Tb_{(p,\upsilon)}}$, is proportional with the monthly emissivity and physical temperature, $\overline{\varepsilon_{(p,\upsilon)}.T_{eff}}$. The emissivity should be nearly constant for a given frequency and incidence angle if moisture and vegetation are not changing too

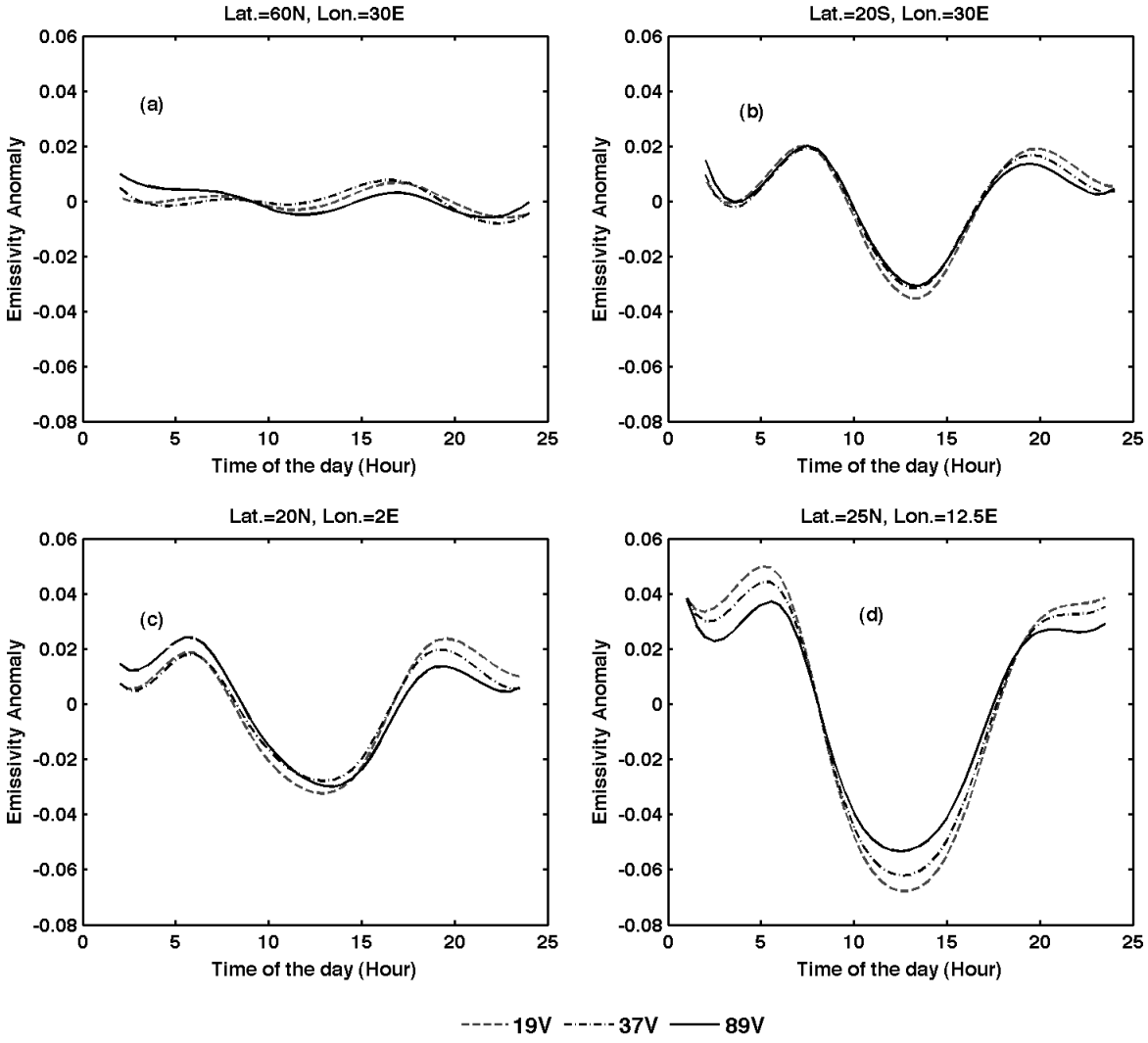

Figure 5- 5: Diurnal cycle of estimated emissivity at 19V, 37V, and 89V for July 2003.

rapidly. This is confirmed by our previous study, when we found that the global RMS of emissivity standard deviation within a month is less than 0.015 (Norouzi et al., 2011). Thus, a similar diurnal variation of the brightness temperature and effective physical temperature is expected, and equation 4 can be rewritten as:

$$Tb^{*}_{(p,v)} \approx \overline{\varepsilon_{(p,v)}}.T^{*}_{eff} \quad (5\text{-}5)$$

which $Tb^{*}_{(p,v)}$ and T^{*}_{eff} are diurnal microwave brightness temperatures and effective temperatures.

Finally, the diurnal effective temperature from time t_1 and t_2 within a day would be:

$$T^{*}_{eff\,2} - T^{*}_{eff\,1} = \frac{Tb^{*}_{(p,v)_2} - Tb^{*}_{(p,v)_1}}{\overline{\varepsilon_{(p,v)}}} \quad (5\text{-}6)$$

Therefore, the shape of the effective temperature diurnal variation is proportional with the shape of the brightness temperature variation over the emissivity.

Based on the PCA, the first three components could explain almost 98 percent variability of Tb diurnally (chapter 4). We use the first three PCA components over emissivity to reconstruct diurnal variations of effective temperature for each frequency and polarization. For emissivity, $\varepsilon_{(p,v)}$, the previously monthly mean emissivities (chapter 3) are used. According to the physical model, the effective temperature diurnally oscillate about the average of the skin temperature (Prigent et al., 1999; Grody and Weng, 2008). The reason is that the temperature eventually tends to make balance according the heat transfer model. This is confirmed separately when we tested for the time that takes to have constant temperature at deeper layer with having constant source of heat. The maximum time that is needed to reach this equilibrium was found to be less than a day around 17 hours. Therefore, the final formula for the effective temperature can be written as:

$$T_{eff_{(p,v)}} = T_{S\,mean} + TB_{PCA_{\cdot(p,v)}} / \varepsilon_{(p,v)} \quad (5\text{-}7)$$

$TB_{PCA_{\cdot(p,v)}}$ is PCA reconstructed diurnal cycle of brightness temperature and $T_{S\,mean}$ is daily average of the skin temperature and may vary day to day, however the variation of the second term is not significant, as it's centered about zero. We can reserve the second term on right in equation 5-7 for each channel and each month of the year as a lookup table of the shape of effective temperature diurnal cycle. This lookup table can be used later to estimate the effective temperature simply by adding the average of the skin temperature. The revised temperature here instead of skin temperature then can be used to retrieve emissivity instantaneously according the previously implemented methodology (Prigent et al., 1997; Prigent et al., 2006; Norouzi et al., 2011).

5.4. Results and discussion

Figure 5-6 shows some examples of the centered diurnal effective temperature (look up table) at 18.7 and 36.5 GHz (vertical polarization) for three different locations based on described methodology. It shows that different regions consist of different diurnal variation at different month of the year. At the location with sand dune land cover according (Jimenez et al., 2010) (Figure 5-6 second row), both frequencies show very small diurnal amplitude with small monthly change. However, in other regions larger diurnal amplitude and more different monthly diurnal shapes are noticed. The difference in diurnal amplitudes at different month can be more than 10 k in this location (figure 5-6 first row). Generally, 37V (figure 5-6 right column) shows larger amplitude than 19V (left column), as 37GHz is less sensitive than 19V to the subsurface and originates from the depth closer to the surface. This confirms that 19V or lower frequencies with larger alpha and penetration depth have smaller diurnal variation than higher frequencies (Prigent et al., 1999).

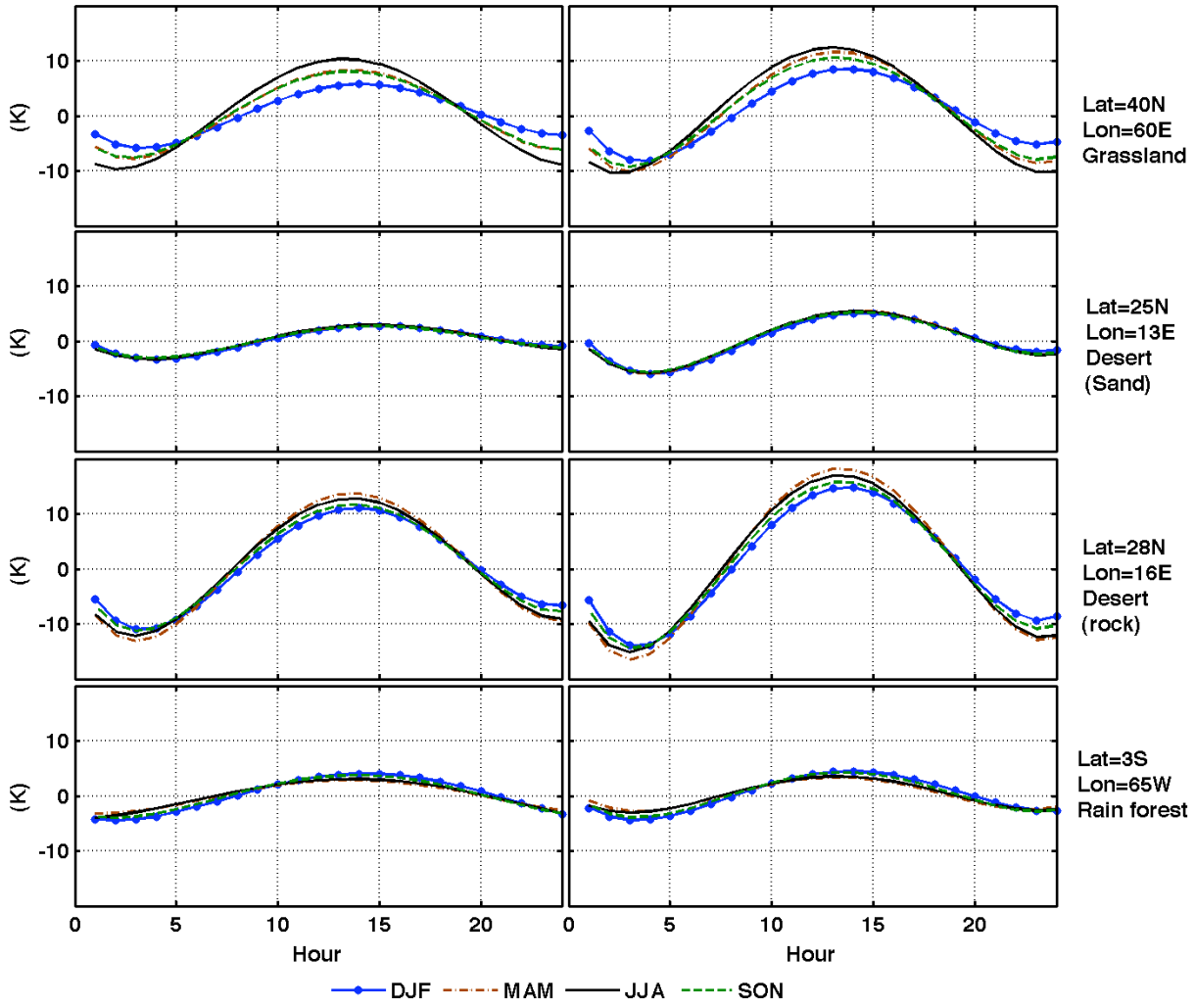

Figure 5- 6: Lookup table of effective temperature diurnal cycle at 19V (left) and 37V (right) at different locations averaged over different seasons.

The obtained lookup table of effective temperature diurnal cycles is then tested to see if they are stable enough to be used in later years as constant shape of the diurnal cycle. De-seasonalized anomalies of the amplitude value of the monthly effective temperatures are studied (figure 5-7) for different land vegetation cover (Matthews, 1983). For all shown land cover types (rain forests, deciduous woodland, and desert areas) the anomalies are mostly between -1 and 1 Kelvin with standard deviation 0.4 K. At other land covers also we found small anomalies (not

shown). This shows that year-to-year variation of amplitude is small, and the obtained effective temperature diurnal cycles for each month can be used for later years as lookup table.

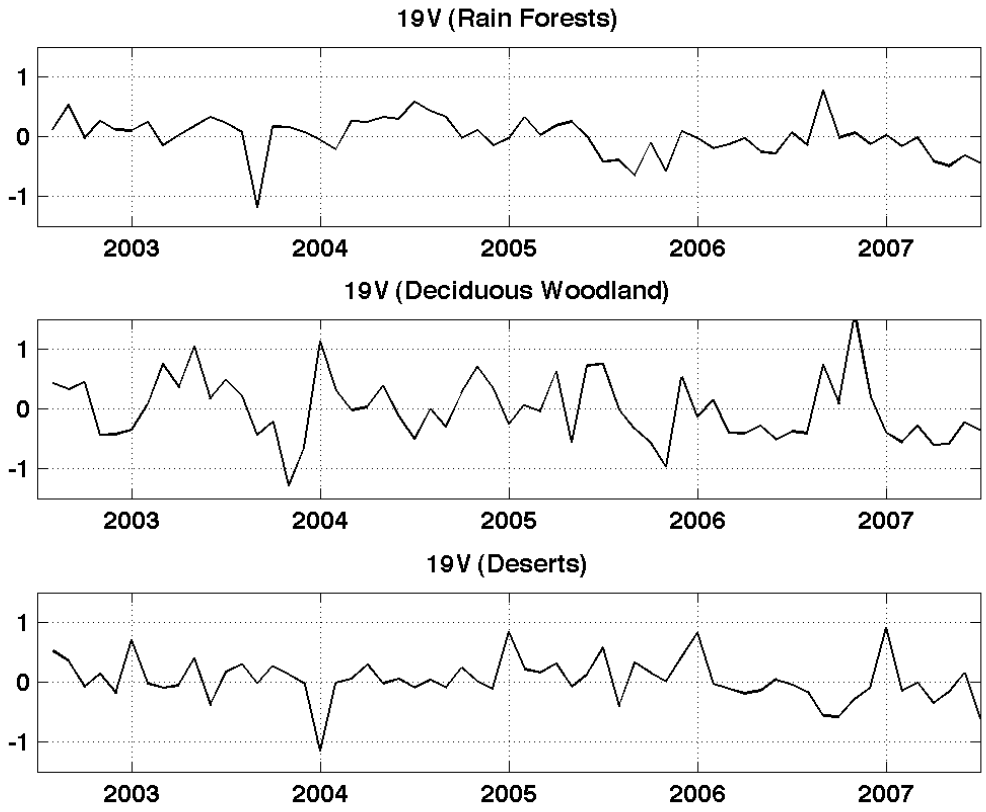

Figure 5- 7: De-seasonalized monthly mean anomaly variation of diurnal amplitude of microwave brightness temperature at 19V at rain forests, deciduous woodland, and desert regions.

Instantaneous emissivity at different AMSR-E channels for each ascending and descending observation is estimated using the proposed effective temperature diurnal cycle lookup table. Just clear sky observations are used in emissivity retrieval. First, the anomaly of the diurnal variation of effective temperature at AMSR-E overpass time is extracted from the lookup table. Then, it is added to daily mean of skin temperature according equation (5-7) and it is used in our emissivity retrieval. The monthly mean composite maps of new emissivities are estimated

by averaging over the retrieved instantaneous emissivities for both ascending and descending. Note that only the channels higher than or equal to 18.7 GHz are used in this method, as the effective temperatures are just available for common channels between AMSR-E and SSM/I. Figure (5-8) shows the monthly mean composite of emissivity at 18.7, 36.5, and 89.0 GHz (both vertical and horizontal polarization) for July 2003. The general patterns of the obtained emissivities at different frequencies are similar to our previous retrievals (chapter 3). For instance, at horizontal polarization frequencies, deserts such as North Africa, West of US, and deserts in Australia show smaller emissivity values than more vegetated area such as Amazon, Congo, and East of US. In vertical polarization, the opposite situation between deserts and vegetated area happens, as the deserts show greater emissivities at 18.7 GHz than the vegetated area.

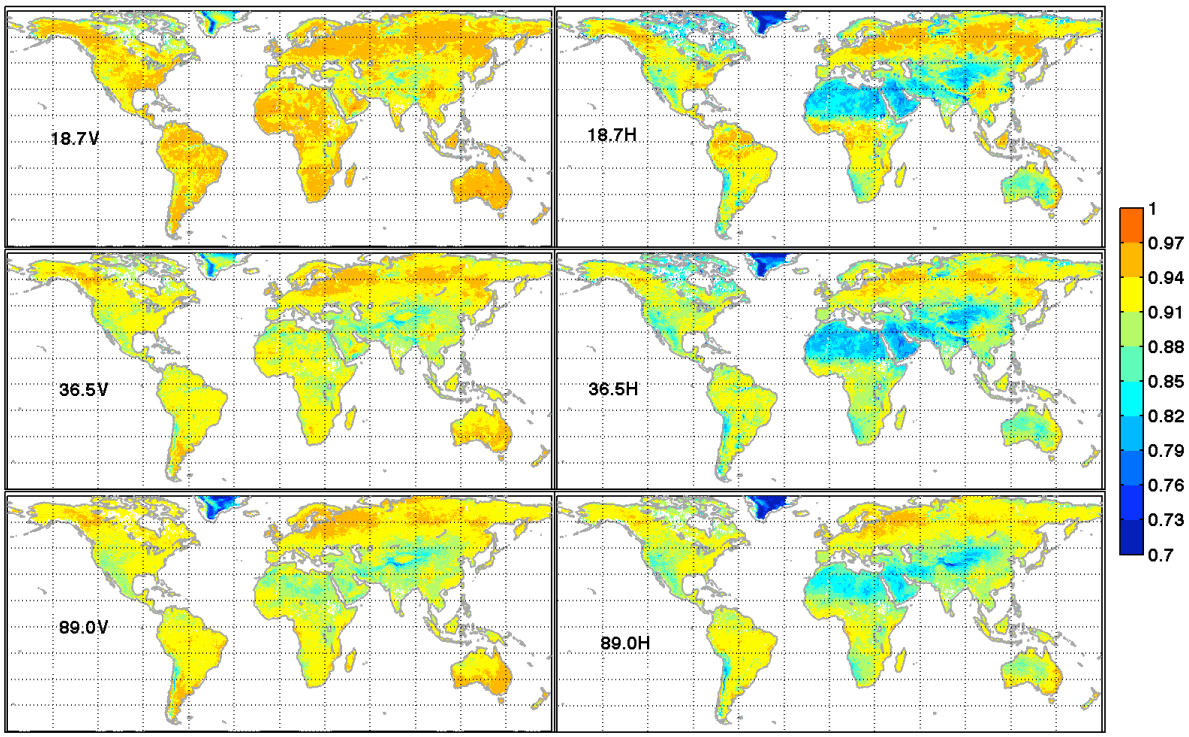

Figure 5- 8: Global monthly emissivity maps of emissivity at different channels using the proposed effective temperature diurnal cycles for July 2003.

The main objective of this study is to mitigate the differences between day and night emissivities. Figure (5-9) shows the map of difference between ascending and descending emissivity maps for 18.7, 36.5, and 89 GHz (vertical polarization) before using the proposed effective temperatures and after applying them for July 2003. Arid and semi-arid regions show up to 10 percents difference between day/night (ascending/descending) emissivities using the previous method without adjusting the effective temperature. There are also some differences that ascending estimate is greater than descending. These are belonging to coastal regions with more open water in the pixel. The difference between day and night significantly decreases after applying the proposed look up table. Almost no systematic difference is noticed with new method, and differences are very small (mostly less than 0.01). However, the number of places with positive emissivity differences is increased without any systematic pattern. The differences increase with frequency that could because of small atmospheric contamination in the retrieval.

Figure (5-10) presents the normalized histogram of difference of the newly estimated emissivities from ascending and descending observations separately using the proposed effective temperatures, and the previously retrieved emissivity differences. Histograms show the differences at 18.7, 36.5, and 89.0 GHz (vertical polarization) for deserts and over the globe. In all frequencies, the differences between ascending and descending emissivities have been decreased significantly in global scale. The mean difference globally between ascending and descending is about -0.003 with standard deviation of 0.0098 for July 2003 at 18.7 GHz vertical polarization. The results in terms of global mean and standard deviation at different frequencies before and after applying the proposed method are summarized in table 5-1. The global mean is reduced about 0.02 globally after using the proposed effective temperature diurnal cycle. In desert regions, there is an obvious improvement in reducing the differences of day and night

emissivities.

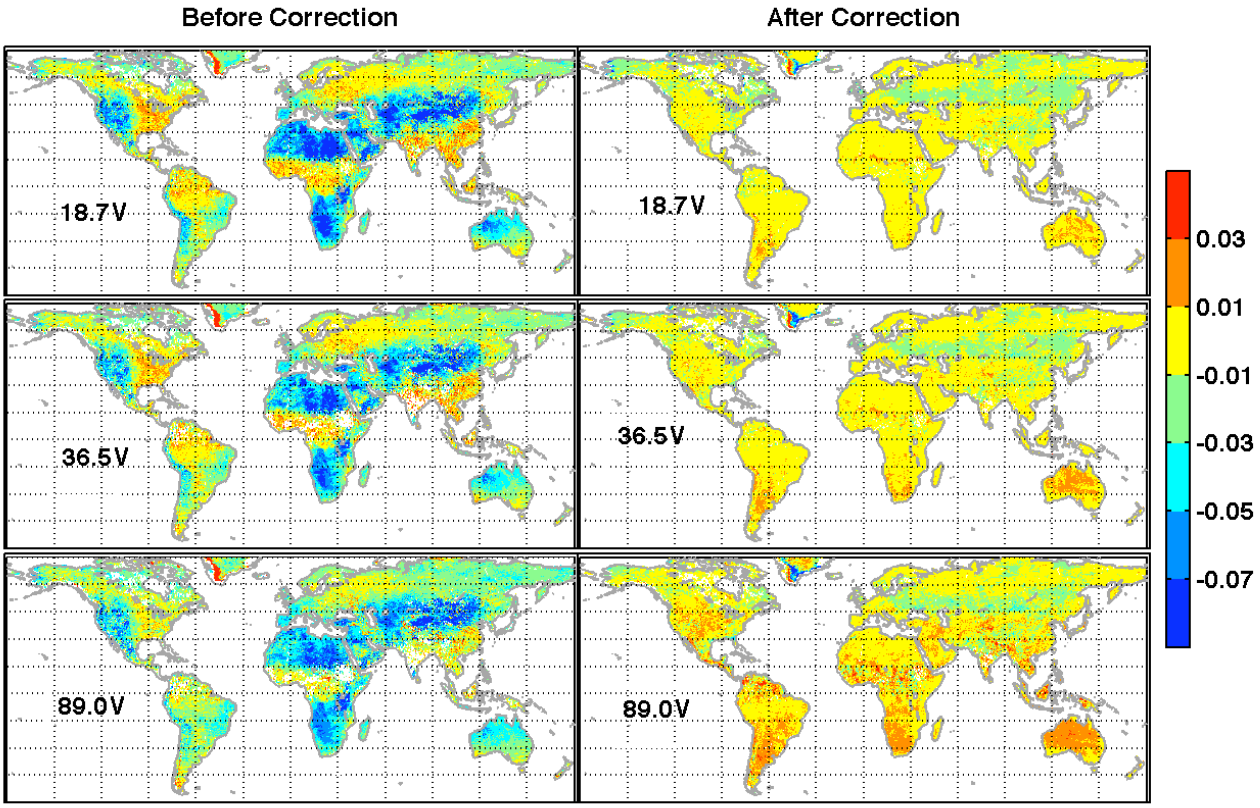

Figure 5- 9: Map of difference between ascending and descending emissivity at 18.7, 36.5, 89.0 GHz (vertical polarization) before and after using the proposed effective temperature diurnal cycles for July 2003.

The differences are slightly larger at 89 GHz after applying the method (about 0.005 greater) compared to other channels. The reason could be because of ignoring the effect of the atmosphere in equation (5-5) for generating the diurnal effective temperature look up table. As the frequency increases, the sensitivity of emissivity to atmospheric effect increases (Weng et al., 2001; Weng, 2007; Prigent et al., 2008). The simplification in equation (5-5) affects the retrieval stronger at higher frequency. Moreover, the atmospheric information that is used in emissivity retrieval comes from daily TOVS observation. Using the daily observations for both ascending

and descending emissivity retrieval means that diurnal cycle of the atmospheric parameters such as air temperature and water vapor profile are ignored. This can further affect the difference between day and night emissivity, and can explain the remainder differences. The effect of the atmospheric opacity that was ignored in this method is included to see its effect on the proposed method. Figure 5-11 shows that the introduction of this parameter in the determination of effective temperature reduced the effect of diurnal variation on the output in terms of differences between emissivities during day and night.

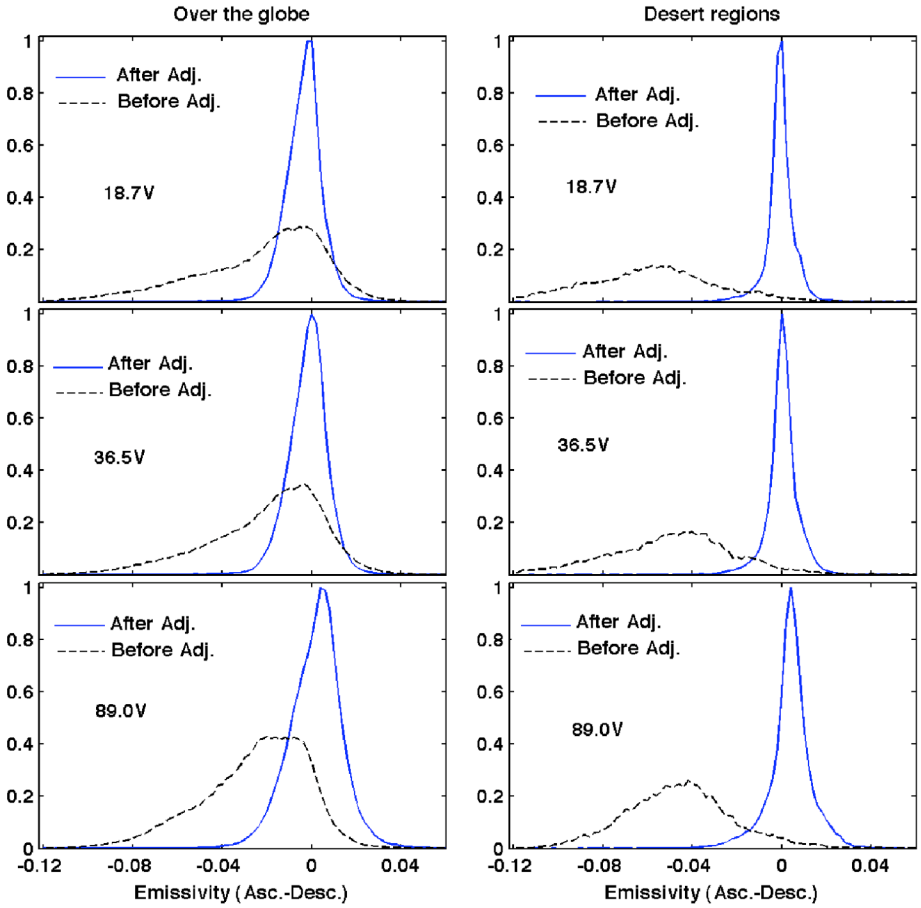

Figure 5- 10: Normalized histogram of ascending and descending emissivity difference at 18.7, 36.5, and 89.0 GHz (vertical polarization) before and after using the proposed effective temperature diurnal cycles over the globe and just desert regions for July 2003.

Channel	Global Mean of Asc.-Desc. (After)	Global Mean of Asc.-Desc. (Before)	Global Asc.-desc. STD (After)	Global Asc.-desc. STD (Before)
18.7V	-0.0029	-0.0220	0.0098	0.0293
18.7H	-0.0051	-0.0225	0.0157	0.0280
23.8V	-0.0024	-0.0254	0.0086	0.0285
36.5V	-0.0011	-0.0192	0.01	0.0273
36.5H	-0.0033	-0.0183	0.0153	0.0265
89.0V	0.0025	-0.0238	0.013	0.0252
89.0H	0.0016	-0.0243	0.0142	0.0257

Table 5- 1: Global mean and standard deviation of ascending and descending emissivity differences before and after applying the proposed effective temperature.

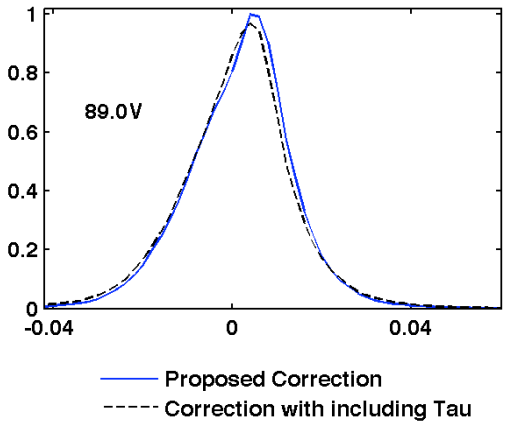

Figure 5- 11:Normalized histogram of day and night emissivity differences at 89.0 GHz using the proposed effective temperature with and without including atmospheric opacity in the correction.

One of the assumptions in this study is that the mean diurnal temperatures at the skin and deeper layers are the same (equation 5-7). Several studies have been conducted to investigate the diurnal variation of soil temperature at different layers and contradictory results about this assumption have been reported. Some believe that according heat conduction the mean diurnal temperature should be the same at all layers (Massman, 1993; Prigent et al., 1999) while other studies show that another sources and sinks can exist due to evaporations (Holmes et al., 2008;

Rutten et al., 2010). For further investigation, the ground measurement of soil temperature profile was analyzed (figure 5-12). This case study shows that deeper layers have smaller amplitude and a phase lag compared to layers closer to the surface. This example shows a case in vegetated regions which smaller penetration depth by microwave is expected. Therefore, 3 k difference (at 30 cm) in mean diurnal temperature is unlikely for AMSR-E channel penetration depths with few centimeters in non-arid regions. In arid regions with greater penetration depth of microwave due to scarcity of the moisture in soil, the new source or sink of heat is negligible (Holmes et al., 2008; Rutten et al., 2010) and similar mean temperature to mean of skin temperature at deeper layers is expected. The sensitivity analysis in chapter 3 shows that this possible 3 k can change emissivity by 0.01. One should note that in previous emissivity retrievals skin temperature are directly utilized in retrieval, and the assumption in this study is somehow embedded in them.

The other assumption in this study is that the emissivity or dielectric constant of the surface doesn't change with temperature during day and night. Some studies have investigated the effect of temperature on dielectric constant. The temperature dependence of the soil bulk dielectric permittivity, ε_b, of the selected soils is presented in figure 5-13. The majority of tested soils show similar trends that confirm other experimental data (Pepin et al., 1995; Or and Wraith, 1999). For small and medium moisture values there is a negligible temperature effect and the linear trend lines in figure 5-13 are almost in parallel to the horizontal axis representing no or a small positive temperature change. This is especially evident for the two trend lines representing the lowest moisture values in ε_b and T relations for all soils in figure 5-13. For higher moisture values there is a tendency to decrease ε_b with temperature proving that the dominant reason for this behavior is the decrease of free water dielectric permittivity with the temperature increase.

Therefore, this assumption in our study sounds reasonable especially mostly in arid regions large differences between day and night were found due penetration depth effect and not because of temperature effect on dielectric (Skierucha, 2011).

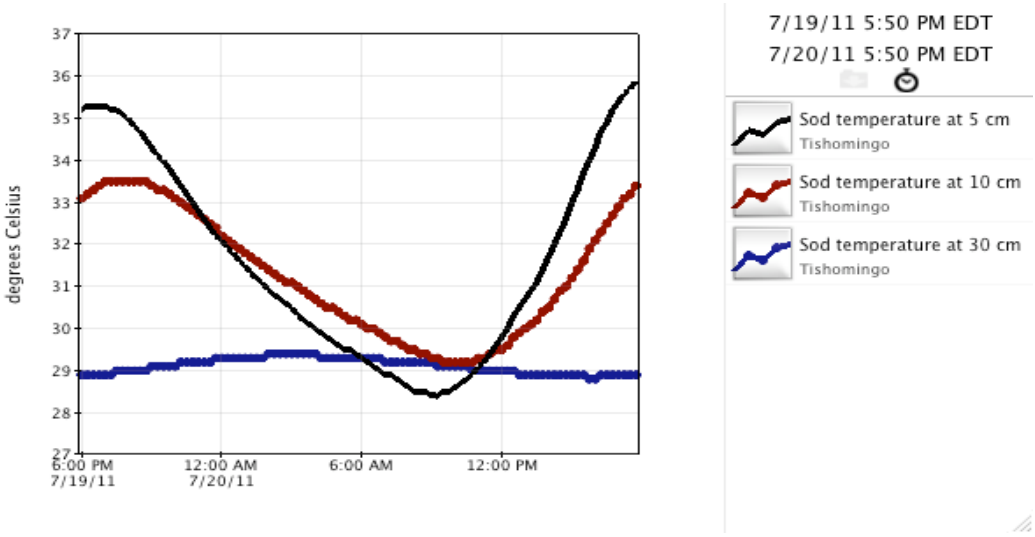

Figure 5- 12: ground measurement of diurnal cycle of temperature profile at Tishomingo, Oklahoma (http://www.mesonet.org)

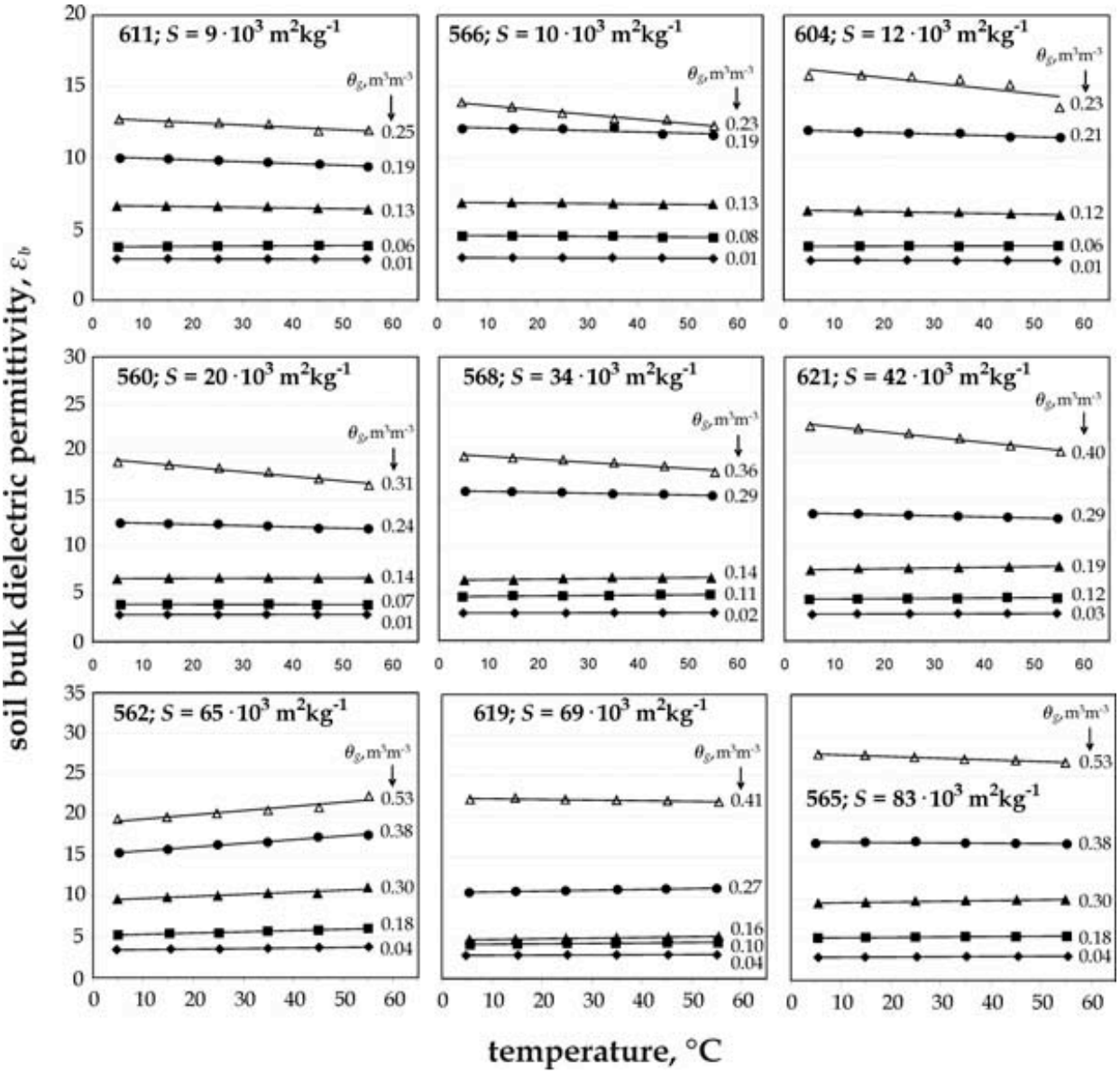

Figure 5- 13: Bulk dielectric permittivity temperature dependence of selected soils bulk dielectric permittivity for different soil volumetric water contents (θg stands for thermo gravimetrically determined soil water content) (Skierucha, 2011)

Note again, that in stable condition in terms of moisture, small difference is anticipated between day and night observations. However, the possible wet and dry conditions can happen during the day and night, which can affect the emissivities and the brightness temperatures. For instance, after a light rain at night, the surface can dry out and causes some differences between

emissivities at ascending and descending. This surface moisture variation can affect the microwave brightness temperature. The shape of the effective temperature diurnal cycle is assumed constant, while the effects of the brightness temperature still can show the difference between emissivities during the day and night due to moisture content variation.

The proposed method in this study is limited to similar frequencies between SSM/I and AMSR-E, i.e. lower frequencies at 06.925 and 10.65 GHz (C- and X-bands) are not included. A possible study to resolve the discrepancies at these lower frequencies is using the obtained lookup table effective temperature diurnal cycle and extrapolating to C- and X-bands. Moreover, the WindSat and TMI channels at lower frequency can be used to construct the microwave brightness temperature at these channels. All steps including the principal component analysis, and generating effective temperature diurnal cycle look up table then can be applied on. Another solution to mitigate the discrepancies between estimates during day and night is using physical model proposed by (Prigent et al., 1999). This model can be used for several years to extract the climatology of Alpha parameter. Then, this alpha can be used similar to look up table in this study to estimate the land surface emissivity instantaneously.

5.5. Conclusion

To retrieve microwave emissivities, estimates of the variation of physical temperatures with depth are necessary. However, there is no global of such information, and infrared thermal temperatures are used as surrogate. This leads to a discrepancy between day and night emissivity retrieval that in stable surface condition is not realistic. A look up table of the diurnal variation of the brightness temperature, which is centered at zero, was adopted based on the diurnal variation of passive microwave brightness temperature at each pixel globally. These diurnal cycles can be

added to the daily average of the skin temperature to find the effective temperature for each channel and month of the year. Applying the obtained effective temperature in emissivity retrievals reduced significantly the differences in estimated day and night emissivities comparing with the case that was just based on infrared thermal temperature as physical temperature. An error analysis was conducted to account for the uncertainty of the assumption and input data in proposed model, and confirms that the mitigation of the discrepancies is promising and can be used for later studies.

CHAPTER 6: CONCLUSION AND PROSPECTIVE WORKS

This research dissertation aimed to provide a better understanding of the land surface emissivity from microwave observations. Several estimates and algorithms are available from different sensors. However, due to lack of global ground-truth measurement of this parameter, it is very difficult to validate the estimations. We tried to target another sensor (AMSR-E) in this research. This sensor has two characteristics; first, it has two lower frequencies that are more sensitive to the surface, and second, its unique local overpass times allow having better diurnal coverage along with other sensors that have overpass times of near dusk and dawn. Although, these characteristics are useful in our atmospheric and geophysical understanding and studies, attention should be paid to issues that are caused by lower frequencies with higher penetration depth and different diurnal cycle variations than the IR measurements used in emissivity retrieval. This chapter summarizes the results of this dissertation and discusses about some possible extensions of this study.

6.1 Summary of results

The results and conclusions of this study therefore can be summarized as following:

6.1.1. Land surface emissivity retrieval from AMSR-E observations

In chapter 3, instantaneous land surface emissivities were estimated from AMSR-E observations under clear sky conditions at all frequencies and both polarizations. Monthly mean composite maps are produced at all frequencies and polarizations for more than six years. The

ISCCP-DX IR-based temperature was used as physical surface temperature in emissivity retrievals. The methodology is similar to previous studies for SSM/I and AMSU products with few adjustments. Having these emissivity estimates along with other estimates from different algorithms and sensors can help to have better chance for spectral analysis and also intercomparison. The results were consistent with previous studies from SSM/I. The remaining differences, after accounting for the differences due to the geometry and frequency, can be explained mostly by the difference in overpass times between two different sensors (AMSR-E and SSM/I). Several quality assessments were conducted. A sensitivity analysis confirmed the importance of the skin temperature at lower frequencies and higher sensitivity of the higher frequencies to atmospheric effects. The day-to-day variability was tested and global RMS of standard deviation of 0.015 was observed. This small variability for estimates within a month confirms the stability of estimates. However, larger standard deviations appeared in arid and semi-arid region.

The difference between day and night emissivities was also examined. Larger differences are found in arid regions at lower frequencies than at higher frequencies, which can be explained by the difference between the skin temperature diurnal variations (amplitude and phase) and the temperature variations at the differing penetration depths for different frequencies. This effect is especially large for AMSR-E because its overpass times are closer to the daily extremes of the skin temperature.

6.1.2. The sensitivity of retrieved emissivities at C and X bands to surface properties

As there is no global direct measurement of emissivity parameters, assessing the estimated emissivities with geophysical properties that affect emissivity can be an interesting

evaluation of the retrieval. Differences between the vertical and horizontal polarizations at C- and X-band were in good qualitative agreement with known variations of vegetation density and surface roughness and can be used as additional indicators of land cover or vegetation type variation at global scales. The two lower frequencies were found to have larger polarization differences at deserts and semi-arid regions. Large correlations were found in moderately vegetated areas with the large seasonal variations of the lower frequency polarization differences and physical properties such as soil moisture and vegetation density (represented by NDVI). The seasonal variations of the polarization difference may be used for quantifying changes in the amount of vegetation. The results confirm that correlation of emissivity monthly variation with vegetation density variation is very small in desert areas (North Africa; Saudi Arabia) and in densely vegetated area such as Amazon and Congo basins. There are some difficulties in analysis of estimation with respect to soil moisture and vegetation density, when these two parameters are mixed and large amounts of soil moisture and vegetation density occur, and it is difficult to determine exactly which parameter the emissivity is more sensitive to.

6.1.3. Spatial variability of microwave brightness temperature diurnal cycle

AMSR-E unique overpass time is an improvement in diurnal coverage of the passive microwave observations. New study was done with considering some more information to extract diurnal characteristics of the brightness temperature globally. Diurnal cycles of microwave brightness temperature were constructed using AMSR-E and SSM/I observations at similar channels. A principal component analysis was conducted to study the spatial variability of the microwave diurnal cycle. The first three components are related to the diurnal amplitude, the duration of daytime, and peak time of the diurnal cycle of the brightness temperature. Strong frequency dependency was found in diurnal amplitude of microwave temperature as the high

frequencies showed greater diurnal amplitude with smaller penetration depth. The diurnal variation of the microwave was studied for different land cover types. It confirmed that in highly vegetated areas the diurnal amplitude is smaller and deserts have the greatest diurnal variation except places with sand dunes soil type. Overall, it was noticed that the brightness temperature diurnal variation does not match with the diurnal variation of the physical temperature. The similar inconsistency is noticed in the diurnal amplitude of thermal and microwave temperatures, as diurnal amplitude of the microwave is significantly smaller in sand dunes.

6.1.4. Effective temperature diurnal cycle lookup table and improvement of land surface emissivity retrievals

With all results from chapter 3 and 4, we concluded that an effective temperature, which is representative of emanating microwave layers, should be developed diurnally consistent with brightness temperature diurnal cycle. The issue was more carefully investigated by looking at different emissivity results and also apparent emissivity diurnal variation. The regions with larger differences in emissivities between day and night had more discrepancies in their diurnal amplitude of skin temperature and brightness temperature. This inconsistency was shown that can affect significantly on emissivity retrievals when the day and night emissivities are compared with as much as 0.1 difference. The differences in stable condition in terms of moisture and vegetation cannot be physical. A look up table of the diurnal variation of the brightness temperature, which is centered at zero, was adopted based on the diurnal variation of passive microwave brightness temperature at each pixel globally. These diurnal cycles can be added to the daily average of the skin temperature to find the effective temperature for each channel and month of the year. Applying the obtained effective temperature in emissivity retrievals reduced significantly the differences in estimated day and night emissivities compared to the case that

was just based on infrared thermal temperature as physical temperature. An error analysis was conducted to account for the uncertainty of the assumption and input data in proposed model, and confirms that the mitigation of the discrepancies is promising and can be used for later studies.

6.2. Prospective works and remaining issues

The results of this study can add more information to estimates of emissivities from other sensors and algorithms. There is a PMM Land Surface Working Group, which specifically focuses on a better understanding of the surface emission and characterization for future rainfall algorithms. Spectral analysis is more feasible with having estimation from AMSR-E with frequencies ranging from 6.925 to 89.0 GHz.

There are still several issues in emissivity retrieval that should be addressed. Some of these issues can be addressed as following:

- The proposed method in this study is limited to similar frequencies between SSM/I and AMSR-E, i.e. lower frequencies at 06.925 and 10.65 GHz (C- and X-bands) are not included. A possible study to resolve the discrepancies at these lower frequencies is using the obtained lookup table effective temperature diurnal cycles and extrapolating them to C- and X-bands. Moreover, the WindSat and TMI channels at lower frequency can be used to construct the microwave brightness temperature at these channels. All steps in this dissertation including the principal component analysis, and generating effective temperature diurnal cycle look up table then can be applied.

- Skin temperature estimates from different products and algorithms have shown significant differences (Jimenez et al., 2011). In chapter 3, the sensitivity analysis showed that skin temperature has significant effect in emissivity retrieval. More efforts are needed to find the best skin temperature globally from infrared thermal observations for emissivity retrievals.
- The effect of the topography was not included in our emissivity retrieval. Topography can affect the retrieval as macro-scale roughness. The scattering of microwave observations in mountainous regions therefore can be significant. Previous studies have shown that the changes in the local observation angle tend to lower the apparent emissivity of a radiometric pixel with respect to the corresponding flat surface characteristics. The effect of the rotation of the polarization plane enlarges (vertical polarization), or attenuates (horizontal polarization) this decrease (Pulvirenti et al., 2008; Pierdicca et al., 2011). Moreover, the topography can affect the radiative transfer model that we used for accounting the atmospheric contribution due to assumption of specular surface.
- In our emissivity retrieval, the diurnal cycle of the atmosphere has been ignored, as TOVS observations just provide daily estimates. This diurnal variation can be important at some places with higher humidity. This ignorance showed some atmospheric residuals in the results of emissivity retrieval in this research especially at higher frequencies. Other products such as NCEP and ECMWF can be used for retrievals.
- The RFI contamination was not considered in this study. The C and X bands are contaminated with Radio Frequency Interference (RFI) especially over US, the

Middle East, and Europe. A spectral difference technique has been developed for AMSR-E and WindSat to quantify the RFI magnitude and extent over the U.S. and at global scale (Njoku et al., 2005; Li et al., 2006). However, it might be possible to use the microwave emissivities at different frequencies to screen out the contaminated regions, as emissivity is "surface temperature free" and the uncertainties in brightness temperature would not be an issue. Our preliminary results from emissivity difference have had similar results to the ones that have been reported before (Not shown in this dissertation).

- This research has just dealt with clear sky condition. However, in most cases (more than 50% over land) the sky condition is cloudy. Several studies extended the clear sky condition to all weather situations using neural network and data assimilation technique (Aires et al., 2001; Boukabara et al., 2007). The results of this research may be extended to cloudy conditions. With using multiple sensor emissivity retrieval, it is possible to extract the emissivity for cloudy condition from clear condition at different time of the day. This idea can be used to extract the surface temperature under cloudy sky.
- Another solution to mitigate the discrepancies between estimates during day and night is using physical model proposed by (Prigent et al., 1999). This model can be used for several years to extract the climatology of Alpha parameter. Then, this alpha can be used similar to look up table in this study to estimate the land surface emissivity instantaneously.

There are also some other studies that can be done to improve our knowledge in geophysical research studies. The emissivity can be converted to different physical properties of the surface. Some prospective studies could be summarized as following:

- The passive microwave brightness temperatures are sensitive to different layers of the surface depending on the frequency. For instance, in vegetated areas, the higher frequencies are sensitive to the top of canopy, while lower frequencies originate from deeper layers. This can be a base to investigate the vegetation structure in densely vegetated areas. Min et al (2010) investigated the structure of vegetation in Amazon regions using microwave emissivity from 19 and 89 GHz. With results of this research study, two more lower frequencies are available that can penetrate deeper and provide more information.
- The snow coverage detection is being investigated from different sources. Microwave observations are less affected by the atmosphere. Several studies have been conducted including using microwave emissivity instead of microwave brightness temperature as the effect of the atmosphere has been removed from the microwave signals. The emissivity difference from different frequencies is used in these snow detection algorithms (Shahroudi et al 2011, private communication). With having two lower frequencies that are much more sensitive to the surface and subsurface, better results can be anticipated.
- Another research possibility is using the instantaneous emissivities to detect the freeze and thaw state. Using this information instead of brightness temperature will reduce the uncertainties by the effect of water temperature between 0 and 4 ^{0}c. As the

water change from liquid phase to ice phase its emissivity will change since its dielectric is changing, even though its temperature may not change.

6.3. Conclusions

Microwave signals from satellite observations have great potential in capturing the atmospheric and geophysical information from the earth. For various applications such as weather, climate, and hydrological studies, recognizing the effect of each component on the microwave observations is necessary. In this research dissertation, several difficulties of estimating of emissivity as well as its sensitivity to surface properties were discussed. It was found that observations from multiple satellites / sensors could be used in emissivity retrieval if the effect and behavior of each of them are considered. In particular, in this research, microwave and infrared temperatures are used for emissivity retrieval. However, just direct application of these measurements (microwave and infrared) causes some discrepancies, as their physics are different. This study tried to remove these discrepancies by providing new information based on diurnal cycle of microwave brightness temperature. The accomplishment of this research is to provide effective temperature diurnal cycle that can be used in emissivity retrievals "instantaneously", while all previous models are able to resolve the issue in a monthly basis.

Another significance of this research and learned lesson in general was to use more information in our research. In particular, this study used several satellites information to construct the diurnal cycle of the brightness temperature. The spatial variability of the diurnal cycle was investigated and found that this diurnal variation has interesting relations with the surface properties such as moisture content, vegetation type, and soil texture.

The emissivity is affected by several surface properties. The retrieved emissivities can be converted to surface properties to enhance our understanding about the earth. The results of this study showed that lower frequency channels have greater potential to capture the surface property variability, as it's less affected by atmosphere and more sensitive to surface and subsurface.

There are still several issues that should be addressed, and several potential studies that can be conducted.

BIBLIOGRAPHY

Aires, F. et al., 2011. A Tool to Estimate Land-Surface Emissivities at Microwave frequencies (TELSEM) for use in numerical weather prediction. Quarterly Journal of the Royal Meteorological Society, 137(656): 690-699.

Aires, F., Prigent, C. and Rossow, W.B., 2004. Temporal interpolation of global surface skin temperature diurnal cycle over land under clear and cloudy conditions. Journal of Geophysical Research-Atmospheres, 109(D4).

Aires, F., Prigent, C. and Rossow, W.B., 2005. Sensitivity of satellite microwave and infrared observations to soil moisture at a global scale: 2. Global statistical relationships. Journal of Geophysical Research-Atmospheres, 110(D11).

Aires, F., Prigent, C., Rossow, W.B. and Rothstein, M., 2001. A new neural network approach including first guess for retrieval of atmospheric water vapor, cloud liquid water path, surface temperature, and emissivities over land from satellite microwave observations. Journal of Geophysical Research-Atmospheres, 106(D14): 14887-14907.

Aires, F., Rossow, W.B., Scott, N.A. and Chedin, A., 2002a. Remote sensing from the infrared atmospheric sounding interferometer instrument - 1. Compression, denoising, and first-guess retrieval algorithms. Journal of Geophysical Research-Atmospheres, 107(D22).

Aires, F., Rossow, W.B., Scott, N.A. and Chedin, A., 2002b. Remote sensing from the infrared atmospheric sounding interferometer instrument - 2. Simultaneous retrieval of temperature, water vapor, and ozone atmospheric profiles. Journal of Geophysical Research-Atmospheres, 107(D22).

Bartalis, Z., Naeimi, V., Hasenauer, S. and Wagner, W., 2008. ASCAT Soil Moisture Product Guide. ASCAT Soil Moisture Report Series, No. 15(Institute of Photogrammetry and Remote Sensing Vienna University of Technology).

Bettenhausen, M.H. et al., 2006. A nonlinear optimization algorithm for WindSat wind-vector retrievals. Ieee Transactions on Geoscience and Remote Sensing, 44(3): 597-610.

Boukabara, S.A., Weng, F.Z. and Liu, Q.H., 2007. Passive microwave remote sensing of extreme weather events using NOAA-18 AMSUA and MHS. Ieee Transactions on Geoscience and Remote Sensing, 45(7): 2228-2246.

Calvet, J.C. et al., 2011. Sensitivity of Passive Microwave Observations to Soil Moisture and Vegetation Water Content: L-Band to W-Band. Ieee Transactions on Geoscience and Remote Sensing, 49(4): 1190-1199.

Choudhury, B.J., 1989. MONITORING GLOBAL LAND SURFACE USING NIMBUS-7 37 GHZ DATA THEORY AND EXAMPLES. International Journal of Remote Sensing, 10(10): 1579-1605.

Choudhury, B.J., 1993. REFLECTIVITIES OF SELECTED LAND-SURFACE TYPES AT 19 AND 37 GHZ FROM SSM/I OBSERVATIONS. Remote Sensing of Environment, 46(1): 1-17.

Colton, M.C. and Poe, G.A., 1999. Intersensor calibration of DMSP SSM/I's: F-8 to F-14, 1987-1997. Ieee Transactions on Geoscience and Remote Sensing, 37(1): 418-439.

Cordisco, E., Prigent, C. and Aires, F., 2006. Snow characterization at a global scale with passive microwave satellite observations. Journal of Geophysical Research-Atmospheres, 111(D19).

English, S.J., 1995. AIRBORNE RADIOMETRIC OBSERVATIONS OF CLOUD LIQUID-WATER EMISSION AT 89 AND 157 GHZ - APPLICATION TO RETRIEVAL OF LIQUID-WATER PATH. Quarterly Journal of the Royal Meteorological Society, 121(527): 1501-1524.

Entekhabi, D. et al., 2010. The Soil Moisture Active Passive (SMAP) Mission. Proceedings of the Ieee, 98(5): 704-716.

Fily, M., Royer, A., Goita, K. and Prigent, C., 2003. A simple retrieval method for land surface temperature and fraction of water surface determination from satellite microwave brightness temperatures in sub-arctic areas. Remote Sensing of Environment, 85(3): 328-338.

Galantowicz, J. et al., 2011. Subsurface Emission Effects in AMSR-E Measurements: Implications for Land Surface Microwave Emissivity Retrieval. Journal of Geophysical Research-Atmospheres: In Press.

Geer, A.J., Bauer, P. and Bormann, N., 2010 Solar Biases in Microwave Imager Observations Assimilated at ECMWF. Ieee Transactions on Geoscience and Remote Sensing, 48(6): 2660-2669.

Greenwald, T.J., Christopher, S.A., Chou, J. and Liljegren, J.C., 1999. Intercomparison of cloud liquid water path derived from the GOES 9 imager and ground based microwave radiometers for continental stratocumulus. Journal of Geophysical Research-Atmospheres, 104(D8): 9251-9260.

Grody, N.C. and Weng, F., 2008. Microwave emission and scattering from deserts: Theory compared with satellite measurements. Ieee Transactions on Geoscience and Remote Sensing, 46(2): 361-375.

Holmes, T.R.H., Owe, M., De Jeu, R.A.M. and Kooi, H., 2008. Estimating the soil temperature profile from a single depth observation: A simple empirical heatflow solution. Water Resources Research, 44(2).

Jackson, T.J., Oneill, P.E. and Swift, C.T., 1997. Passive microwave observation of diurnal surface soil moisture. Ieee Transactions on Geoscience and Remote Sensing, 35(5): 1210-1222.

Jimenez, C., Catherinot, J., Prigent, C. and Roger, J., 2010. Relations between geological characteristics and satellite-derived infrared and microwave emissivities over deserts in northern Africa and the Arabian Peninsula. Journal of Geophysical Research-Atmospheres, 115.

Jimenez, C. et al., 2011. Global intercomparison of 12 land surface heat flux estimates. Journal of Geophysical Research-Atmospheres, 116.

Jolliffe, I.T., 2002. Principal Component Analysis. Springer Series in Statistics. Springer, New York.

Jones, A.S. and VonderHaar, T.H., 1997. Retrieval of microwave surface emittance over land using coincident microwave and infrared satellite measurements. Journal of Geophysical Research-Atmospheres, 102(D12): 13609-13626.

Jones, A.S., Vukicevic, T. and Vonder Haar, T.H., 2004. A microwave satellite observational operator for variational data assimilation of soil moisture. Journal of Hydrometeorology, 5(1): 213-229.

Jones, L.A. et al., 2007. Satellite microwave remote sensing of boreal and arctic soil temperatures from AMSR-E. Ieee Transactions on Geoscience and Remote Sensing, 45(7): 2004-2018.

Jorda, G., Gomis, D. and Talone, M., 2011. The SMOS L3 Mapping Algorithm for Sea Surface Salinity. Ieee Transactions on Geoscience and Remote Sensing, 49(3): 1032-1051.

Kalnay, E. et al., 1996. The NCEP/NCAR 40-year reanalysis project. Bulletin of the American Meteorological Society, 77(3): 437-471.

Karbou, F., Aires, F., Prigent, C. and Eymard, L., 2005a. Potential of Advanced Microwave Sounding Unit-A (AMSU-A) and AMSU-B measurements for atmospheric temperature and humidity profiling over land. Journal of Geophysical Research-Atmospheres, 110(D7).

Karbou, F., Gerard, E. and Rabier, F., 2006. Microwave land emissivity and skin temperature for AMSU-A and -B assimilation over land. Quarterly Journal of the Royal Meteorological Society, 132(620): 2333-2355.

Karbou, F. and Prigent, C., 2005. Calculation of microwave land surface emissivity from satellite observations: Validity of the specular approximation over snow-free surfaces? Ieee Geoscience and Remote Sensing Letters, 2(3): 311-314.

Karbou, F., Prigent, C., Eymard, L. and Pardo, J.R., 2005b. Microwave land emissivity calculations using AMSU measurements. Ieee Transactions on Geoscience and Remote Sensing, 43(5): 948-959.

Kawanishi, T. et al., 2003. The Advanced Microwave Scanning Radiometer for the Earth Observing System (AMSR-E), NASDA's contribution to the EOS for global energy and water cycle studies. Ieee Transactions on Geoscience and Remote Sensing, 41(2): 184-194.

Li, J. et al., 2011. Land surface emissivity from high temporal resolution geostationary infrared imager radiances: Methodology and simulation studies. Journal of Geophysical Research-Atmospheres, 116.

Li, L., Gaiser, P.W., Bettenhausen, M.H. and Johnston, W., 2006. WindSat radio-frequency interference signature and its identification over land and ocean. Ieee Transactions on Geoscience and Remote Sensing, 44(3): 530-539.

Li, Z. et al., 2010. An objective methodology for infrared land surface emissivity evaluation. Journal of Geophysical Research-Atmospheres, 115.

Liebe, H.J., 1989. MPM - AN ATMOSPHERIC MILLIMETER-WAVE PROPAGATION MODEL. International Journal of Infrared and Millimeter Waves, 10(6): 631-650.

Liebe, H.J., Hufford, G.A. and Cotton, M.G., 1993. Propagation modelling of moist air and suspended water/ice particles at frequencies below 1000 GHz. presented at the Specialist Meeting of the Electromagnetic Wave Propagation Panel Symposium, Palma de Mallorca, Spain.

Lin, B. and Rossow, W.B., 1994. OBSERVATIONS OF CLOUD LIQUID WATER PATH OVER OCEANS - OPTICAL AND MICROWAVE REMOTE-SENSING METHODS. Journal of Geophysical Research-Atmospheres, 99(D10): 20907-20927.

Lu, S., Ju, Z.Q., Ren, T.S. and Horton, R., 2009. A general approach to estimate soil water content from thermal inertia. Agricultural and Forest Meteorology, 149(10): 1693-1698.

Massman, W.J., 1993. PERIODIC TEMPERATURE-VARIATIONS IN AN INHOMOGENEOUS SOIL - A COMPARISON OF APPROXIMATE AND EXACT ANALYTICAL EXPRESSIONS. Soil Science, 155(5): 331-338.

Matthews, E., 1983. GLOBAL VEGETATION AND LAND-USE DATA-BASES FOR CLIMATE STUDIES. Bulletin of the American Meteorological Society, 64(7): 793-794.

Matzler, C., 2005. On the determination of surface emissivity from satellite observations. Ieee Geoscience and Remote Sensing Letters, 2(2): 160-163.

McCollum, J.R. and Ferraro, R.R., 2005. Microwave rainfall estimation over coasts. Journal of Atmospheric and Oceanic Technology, 22(5): 497-512.

Min, Q.L., Lin, B. and Li, R., 2010. Remote Sensing Vegetation Hydrological States Using Passive Microwave Measurements. Ieee Journal of Selected Topics in Applied Earth Observations and Remote Sensing, 3(1): 124-131.

Moncet, J. et al., 2011. Land Surface Microwave Emissivities Derived from AMSR-E and MODIS Measurements with Advanced Quality Control. Journal of Geophysical Research-Atmospheres, 116.

Njoku, E.G., Ashcroft, P., Chan, T.K. and Li, L., 2005. Global survey and statistics of radio-frequency interference in AMSR-E land observations. Ieee Transactions on Geoscience and Remote Sensing, 43(5): 938-947.

Njoku, E.G. and Entekhabi, D., 1996. Passive microwave remote sensing of soil moisture. Journal of Hydrology, 184(1-2): 101-129.

Njoku, E.G., Jackson, T.J., Lakshmi, V., Chan, T.K. and Nghiem, S.V., 2003. Soil moisture retrieval from AMSR-E. Ieee Transactions on Geoscience and Remote Sensing, 41(2): 215-229.

Njoku, E.G. and Li, L., 1999. Retrieval of land surface parameters using passive microwave measurements at 6-18 GHz. Ieee Transactions on Geoscience and Remote Sensing, 37(1): 79-93.

Njoku, E.G., Stacey, J.M. and Barath, F.T., 1980. The Seasat scanning multichannel microwave radiometer (SMMR): Instrument description and performance. Oceanic Engineering, IEEE Journal of, 5(2): 100-115.

Norouzi, H. et al., 2011. The sensitivity of land emissivity estimates from AMSR-E at C and X bands to surface properties. Hydrol. Earth Syst. Sci. Discuss., 8(3): 5667-5699.

Or, D. and Wraith, J.M., 1999. Temperature effects on soil bulk dielectric permittivity measured by time domain reflectometry: A physical model. Water Resources Research, 35(2): 371-383.

Owe, M., de Jeu, R. and Walker, J., 2001. A methodology for surface soil moisture and vegetation optical depth retrieval using the microwave polarization difference index. Ieee Transactions on Geoscience and Remote Sensing, 39(8): 1643-1654.

Papa, F., Prigent, C., Rossow, W.B., Legresy, B. and Remy, F., 2006. Inundated wetland dynamics over boreal regions from remote sensing: the use of Topex-Poseidon dual-frequency radar altimeter observations. International Journal of Remote Sensing, 27(21): 4847-4866.

Pepin, S., Livingston, N.J. and Hook, W.R., 1995. TEMPERATURE-DEPENDENT MEASUREMENT ERRORS IN TIME-DOMAIN REFLECTOMETRY DETERMINATIONS OF SOIL-WATER. Soil Science Society of America Journal, 59(1): 38-43.

Pierdicca, N., Pulvirenti, L. and Marzano, F.S., 2011. Simulating Topographic Effects on Spaceborne Radiometric Observations Between L and X Frequency Bands. Ieee Transactions on Geoscience and Remote Sensing, 48(1): 273-282.

Pimentel, S., Haines, K. and Nichols, N.K., 2008. Modeling the diurnal variability of sea surface temperatures. Journal of Geophysical Research-Oceans, 113(C11): 11.

Prigent, C., Aires, F., Rossow, W. and Matthews, E., 2001. Joint characterization of vegetation by satellite observations from visible to microwave wavelengths: A sensitivity analysis. Journal of Geophysical Research-Atmospheres, 106(D18): 20665-20685.

Prigent, C., Aires, F. and Rossow, W.B., 2006. Land surface microwave emissivities over the globe for a decade. Bulletin of the American Meteorological Society, 87(11): 1573-+.

Prigent, C., Aires, F., Rossow, W.B. and Robock, A., 2005a. Sensitivity of satellite microwave and infrared observations to soil moisture at a global scale: Relationship of satellite observations to in situ soil moisture measurements. Journal of Geophysical Research-Atmospheres, 110(D7).

Prigent, C., Chevallier, F., Karbou, F., Bauer, P. and Kelly, G., 2005b. AMSU-A land surface emissivity estimation for numerical weather prediction assimilation schemes. Journal of Applied Meteorology, 44(4): 416-426.

Prigent, C., Jaumouille, E., Chevallier, F. and Aires, F., 2008. A parameterization of the microwave land surface emissivity between 19 and 100 GHz, anchored to satellite-derived estimates. Ieee Transactions on Geoscience and Remote Sensing, 46(2): 344-352.

Prigent, C., Rossow, W.B. and Matthews, E., 1997. Microwave land surface emissivities estimated from SSM/I observations. Journal of Geophysical Research-Atmospheres, 102(D18): 21867-21890.

Prigent, C., Rossow, W.B. and Matthews, E., 1998. Global maps of microwave land surface emissivities: Potential for land surface characterization. Radio Science, 33(3): 745-751.

Prigent, C., Rossow, W.B., Matthews, E. and Marticorena, B., 1999. Microwave radiometric signatures of different surface types in deserts. Journal of Geophysical Research-Atmospheres, 104(D10): 12147-12158.

Prigent, C., Wigneron, J.P., Rossow, W.B. and Pardo-Carrion, J.R., 2000. Frequency and angular variations of land surface microwave emissivities: Can we estimate SSM/T and AMSU emissivities from SSM/I emissivities? Ieee Transactions on Geoscience and Remote Sensing, 38(5): 2373-2386.

Pulvirenti, L., Pierdicca, N. and Marzano, F.S., 2008. Topographic effects on the surface emissivity of a mountainous area observed by a spaceborne microwave radiometer. Sensors, 8(3): 1459-1474.

Rossow, W.B. and Schiffer, R.A., 1991. ISCCP CLOUD DATA PRODUCTS. Bulletin of the American Meteorological Society, 72(1): 2-20.

Rossow, W.B. and Schiffer, R.A., 1999. Advances in understanding clouds from ISCCP. Bulletin of the American Meteorological Society, 80(11): 2261-2287.

Ruston, B.C., 2004. Characteristics of summertime microwave land emissivity over the conterminous United States., Colorado State University, Colorado.

Rutten, M.M., Steele-Dunne, S.C., Judge, J. and van de Giesen, N., 2010. Understanding Heat Transfer in the Shallow Subsurface Using Temperature Observations. Vadose Zone Journal, 9(4): 1034-1045.

Skierucha, W., 2011. Electromagnetic Waves. InTech.

Stephen, H., Ahmad, S. and Piechota, T.C., 2010. Land Surface Brightness Temperature Modeling Using Solar Insolation. Ieee Transactions on Geoscience and Remote Sensing, 48(1): 491-498.

Tedesco, M. and Kim, E.J., 2006. Retrieval of dry-snow parameters from microwave radiometric data using a dense-medium model and genetic algorithms. Ieee Transactions on Geoscience and Remote Sensing, 44(8): 2143-2151.

Weng, F.Z., 2007. Advances in radiative transfer modeling in support of satellite data assimilation. Journal of the Atmospheric Sciences, 64(11): 3799-3807.

Weng, F.Z., Yan, B.H. and Grody, N.C., 2001. A microwave land emissivity model. Journal of Geophysical Research-Atmospheres, 106(D17): 20115-20123.

Wilheit, T., Kummerow, C.D. and Ferraro, R., 2003. Rainfall algorithms for AMSR-E. Ieee Transactions on Geoscience and Remote Sensing, 41(2): 204-214.

Zhang, L.X., Zhao, T.J., Jiang, L.M. and Zhao, S.J., 2010. Estimate of Phase Transition Water Content in Freeze-Thaw Process Using Microwave Radiometer. Ieee Transactions on Geoscience and Remote Sensing, 48(12): 4248-4255.

Zhang, Y.C., Rossow, W.B. and Stackhouse, P.W., 2006. Comparison of different global information sources used in surface radiative flux calculation: Radiative properties of the near-surface atmosphere. Journal of Geophysical Research-Atmospheres, 111(D13).

Zhang, Y.C., Rossow, W.B. and Stackhouse, P.W., 2007. Comparison of different global information sources used in surface radiative flux calculation: Radiative properties of the surface. Journal of Geophysical Research-Atmospheres, 112(D1).